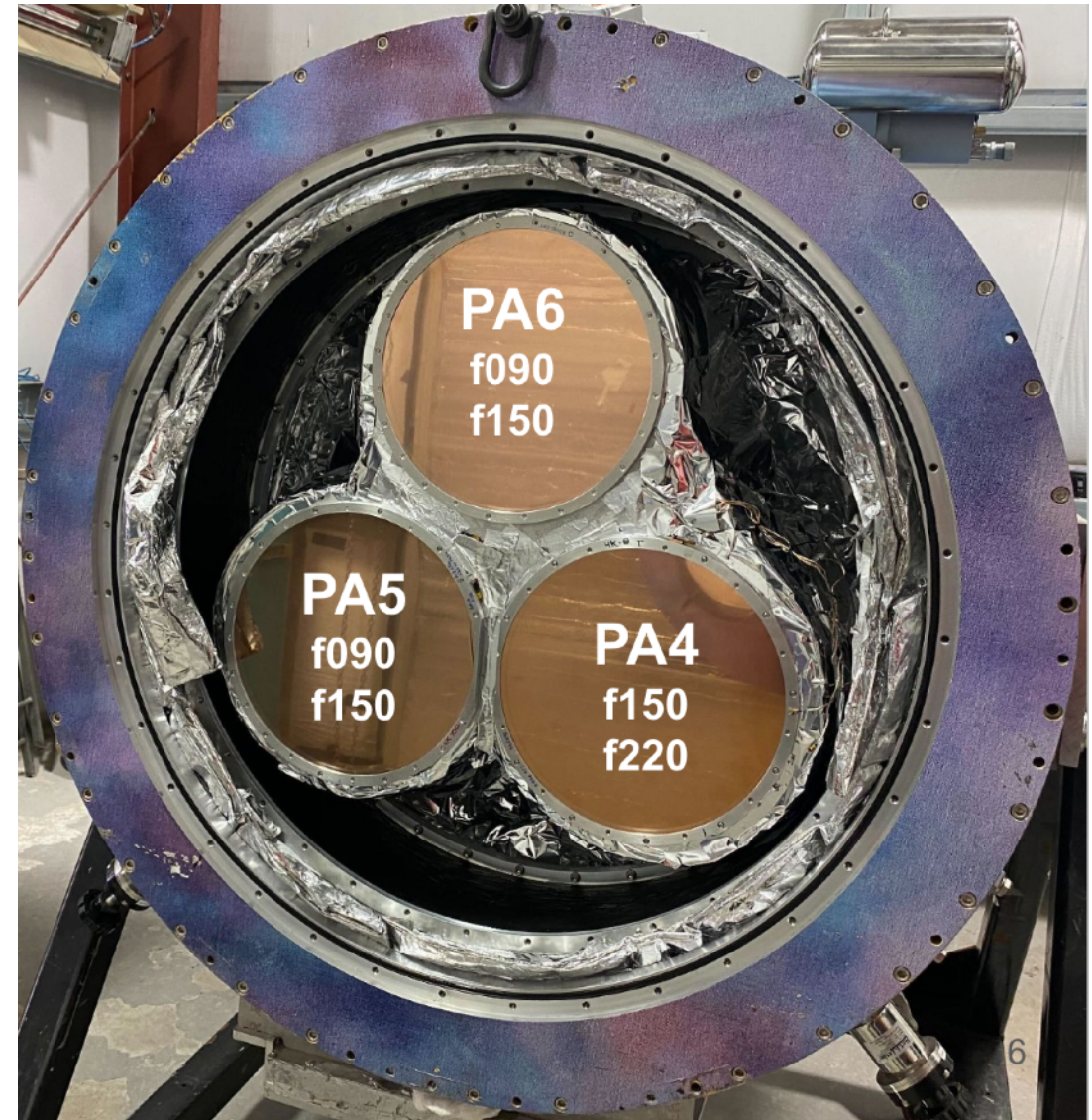
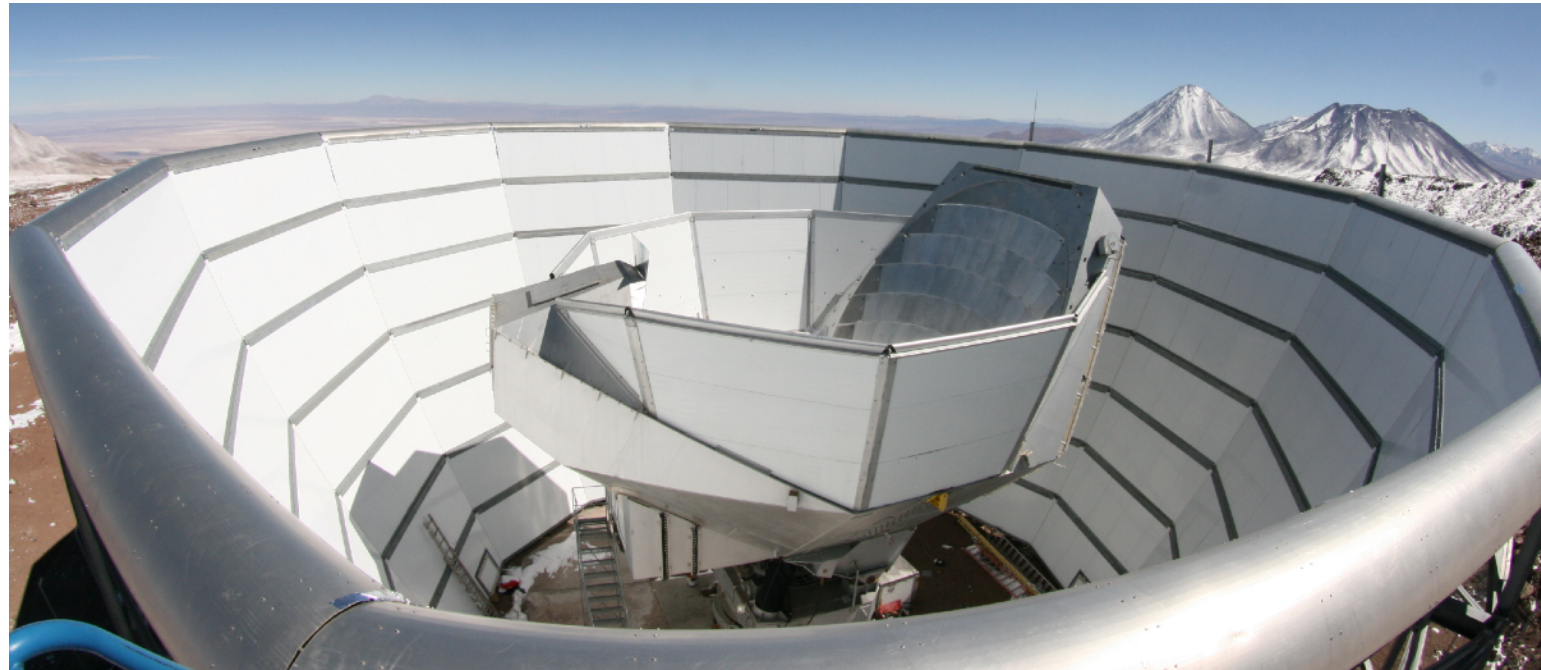


ACT Data Release 6 (2017-2022)

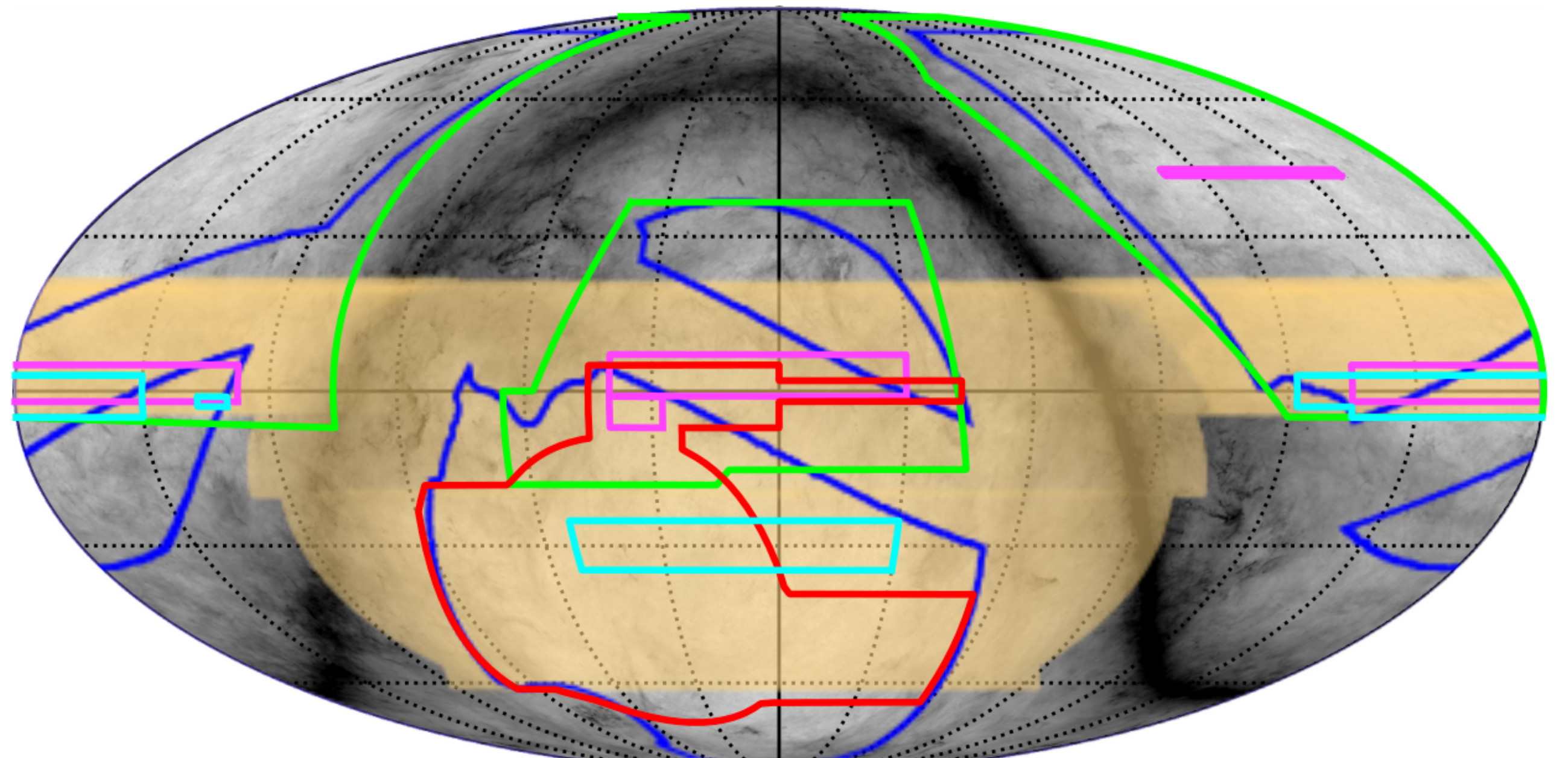
Thibaut Louis



- 3 dichroic detector arrays for DR6: PA4, PA5 and PA6
- 3750 working detectors (70% yield) at 100 mK
- 3 broad bands: f090 (77 – 112 GHz),
f150 (124 – 172 GHz) and f220 (182 – 277 GHz)
- Combined sensitivity of $6.2 \mu\text{K}\sqrt{\text{s}}$,
and $1.4' \text{ FWHM} @ \text{f150}$



ACT survey: approx. 40% of the sky



ACT Final Data Release: Three main papers

DRAFT VERSION JANUARY 24, 2025
Typeset using L^AT_EX twocolumn style in AASTeX63

The Atacama Cosmology Telescope: DR6 maps

SIGURD NAESS,¹ YILUN GUAN,² ADRIAAN J. DUVENVOORDEN,³ MATTHEW HASSELFIELD,⁴ YUHAN WANG,⁵ AND ET AL, ACT COLLABORATION

¹*Institute of Theoretical Astrophysics, University of Oslo, Norway*

²*Dunlap Institute for Astronomy and Astrophysics, University of Toronto, 50 St. George Street, Toronto, ON M5S 3H4, Canada*

³*Joseph Henry Laboratories of Physics, Jadwin Hall, Princeton University, Princeton, NJ, USA 08544*

⁴*Center for Computational Astrophysics, Flatiron Institute, New York, NY, USA 10010*

⁵*Department of Physics, Cornell University, Ithaca, NY 14853, USA*

The Atacama Cosmology Telescope: DR6 Power spectra, Likelihood and Λ CDM parameters

THIBAUT LOUIS,¹ ADRIEN LA POSTA,² ZACHARY ATKINS,³ HIDDE T. JENSE,⁴ AND ACT COLLABORATION

¹*Université Paris-Saclay, CNRS/IN2P3, IJCLab, 91405 Orsay, France*

²*Department of Physics, University of Oxford, Denys Wilkinson Building, Keble Road, Oxford OX1 3RH, United Kingdom*

³*Joseph Henry Laboratories of Physics, Jadwin Hall, Princeton University, Princeton, NJ, USA 08544*

⁴*School of Physics and Astronomy, Cardiff University, The Parade, Cardiff, Wales, UK CF24 3AA*

The Atacama Cosmology Telescope: DR6 Constraints on Extended Cosmological Models

ERMINIA CALABRESE,¹ J. COLIN HILL,² HIDDE T. JENSE,¹ ADRIEN LA POSTA,³ AND ACT COLLABORATION

¹*School of Physics and Astronomy, Cardiff University, The Parade, Cardiff, Wales, UK CF24 3AA*

²*Department of Physics, Columbia University, New York, NY 10027, USA*

³*Department of Physics, University of Oxford, Denys Wilkinson Building, Keble Road, Oxford OX1 3RH, United Kingdom*

Data and code release

Alongside the papers, we release all the data products needed to reproduce our analysis. *For the first time in CMB data analysis, we also provide the complete power spectrum and likelihood pipeline, enabling users to go from public products to cosmological parameters and to reproduce all the figures from the power spectrum paper.*

	Planck	ACT	SPT3G	BICEP/Keck
Likelihood	Yes	Yes	Yes	Yes
Maps	Yes	Yes	No	No
Analysis Codes	Partial release	Full Release	No	No

Other ground based experiments

Data and code release

As we approach percent-level constraints on parameters, signs of tension (or hints of new physics) have emerged

H₀ tension

$$H_0^{\text{SH0ES}} = 73.17 \pm 0.86 \text{ km/s/Mpc} \text{ (Breuval et al. 2024)}$$

$$H_0^{\text{Planck}} = 67.36 \pm 0.54 \text{ km/s/Mpc} \text{ (Planck 2018 results. VI)}$$

Planck anomalies

$$A_L = 1.180 \pm 0.065 \text{ (Planck 2018 results. VI)}$$

$$\Omega_k = -0.044 \pm 0.018 \text{ (Planck 2018 results. VI)}$$

DESI equation state of dark energy

$$\left. \begin{array}{l} w_0 = -0.752 \pm 0.057 \\ w_a = -0.86^{+0.23}_{-0.20} \end{array} \right\} \begin{array}{l} \text{DESI+CMB} \\ +\text{DESY5}, \end{array}$$

Data and code release

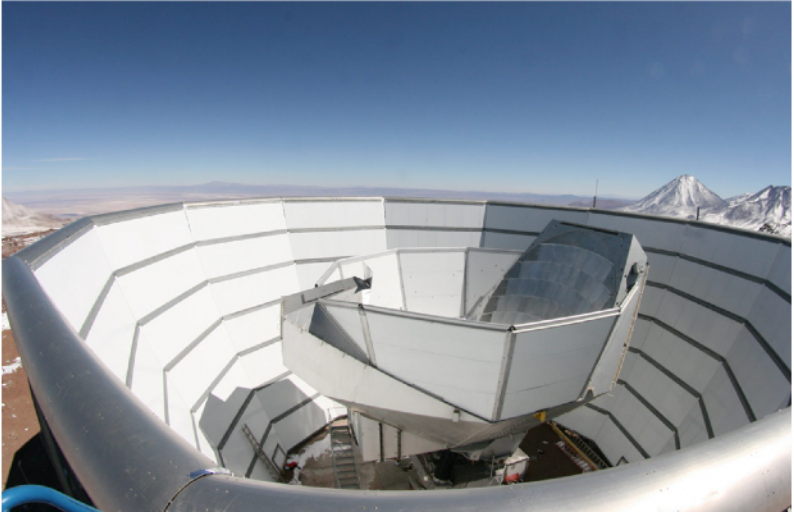
Given this state of the art, within ACT, we have agreed that the only way to make progress as a community is to strive for maximum transparency and reproducibility

LAMBDA - Data Products

Data Hosted Experiment Tables Space-Based Suborbital Astrophysical About Products

Overview ACT (MBAC) ACT (ACTPol) ACT (AdvACT) **ACT (DR6.02)** Publications

ACT (DR6.02) Data Release



ACT Telescope - view looking into the receiver. Image credit Mark Devlin

ANNOUNCEMENT:

- The full DR6.02 release will be here very soon.
- A full copy of the data is stored on NERSC at: /global/cfs/cdirs/cmb/data/act_dr6/dr6.02. Access to NERSC can be requested here: <https://crd.lbl.gov/divisions/scidata/c3/c3-research/cosmic-microwave-background/cmb-data-at-nersc/>
- The link to the web atlas: [DR6 Atlas](#) (does not support Safari, Use the (?) for details)
- The link to the likelihoods: [act_dr6_mflike likelihood](#), [CMB-only likelihood](#)

Description

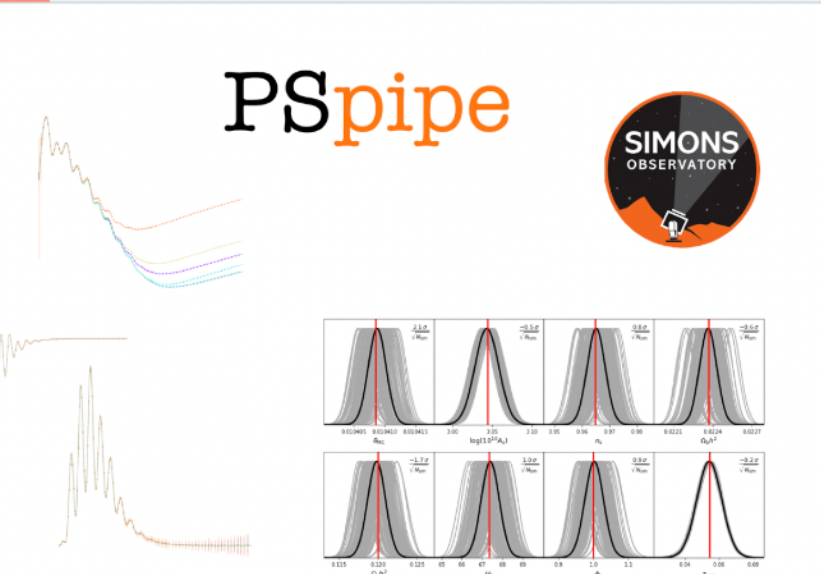
Maps and cosmological results from the 90, 150 and 220 GHz data from the 2017-2022 observing seasons of the AdvancedACT camera.

- Description of the frequency maps in temperature and polarization over 19,000 square degrees, the data reduction pipeline and derived maps (Naess et al. 2025)
- Power spectra, measurements of foreground parameters and cosmological constraints on Lambda-CDM (Louis et al. 2025)
- Constraints on extended cosmological models (Calabrese et al. 2025)

github.com/simonobs/PSpipe

README License

PSpipe



The package

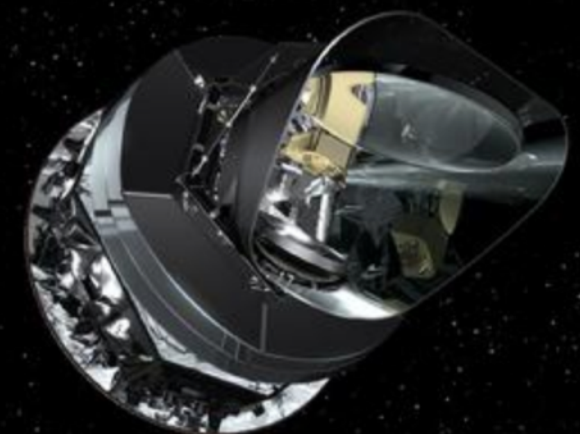
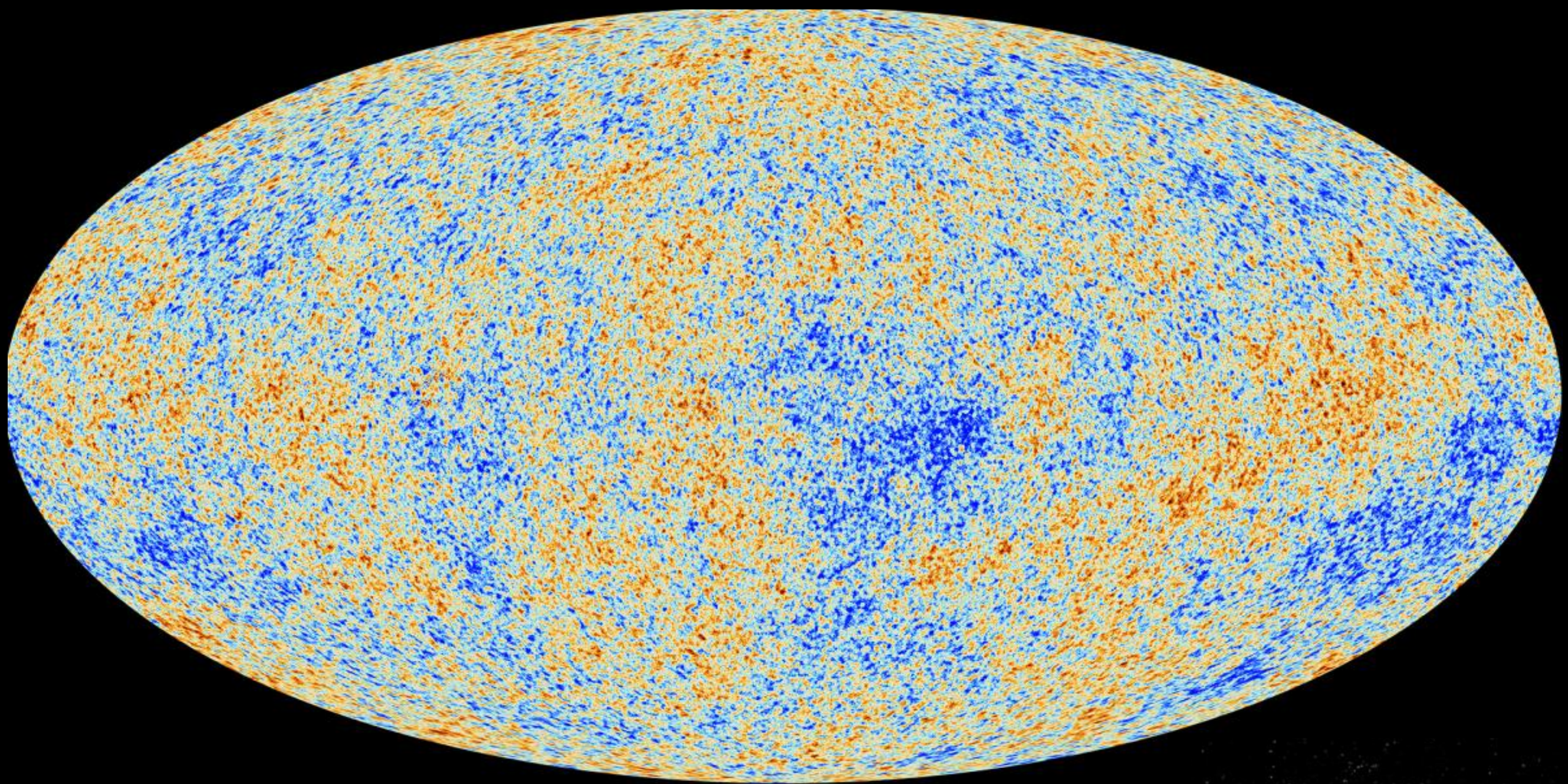
build passing license BSD

PSpipe is a pipeline creator for the analysis of the high resolution maps of the large aperture telescope of the Simons Observatory. It contains tools for estimating power spectra and covariance matrices.

The pipelines are mainly written in python and make use of three different codes,

- `pspy` : a python library for power spectrum estimation (<https://github.com/simonobs/pspy>)
- `pspipe_utils` : a python toolbox library to process and to deal with power spectrum computation (https://github.com/simonobs/pspipe_utils)
- `mflike` : a multifrequency likelihood interfaced with `cobaya` (https://github.com/simonobs/LAT_MFLike)

MAPS



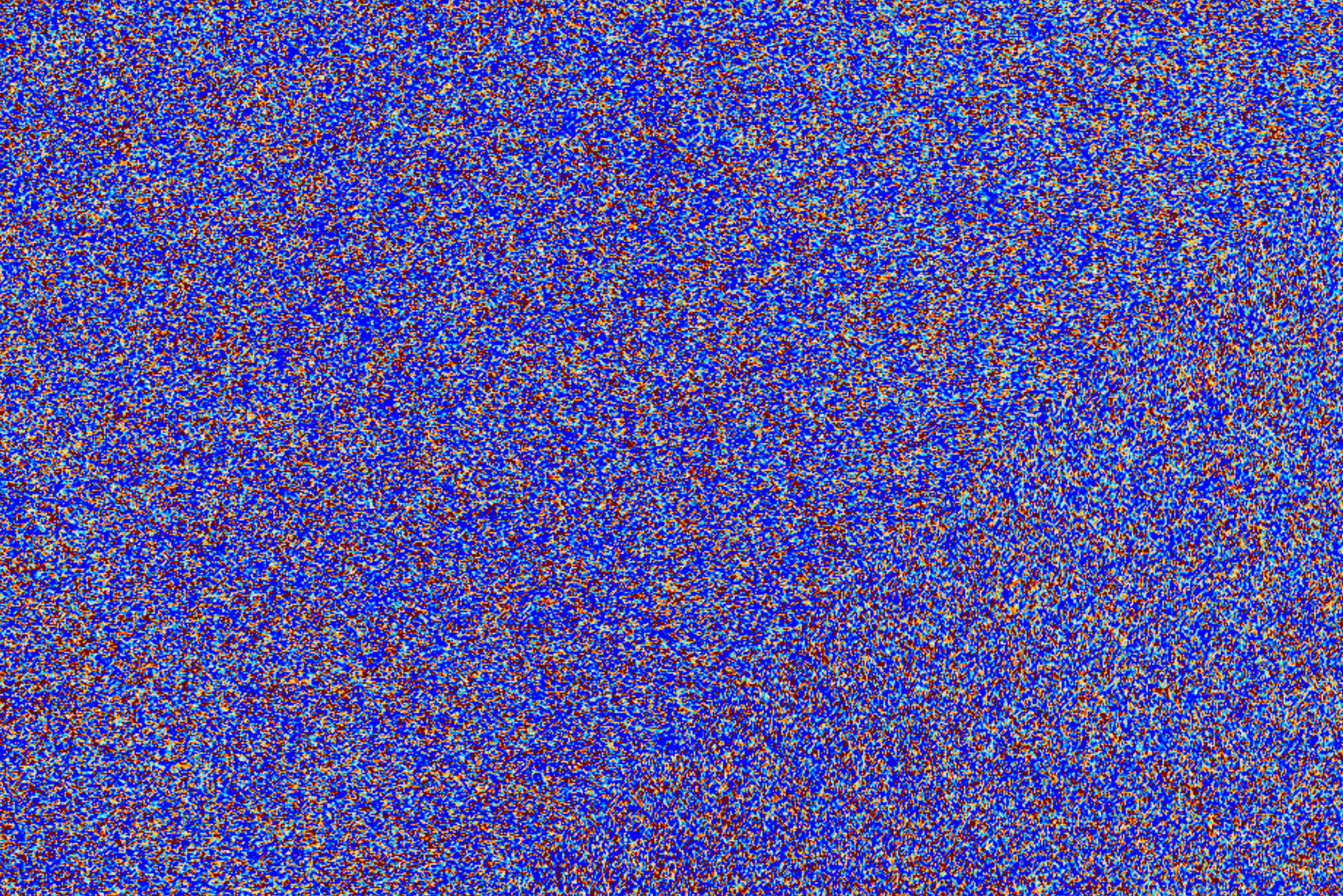
Planck f150 T

13°×7°

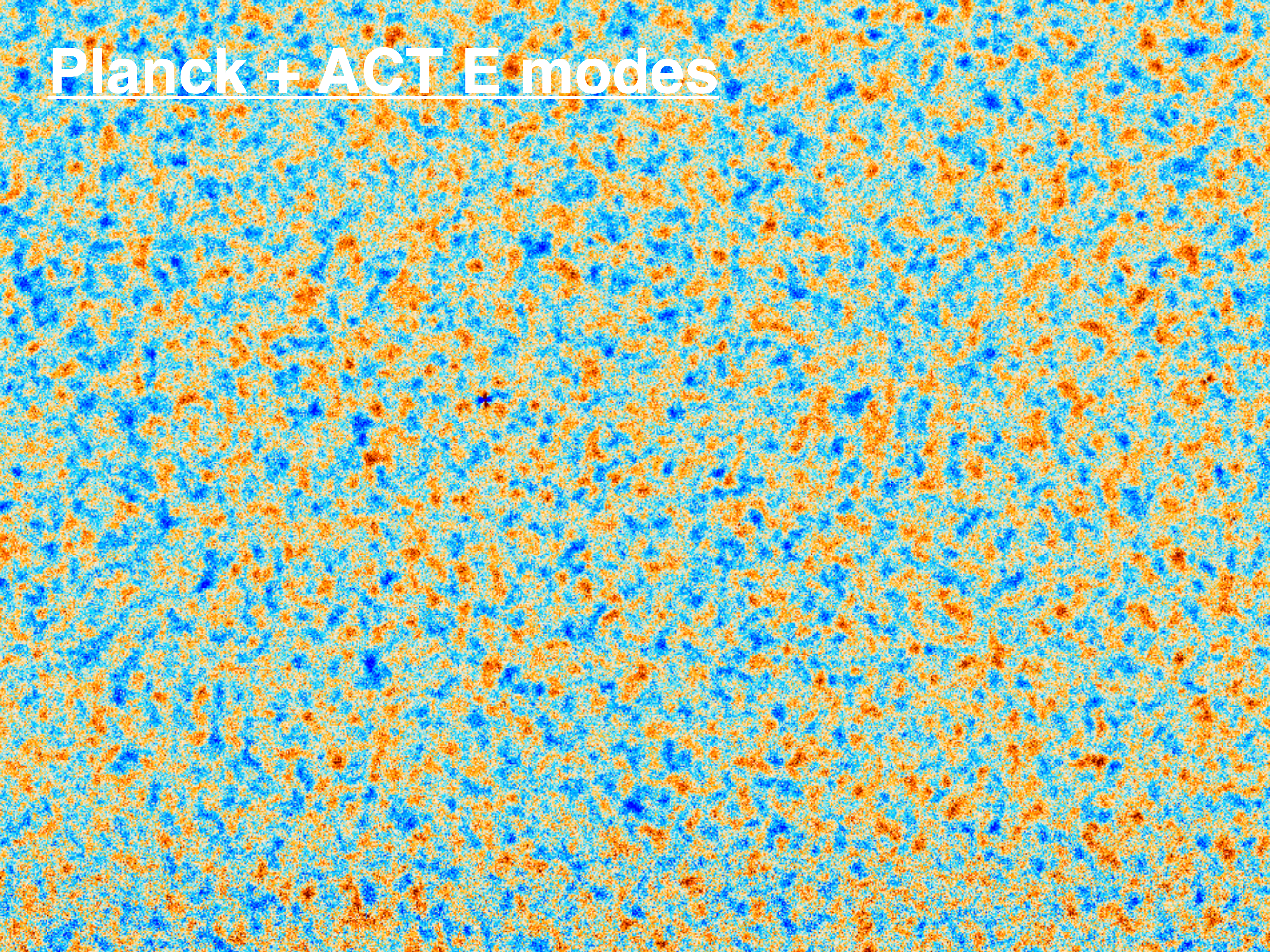
ACT+Planck f150 T

13°×7°

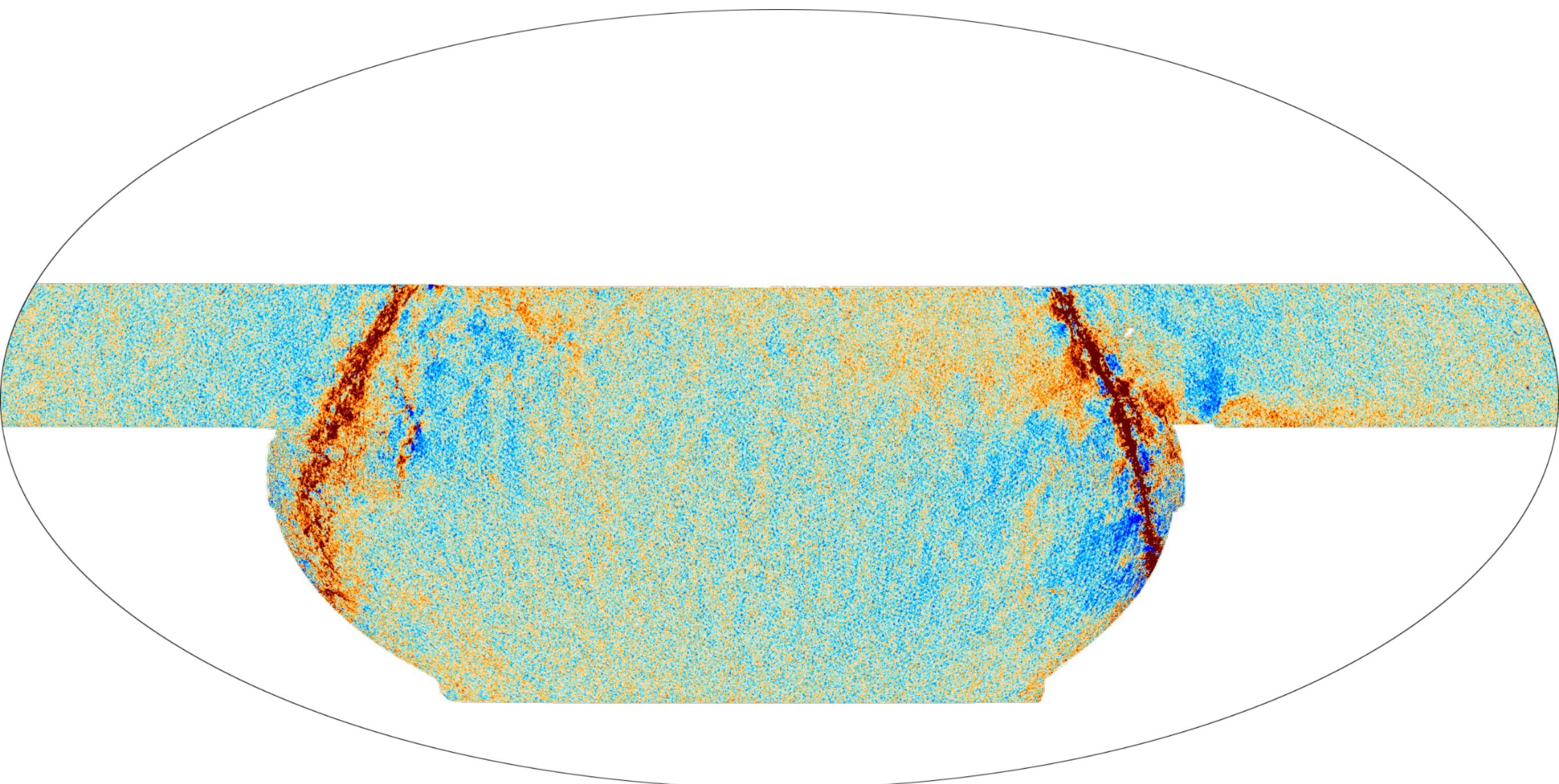
PLANCK E modes



Planck + ACT E modes



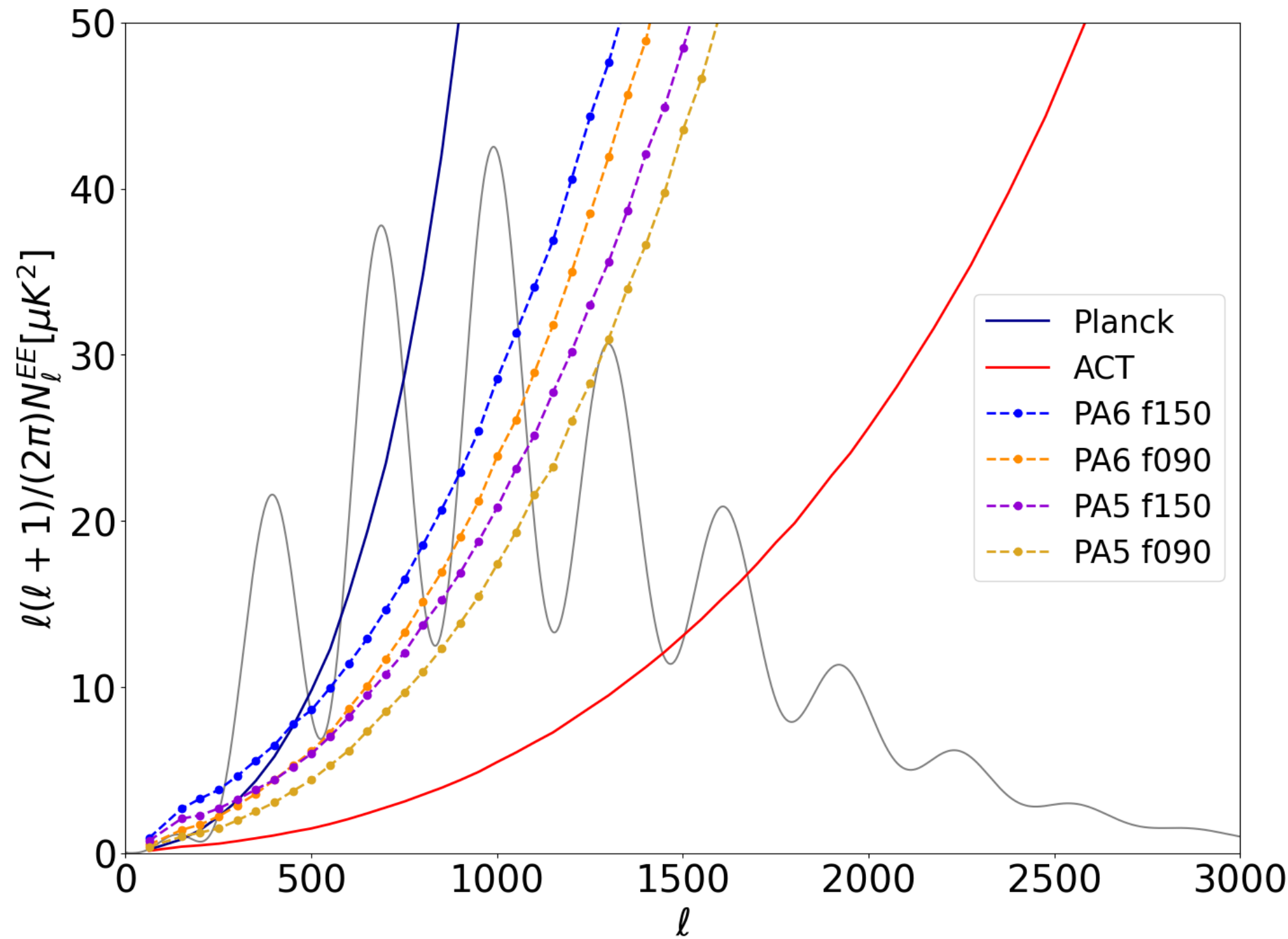
First high S/N E-modes map ever made over
a large portion of the sky



ACT+Planck E

Power spectra

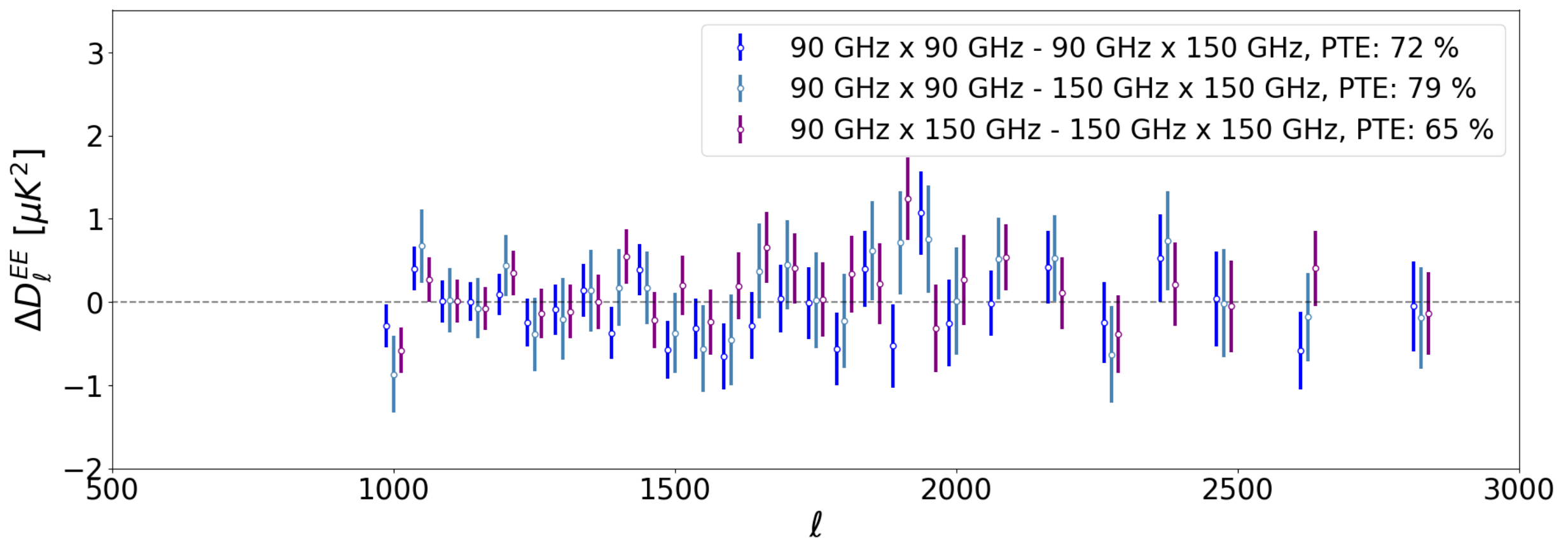
Noise power spectra



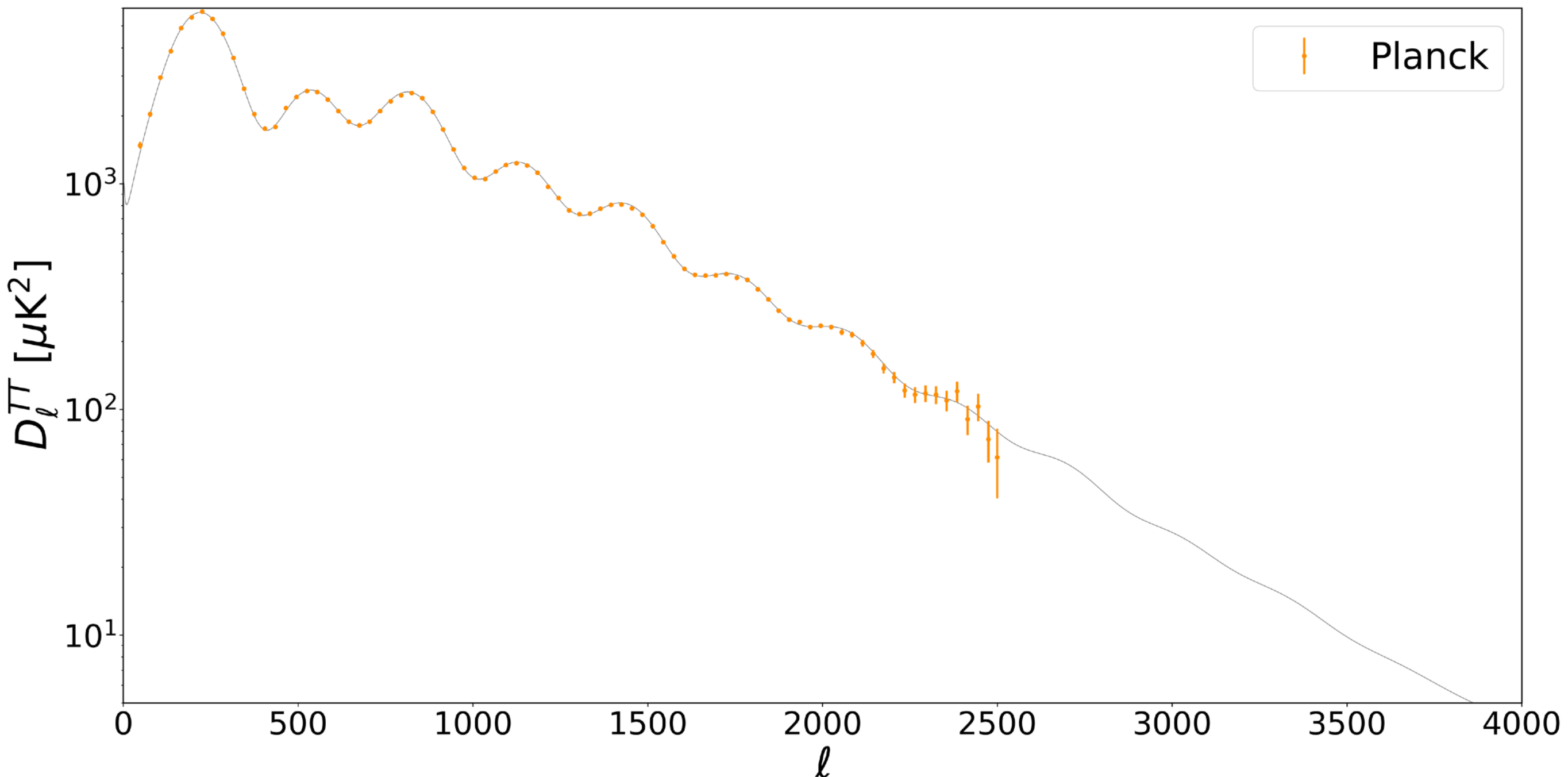
The ACT DR6 polarization data are signal-dominated up to a multipole $\ell=1500$, corresponding to an angular scale of ~ 0.1 degrees. The different array-bands have comparable constraining power, providing useful redundancies.

Before unblinding, we have performed around 2000 null tests on the data, we checked that the results do not depend on

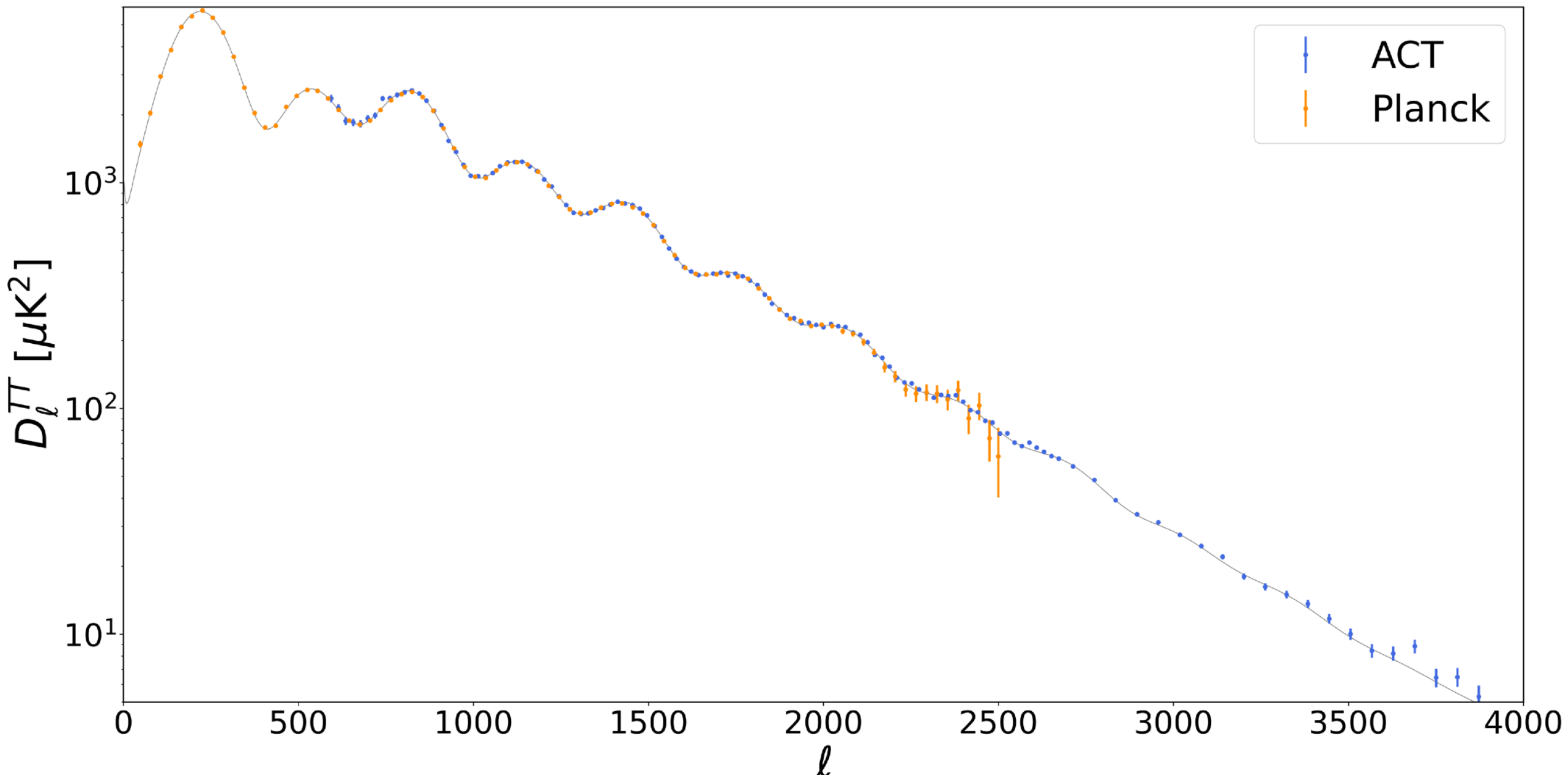
- array bands
- weather conditions
- scan elevation
- sky location
- time of observation
- position of the detectors in the focal plane



Planck temperature power spectrum



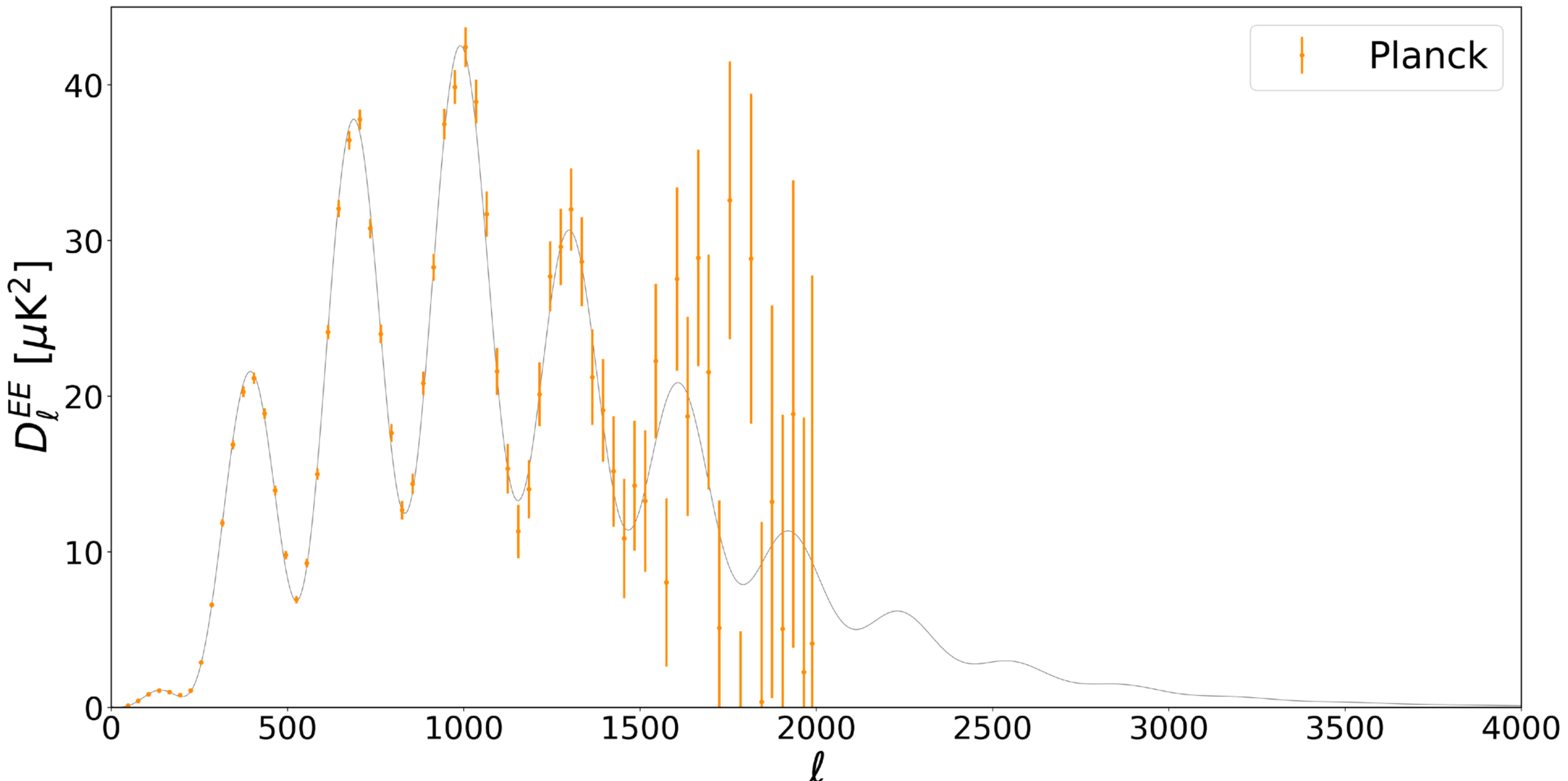
Planck + ACT temperature power spectra



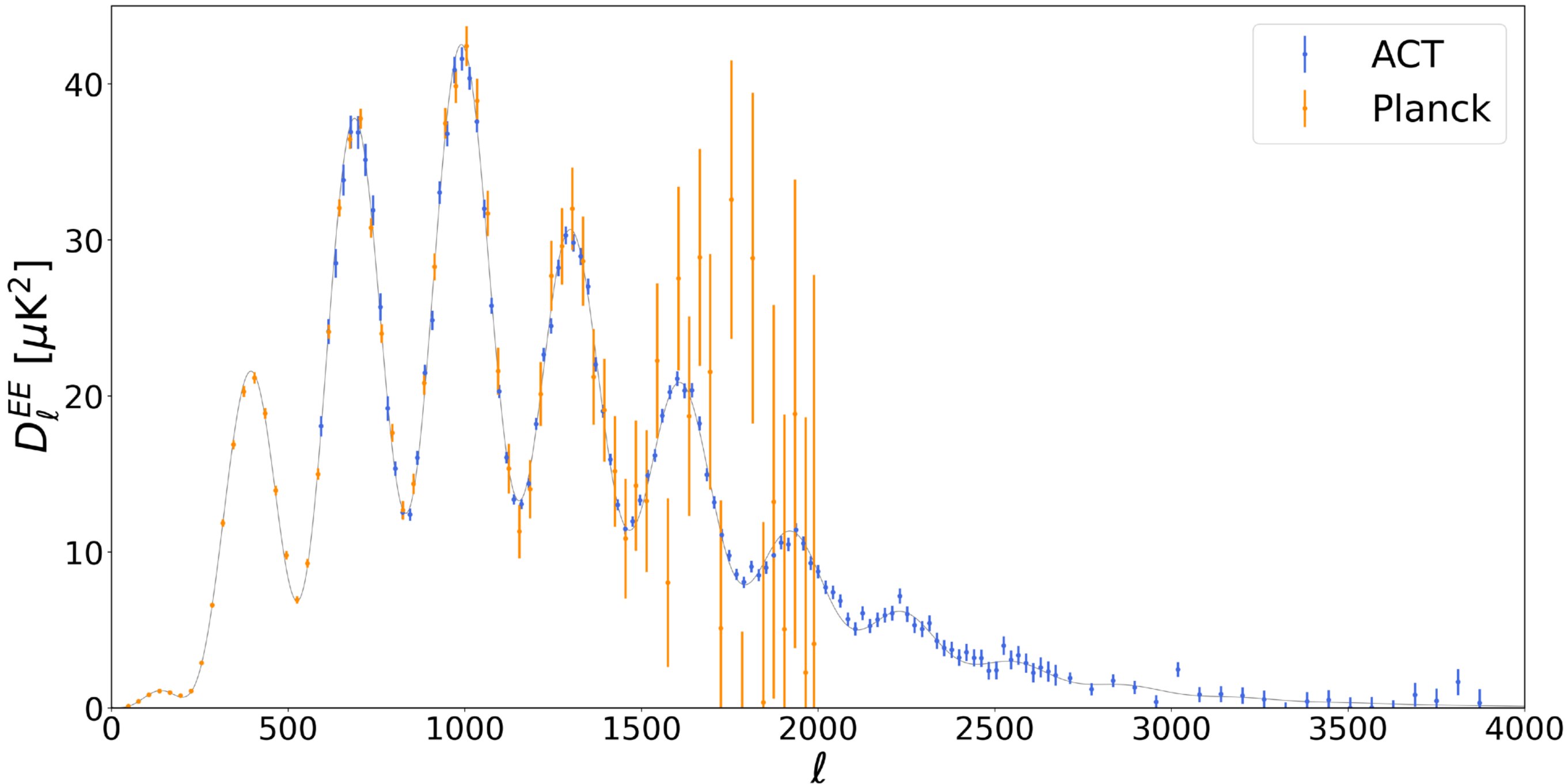
- ACT data

 - 1) extend Planck measurement to small angular scales.
 - 2) are very consistent with Planck data on overlapping angular scales.
 - 3) + Planck data are fitted by a common model

Planck E modes power spectra

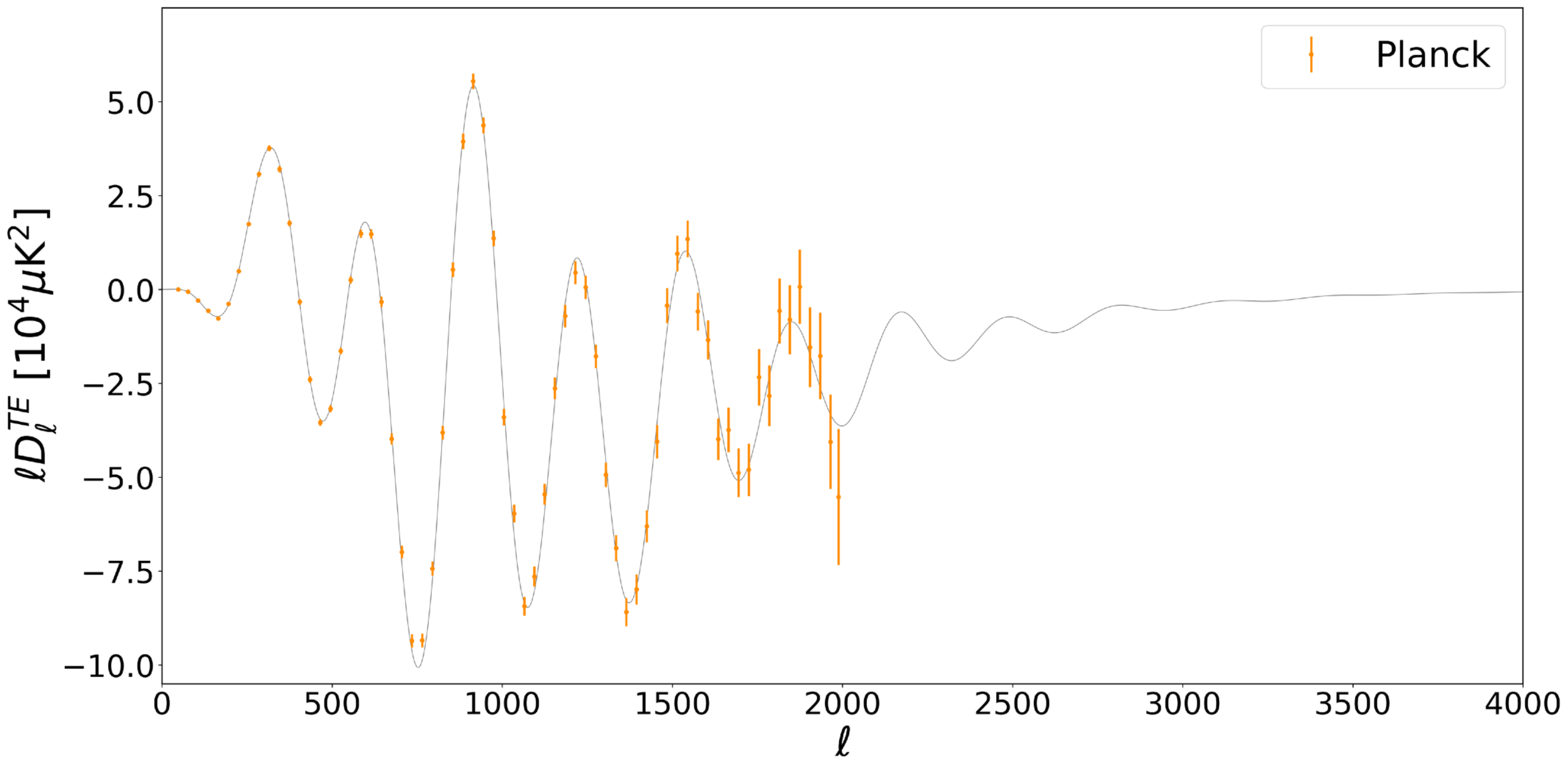


Planck + ACT E modes power spectra

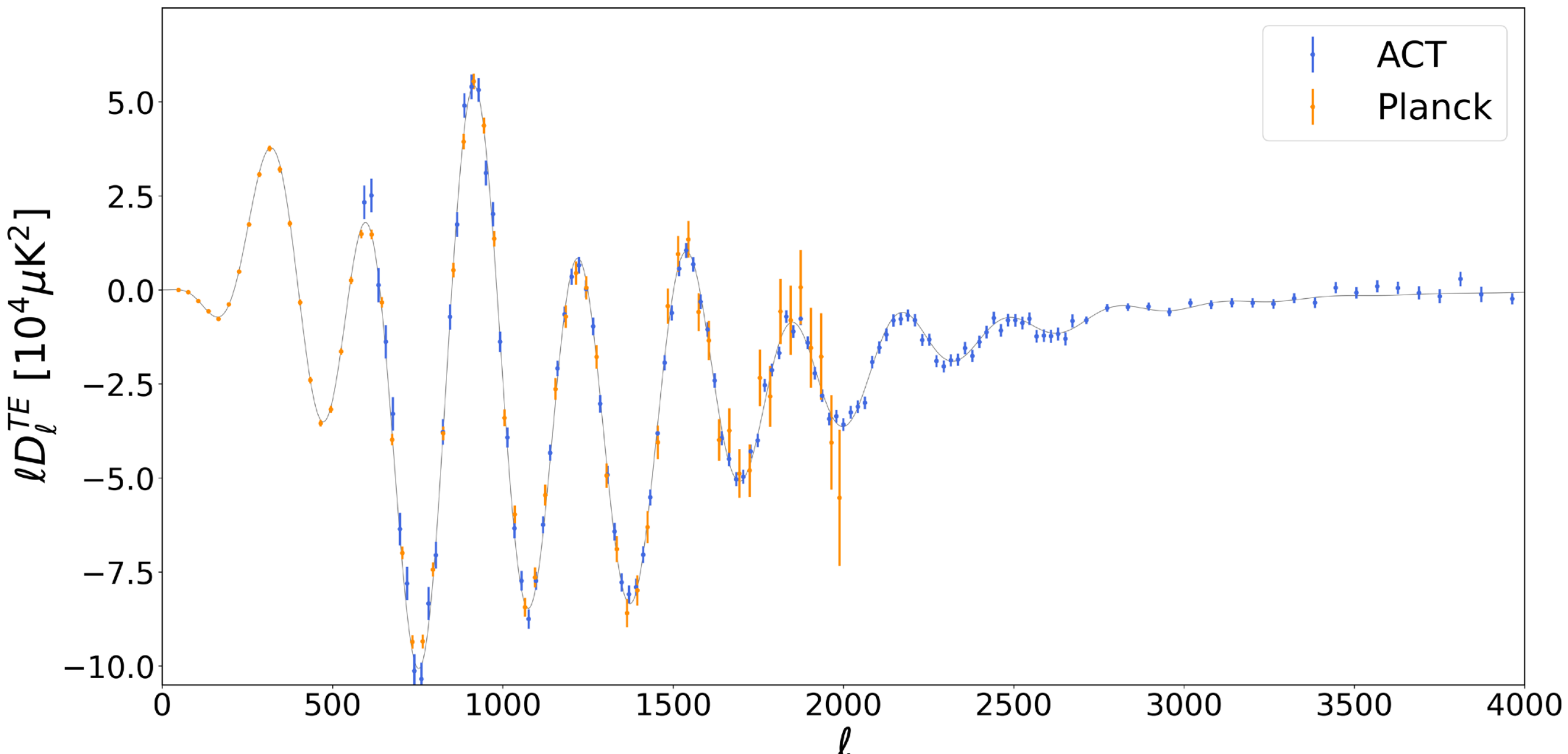


ACT DR6 EE is more sensitive than Planck for multipoles $\ell > 600$

Planck TE power spectrum



Planck + ACT TE power spectrum

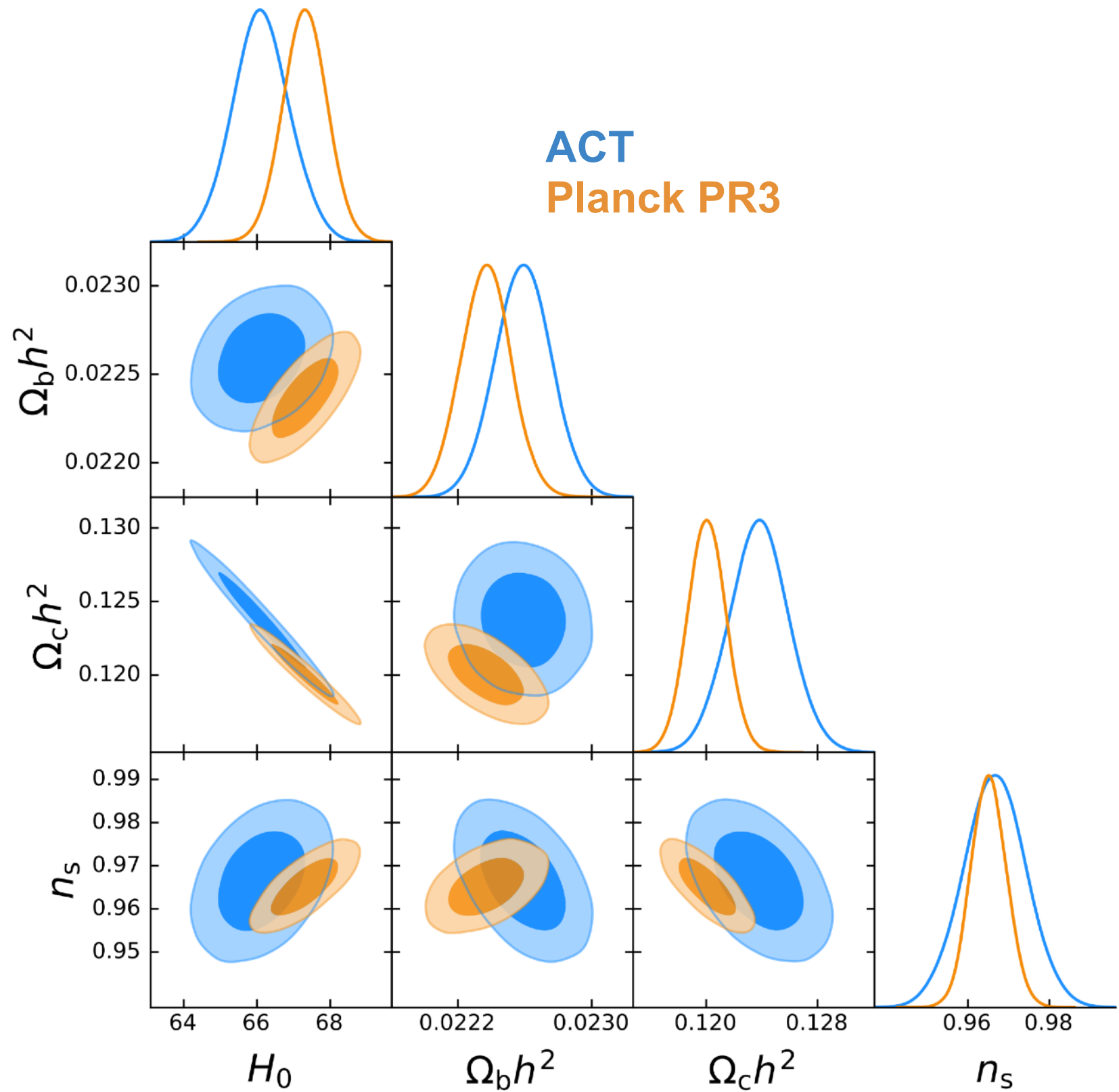


Very clean, foreground free cosmology,
1.1 % constraint on H₀ from TE alone

LCDM

Excellent agreement with Planck (PR3) in LCDM

ACT and Planck
are consistent at the
1.6 sigma level



LCDM provides an excellent fit to both Planck and ACT DR6

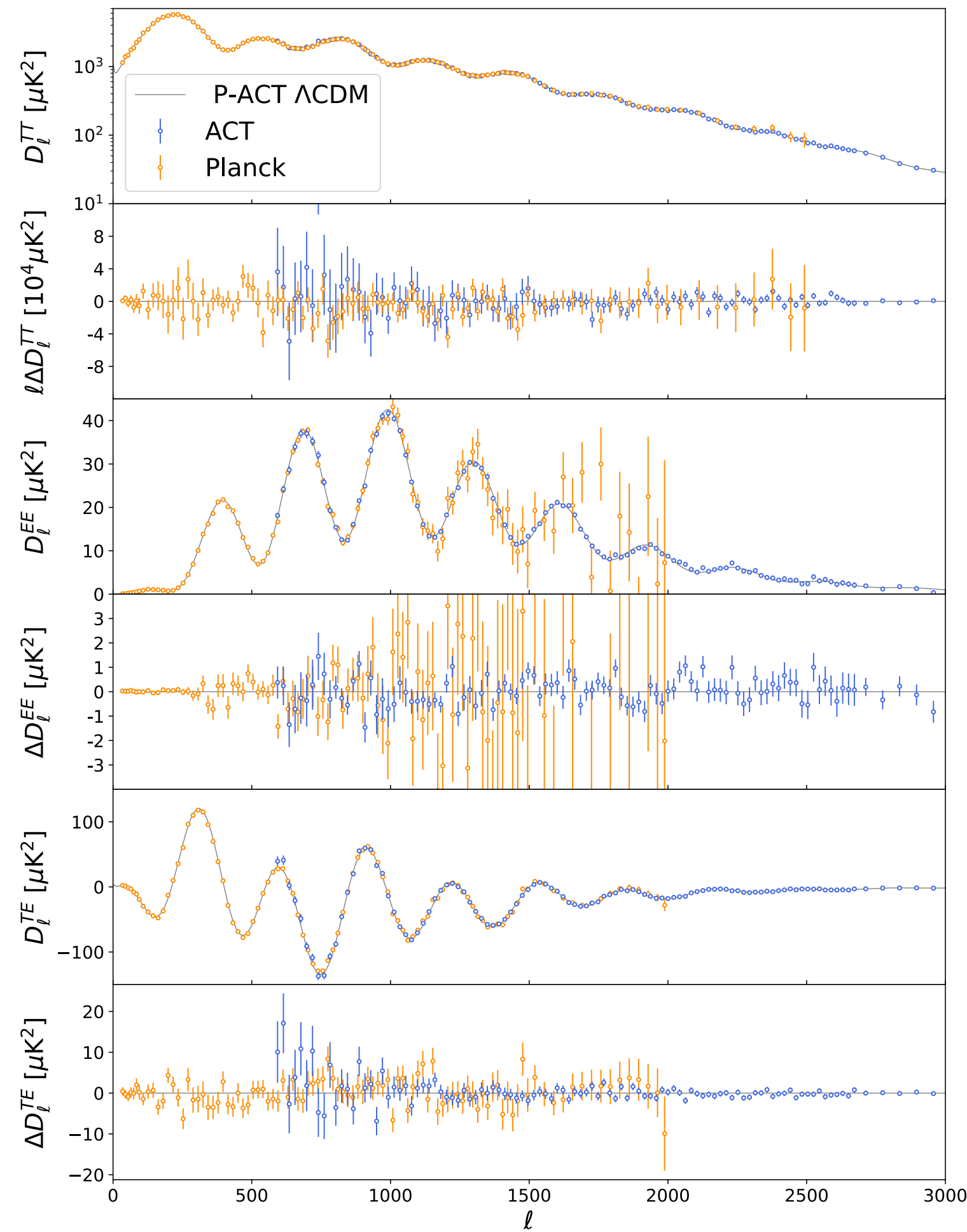
$$\chi^2(\text{ACT}) = 1598/1617 \text{ (63\%)}$$

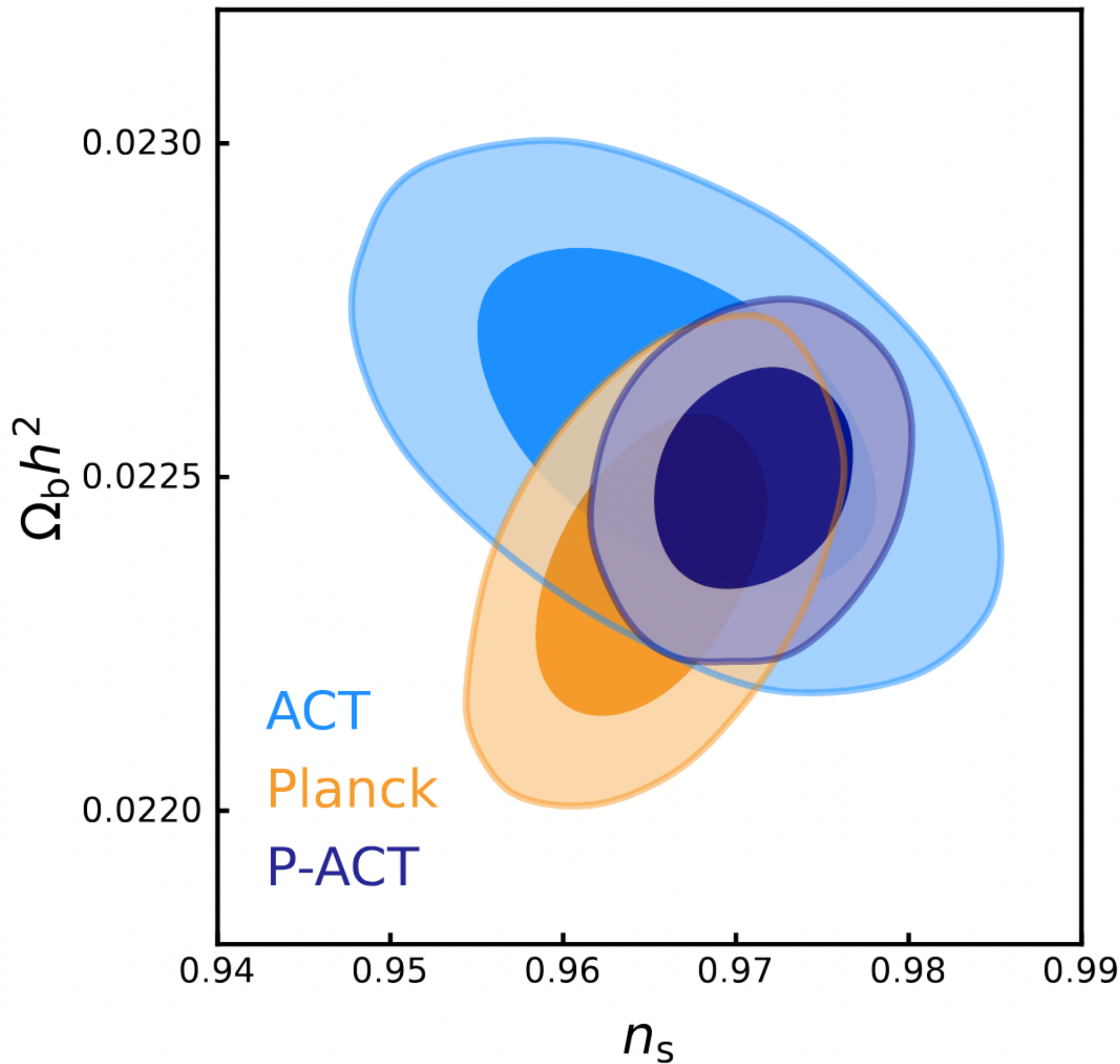
$$\chi^2(\text{P-ACT}) = 1842/1897 \text{ (81\%)}$$

This motivated the creation of a combined data set:

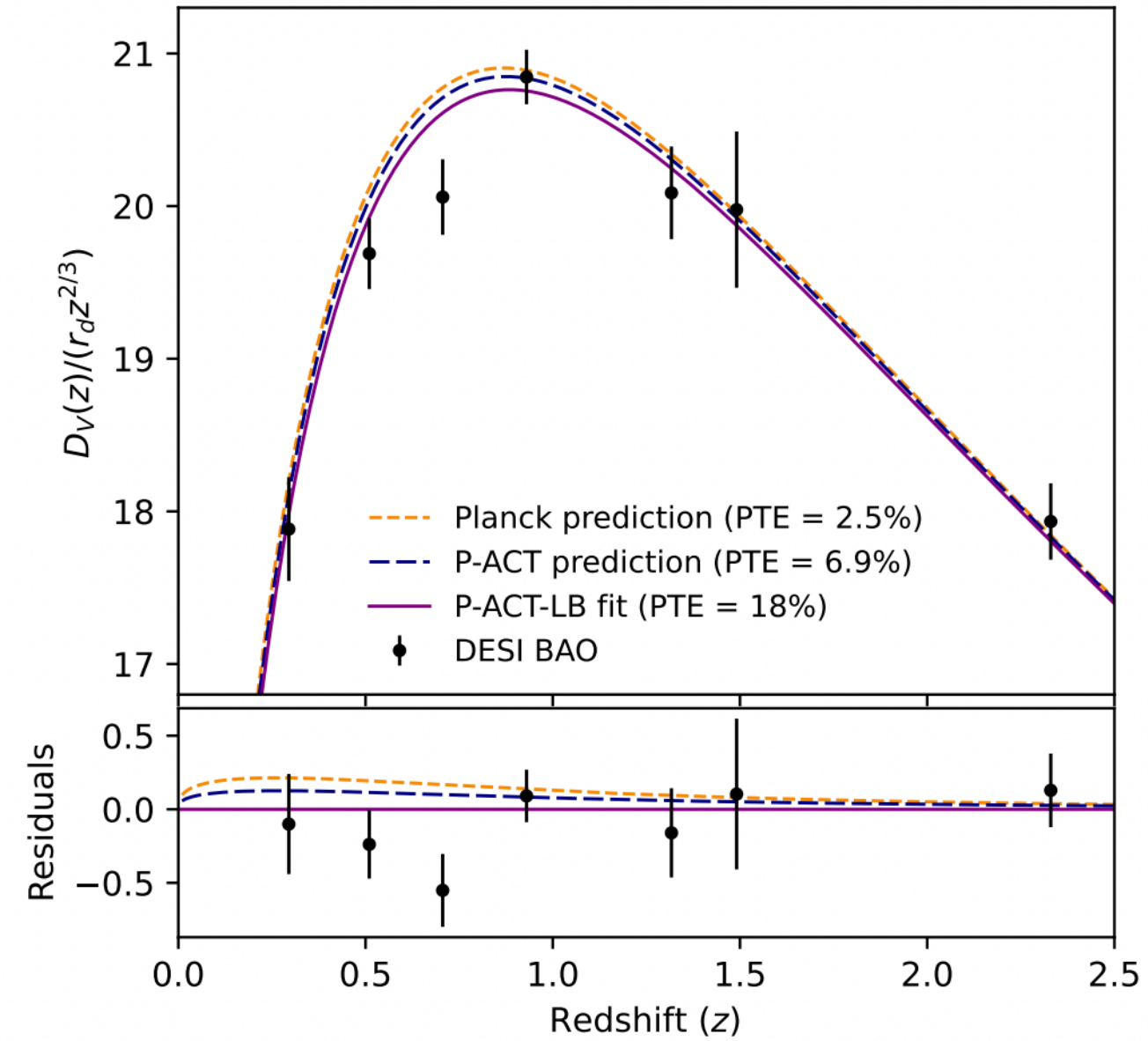
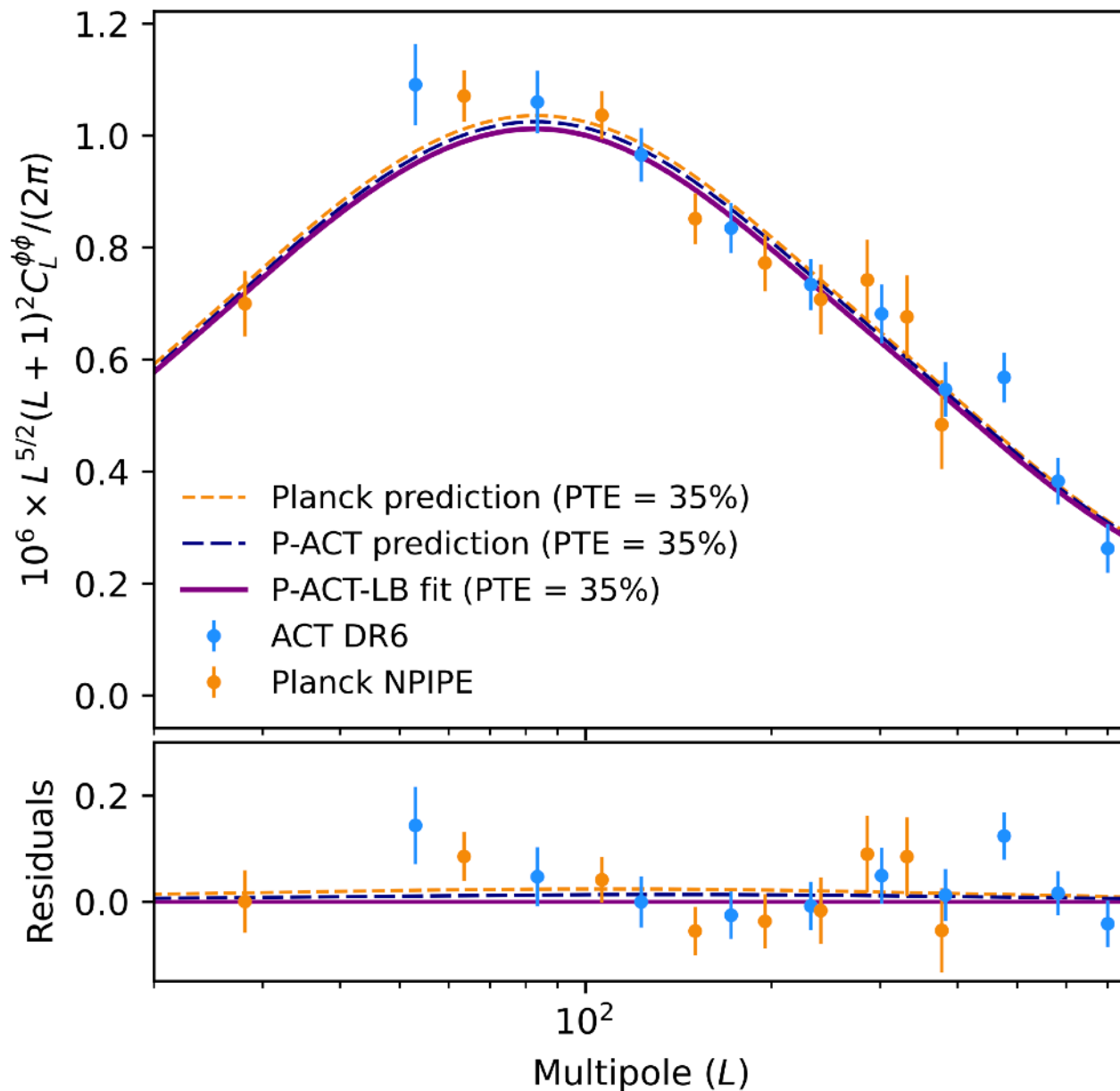
P-ACT = Planck + ACT

This data set leads to state of the art constraints On cosmological model





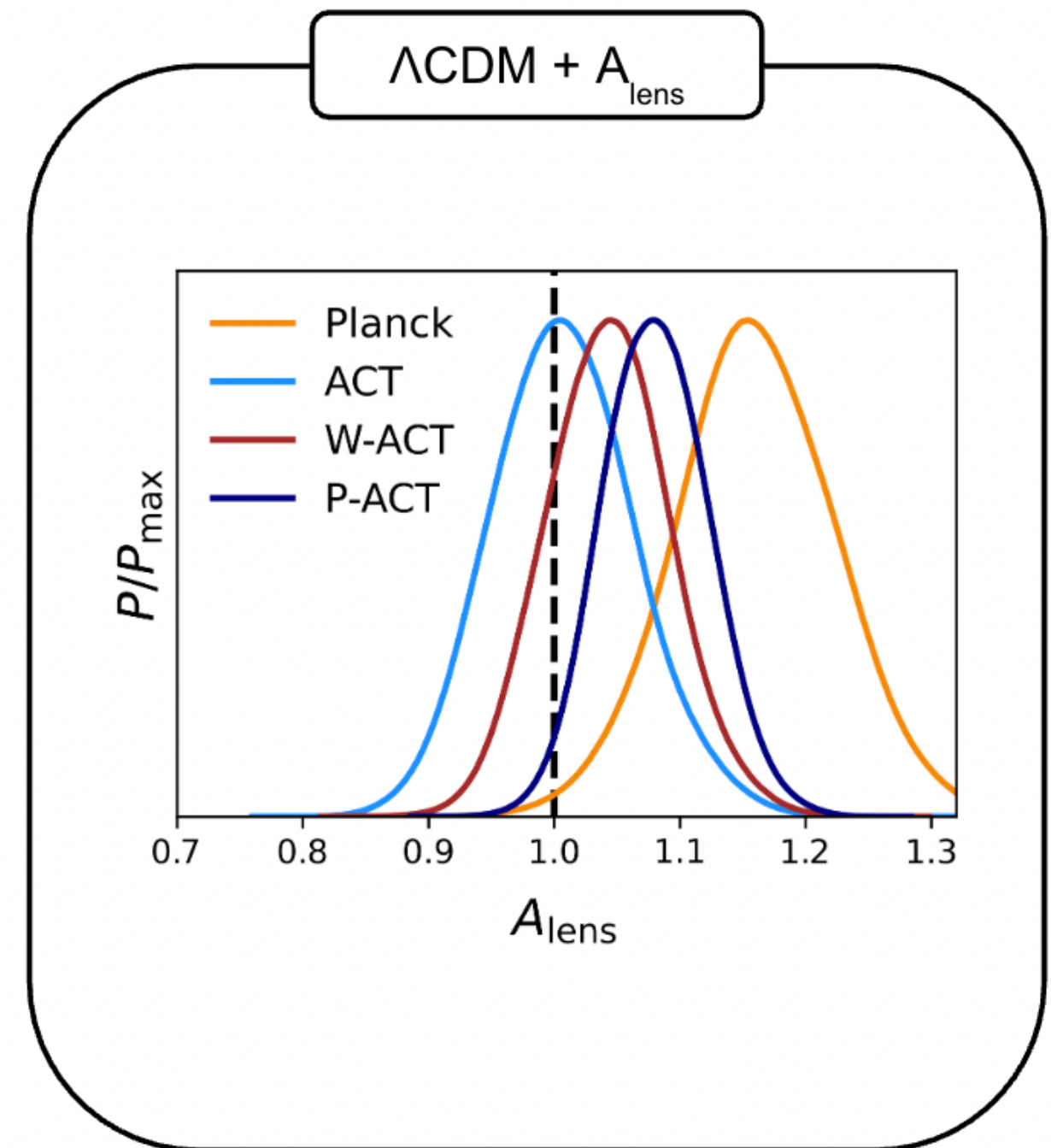
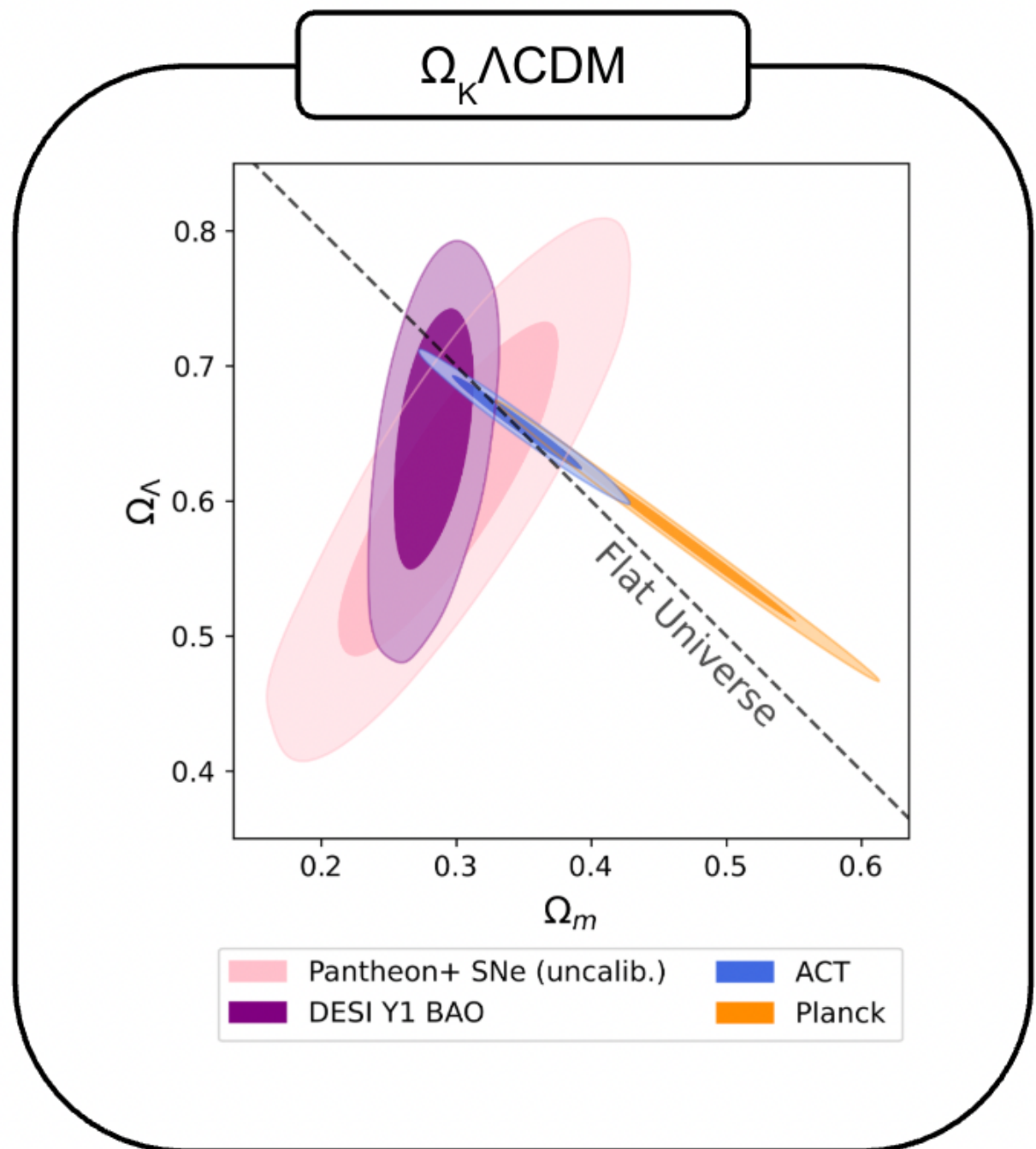
Λ CDM remains a robust model that can be extrapolated over 10 billion years and accurately predict observable at low redshift



P-ACT-LB = Planck + ACT + Lensing (ACT + Planck)
+ BAO from DESI Y1

Beyond LCDM

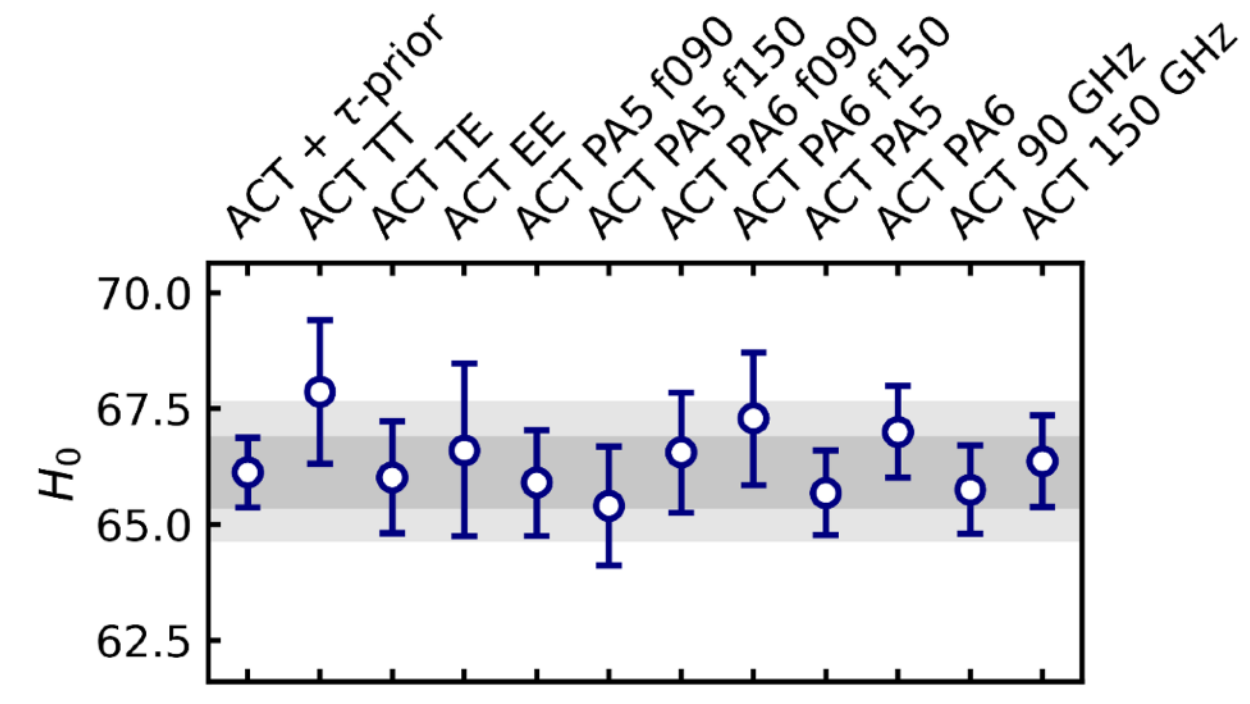
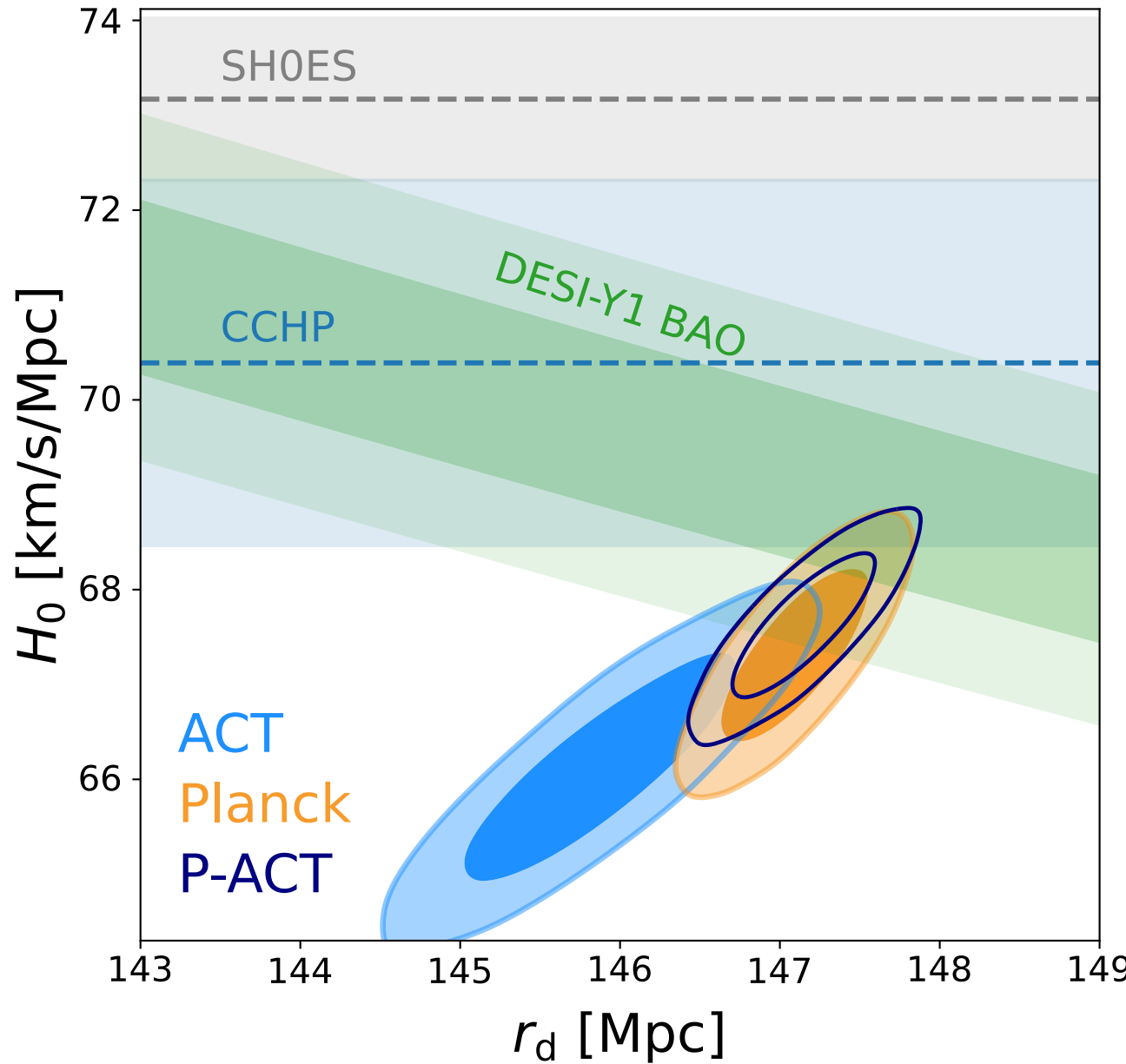
Unlike in Planck legacy result, we don't see evidence for curvature or higher than predicted lensing amplitude from CMB power spectra



The three possible solutions to the H₀ measurement problem

- 1) SH0ES constraint is affected by un-modelled systematics
(leading to artificial high H₀)
- 2) Planck measurement is affected by un-modelled systematics
(leading to artificial low H₀)
- 3) Need new physics beyond LCDM ?

An Hubble constant measurement nowhere near the SH0ES value



None of ACT probes
exceed $H_0 = 68$ km/s/Mpc

SH0ES: Breuval et al. 2024, Riess et al. 2022 (Cepheids)

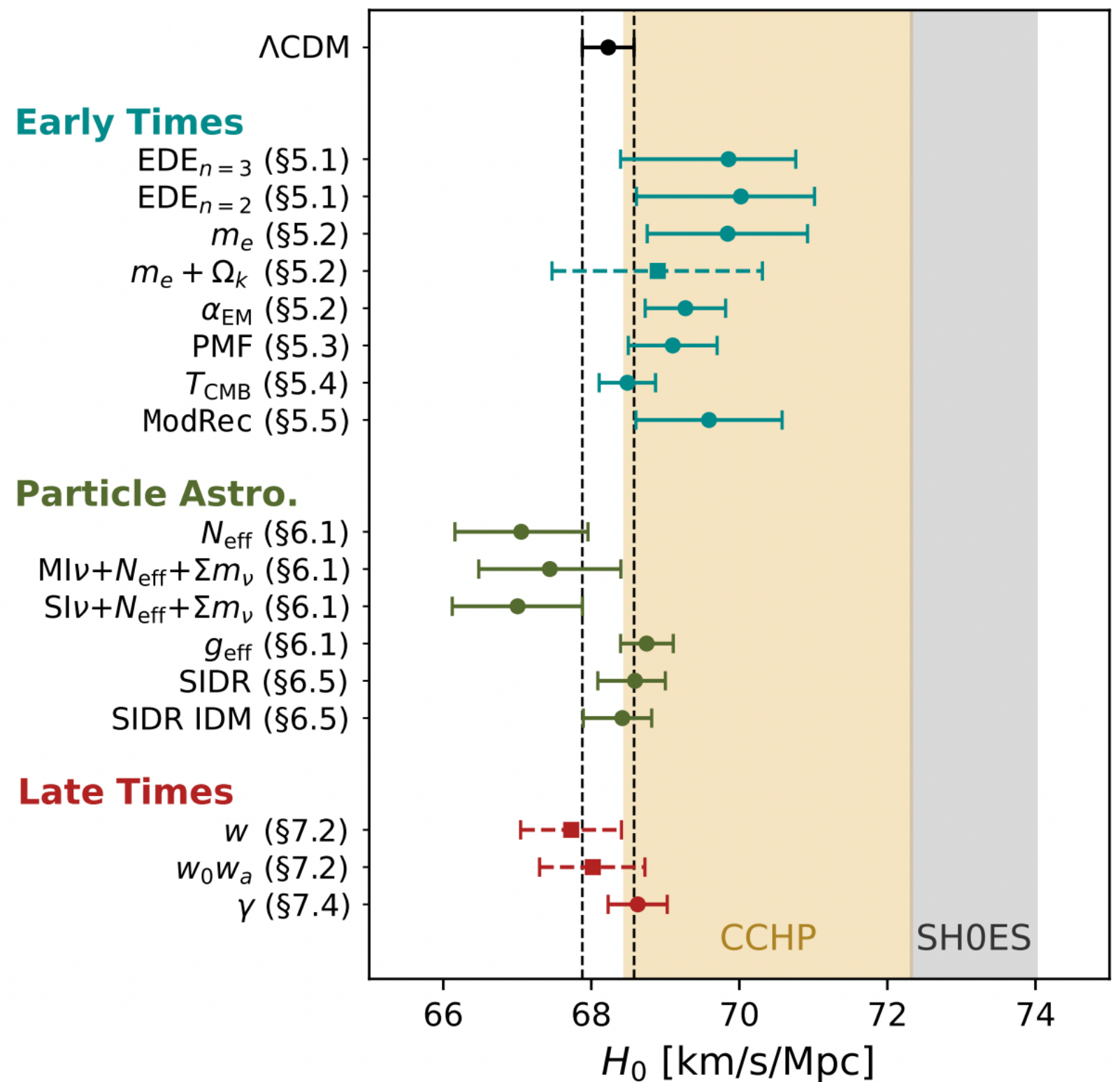
CCHP : Chicago–Carnegie Hubble Program : Freedman et al. 2024 (Tip of the Red Giant Branch and J-Region Asymptotic Giant Branch)

The three possible solutions to the H0 problem

- 1) SH0ES constraint is affected by un-modelled systematics
(leading to artificial high H0)
- 2) ~~Planck measurement is affected by un modelled systematics~~
~~(leading to artificial low H0)~~
- 3) Need new physics beyond LCDM ?

$$66.1 < H_0 < 71.0 \text{ km/s/Mpc}$$

We tested a large class of extensions,
None of them are preferred over Λ CDM.



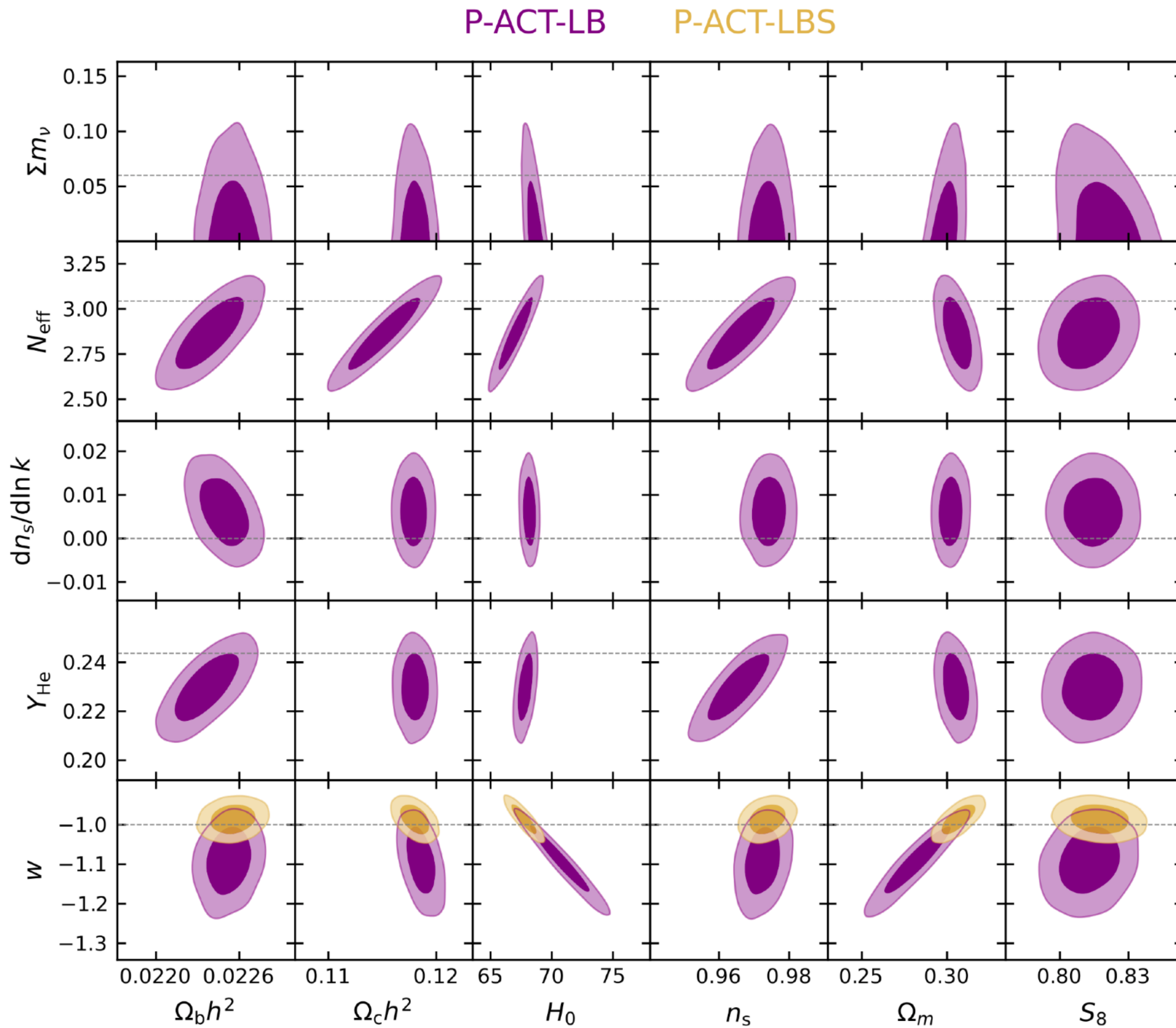
Solid (dashed) bars are constraints at 68% confidence derived from P-ACT-LB (P-ACT-LBS).

The three possible solutions to the H₀ problem

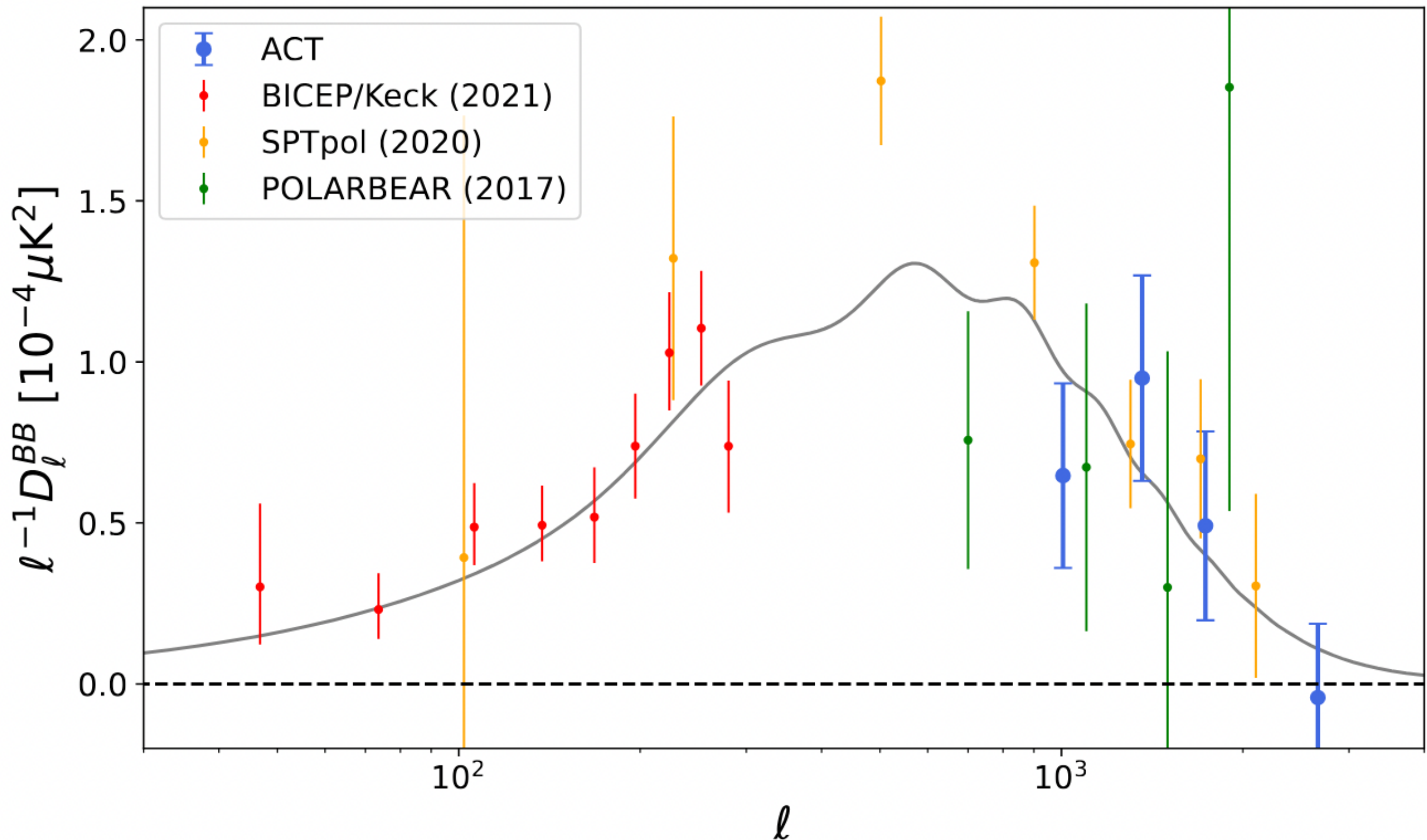
- 1) SH0ES constraint is affected by un-modelled systematics
(leading to artificial high H₀)
- 2) Planck measurement is affected by un-modelled systematics
(leading to artificial low H₀)
- 3) Need new physics beyond LCDM ?

Hard to cross definitely, but P-ACT poses a challenge to the proposed models

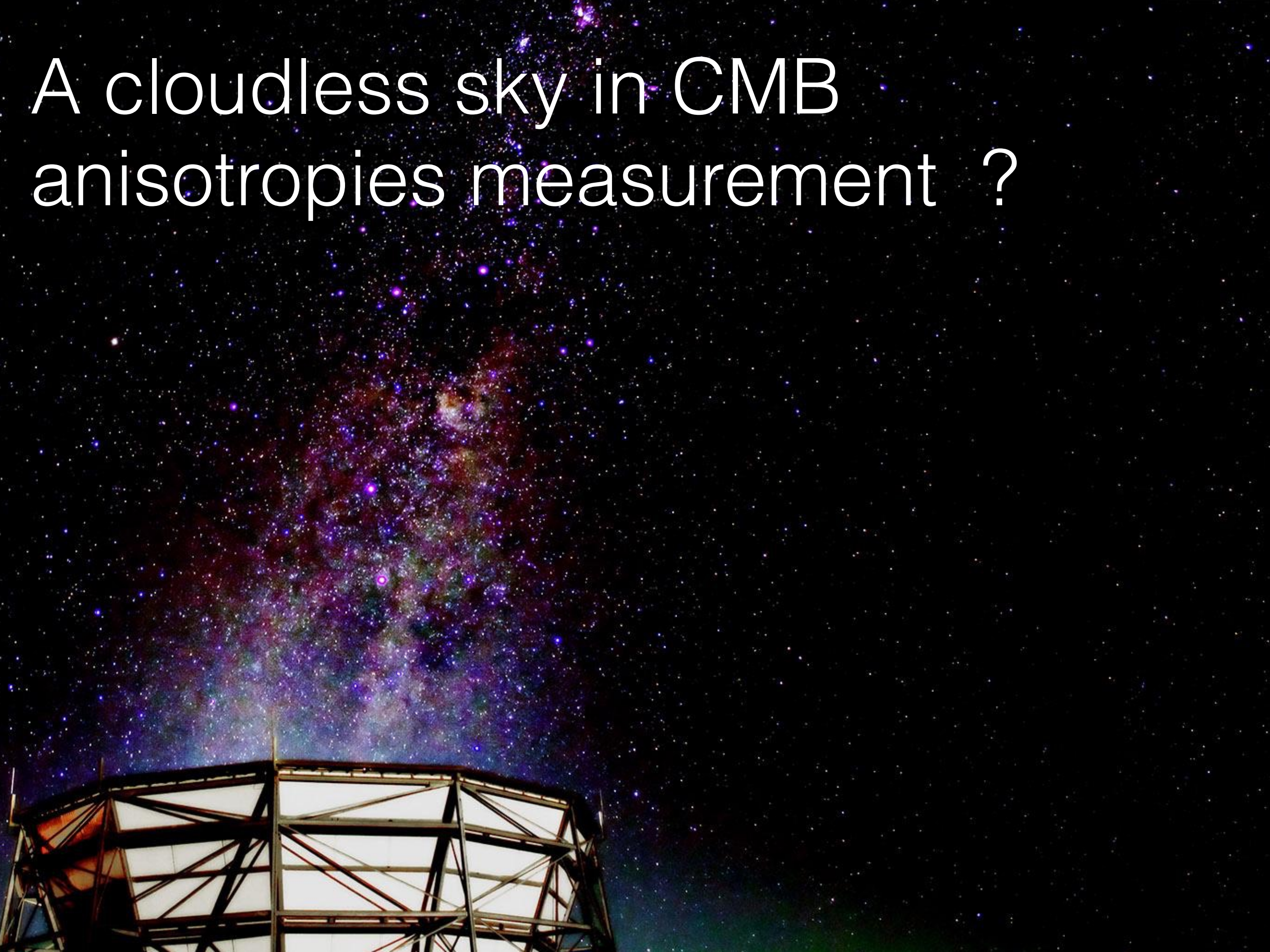
Exploration of others cosmological models



What about B modes ?

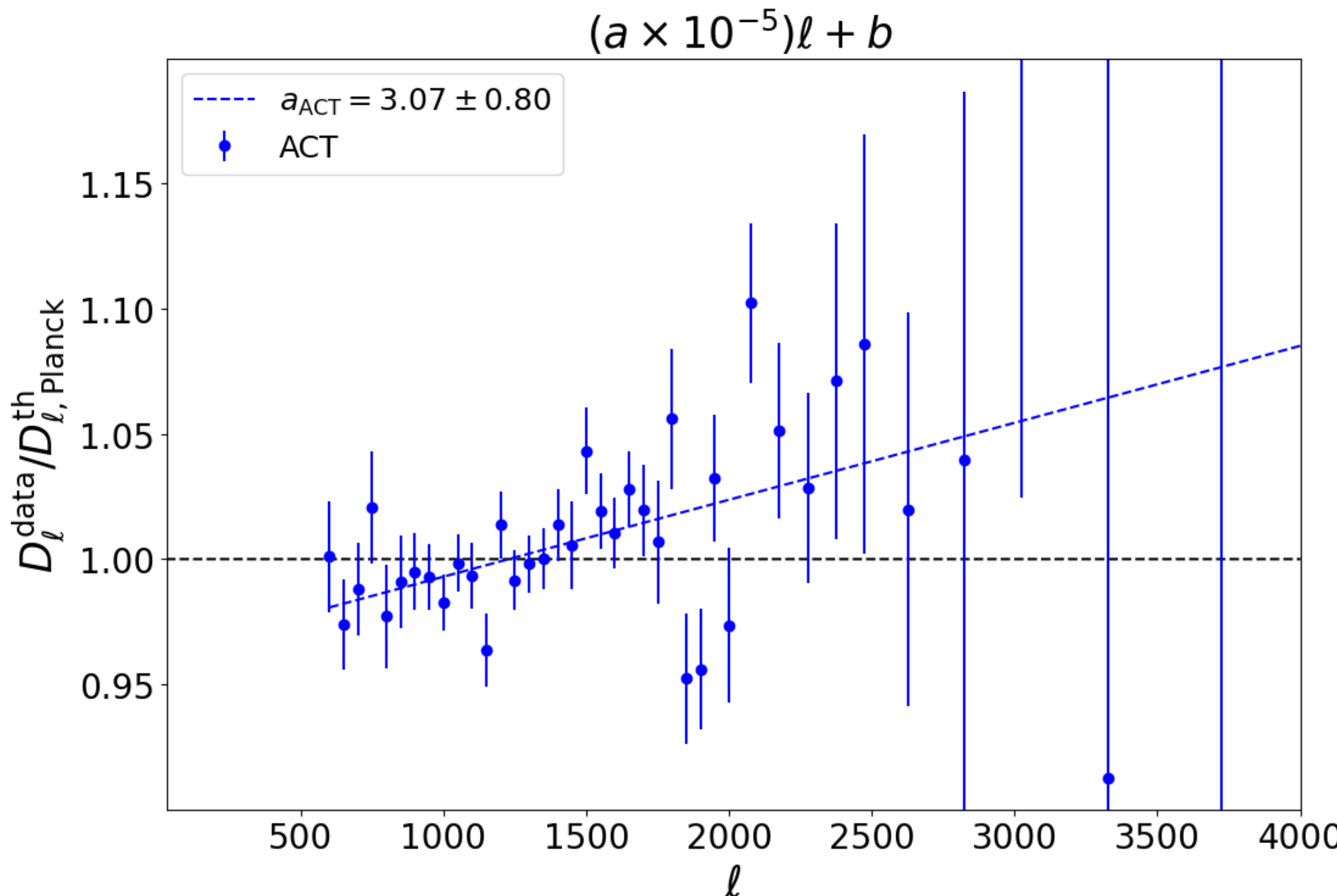


A cloudless sky in CMB
anisotropies measurement ?

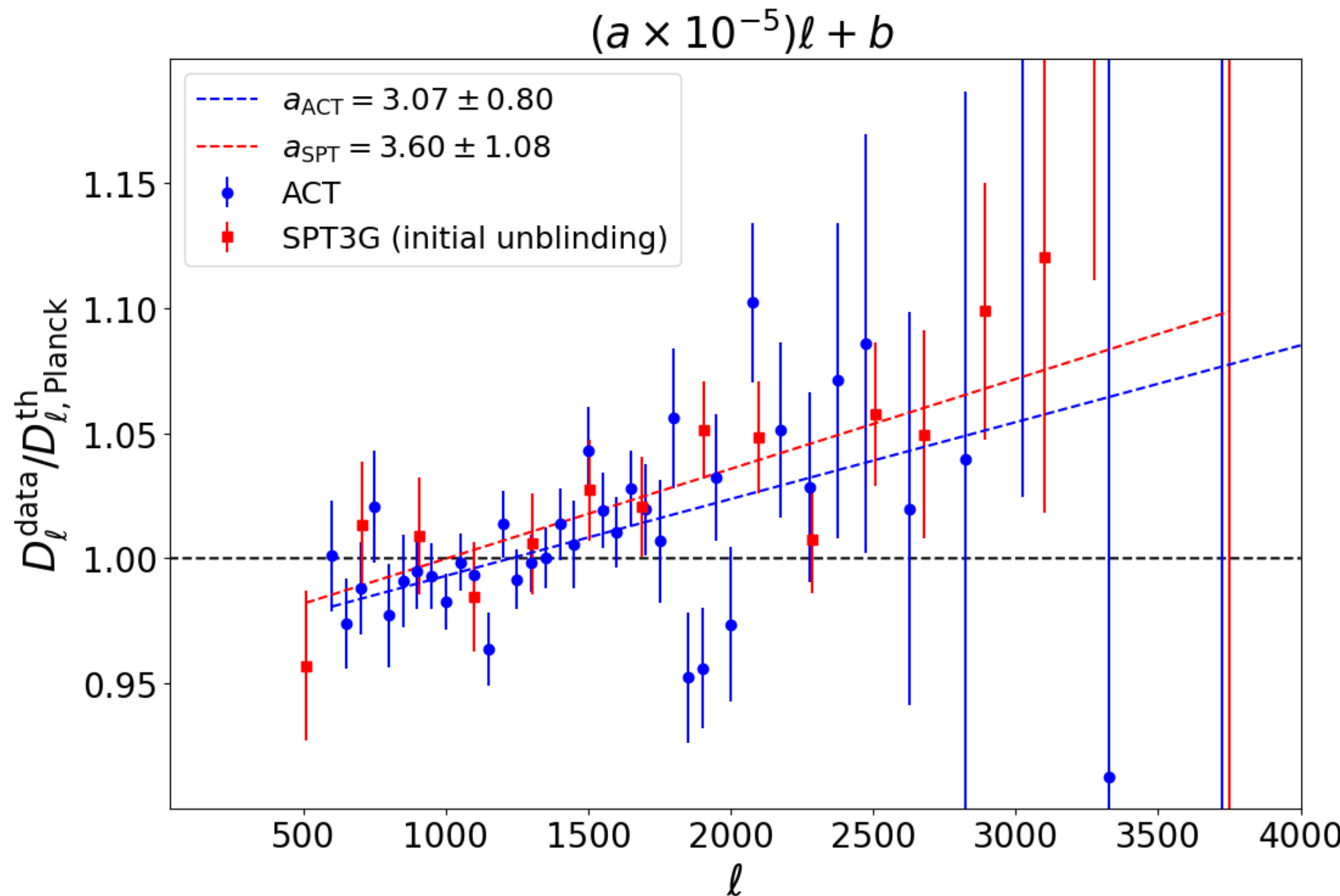


An interesting shape in EE ?

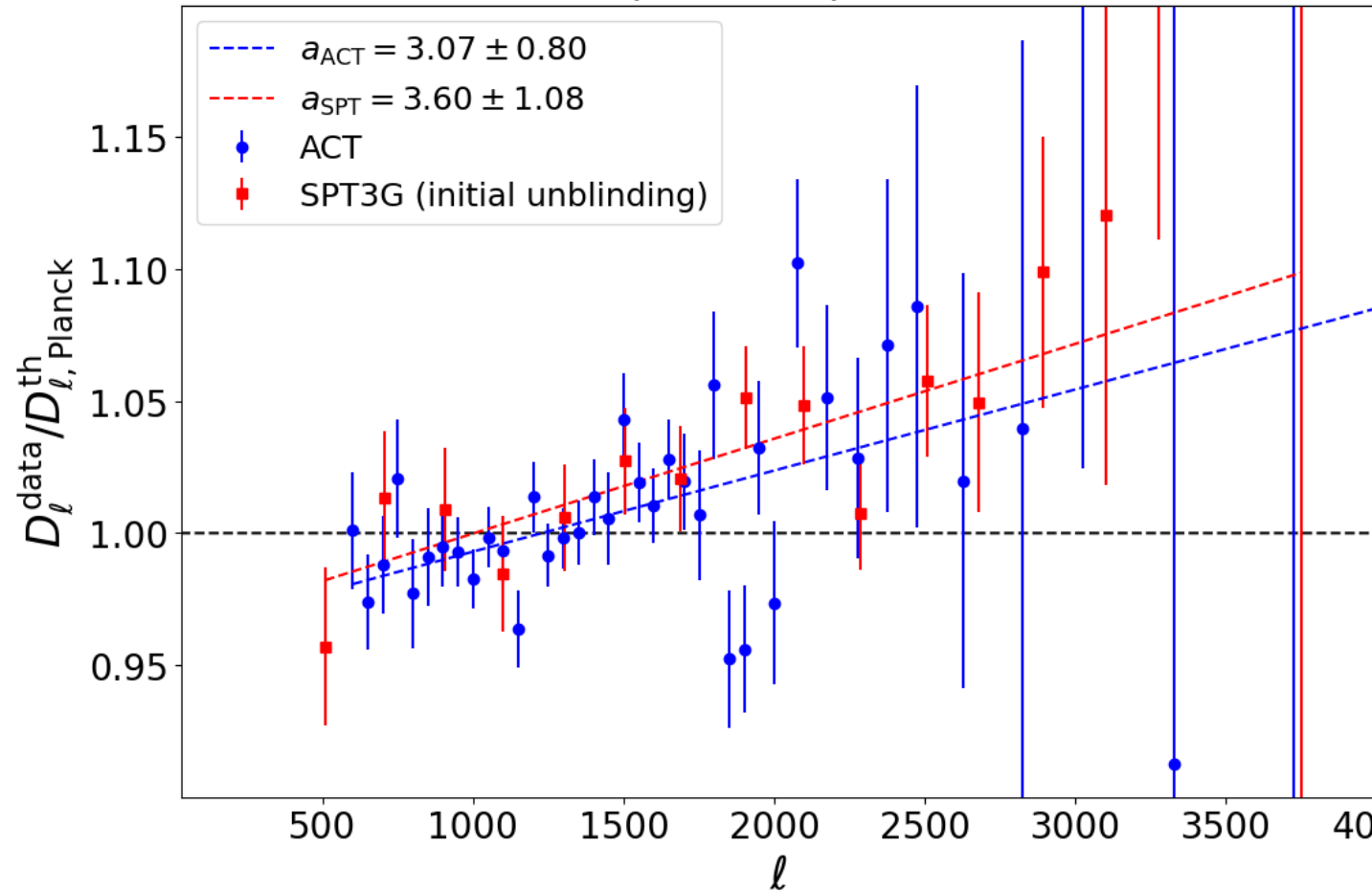
If we compare ACT EE measurement with the expectation from Planck cosmological model, we find a hint of a slope. This slope in ACT is not significative once we propagate Planck uncertainties (our EE cosmology agree with Planck at the 2.3 sigma level).



Very interestingly, SPT was finding a very similar slope in their initial unblinding data. If we were to combine both data set, the slope surely would become significative !

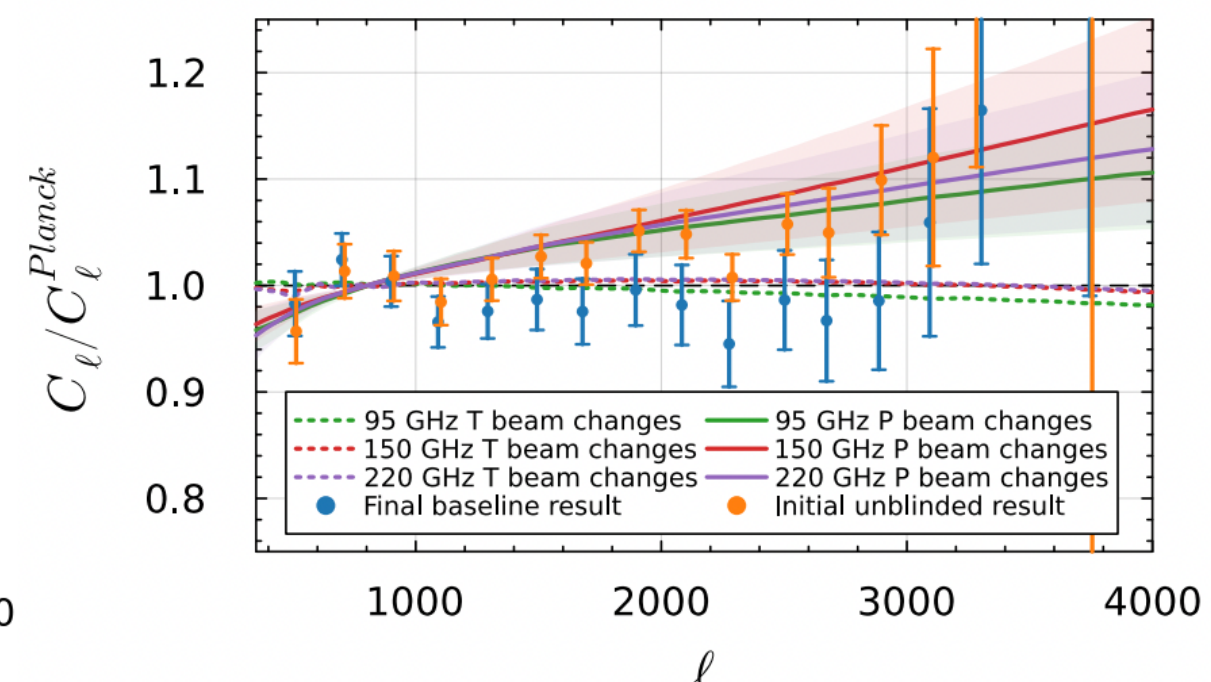


$$(a \times 10^{-5})\ell + b$$



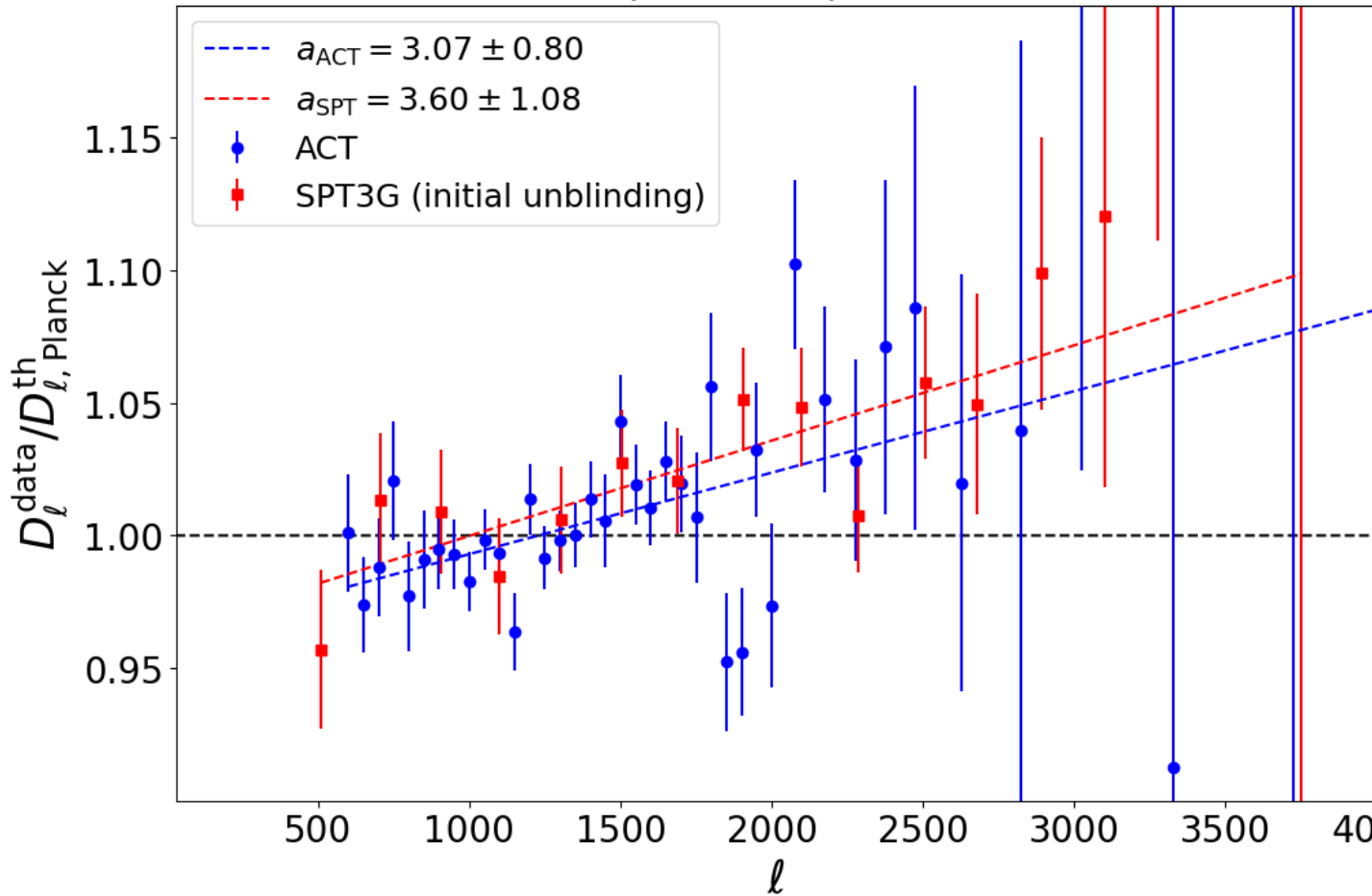
SPT3G: arXiv:2411.06000

EE

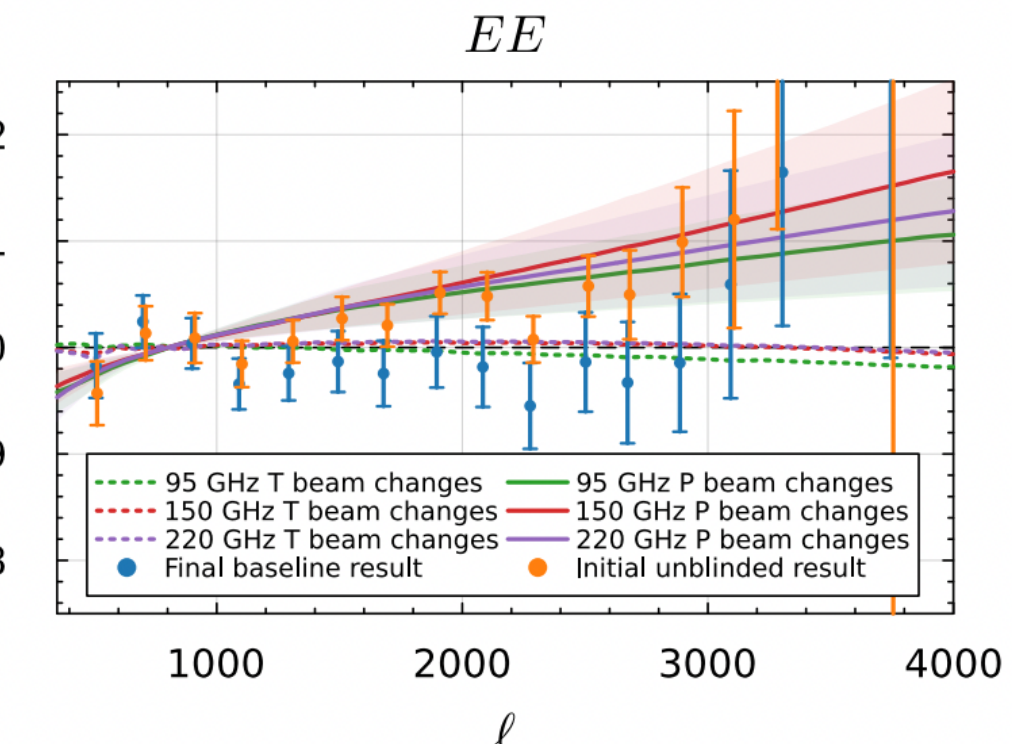


However, SPT, after unblinding their data, and motivated by the mismatch with Planck preferred cosmology, attributed this slope to a mismatch between their beam in temperature and polarisation and included extra parameters to correct for it.

$$(a \times 10^{-5})\ell + b$$



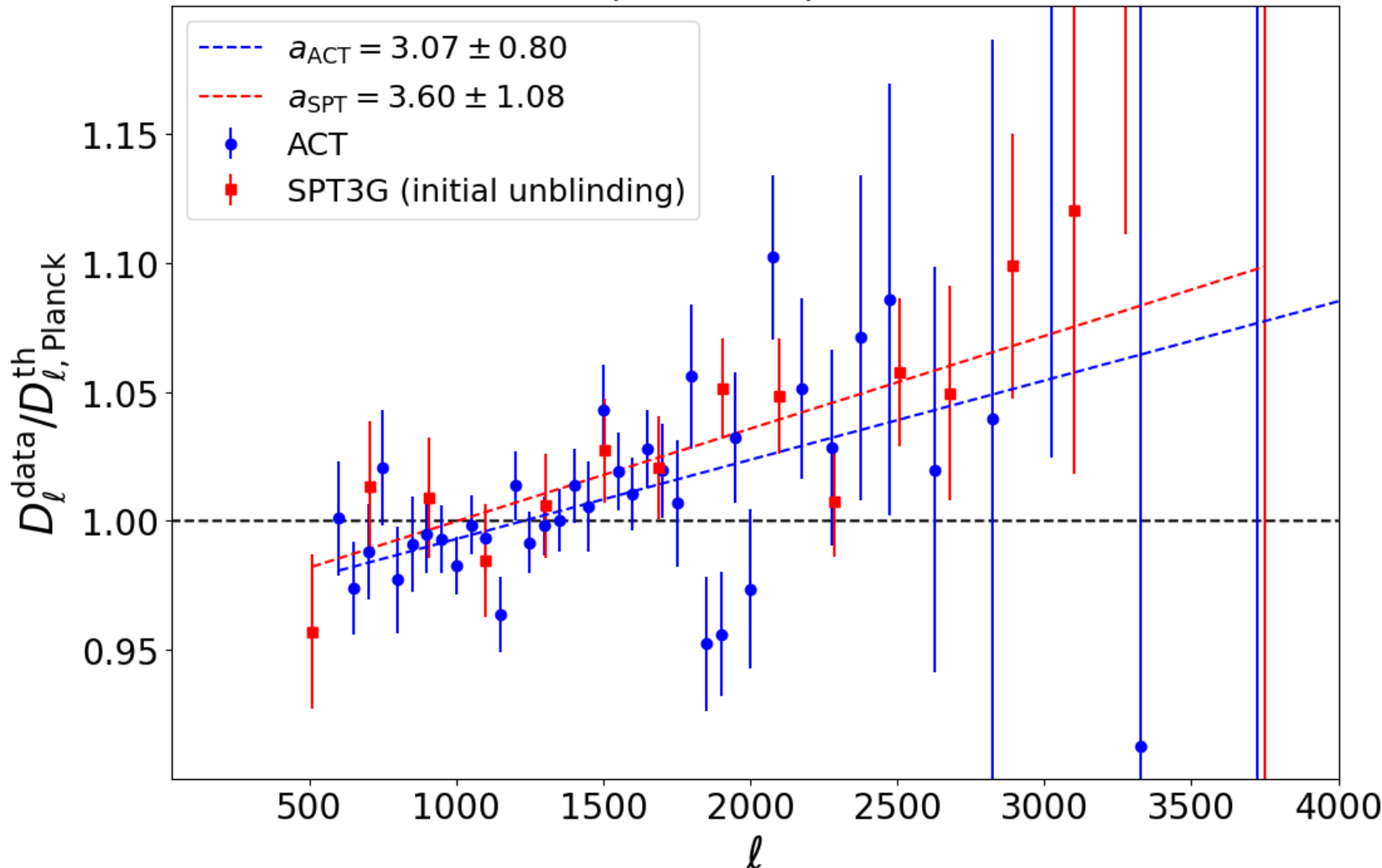
SPT3G: arXiv:2411.06000



To my current knowledge and based on public material,
 SPT do not have strong **model-independent** evidence supporting
 The claim that their polarisation and temperature beam disagree.

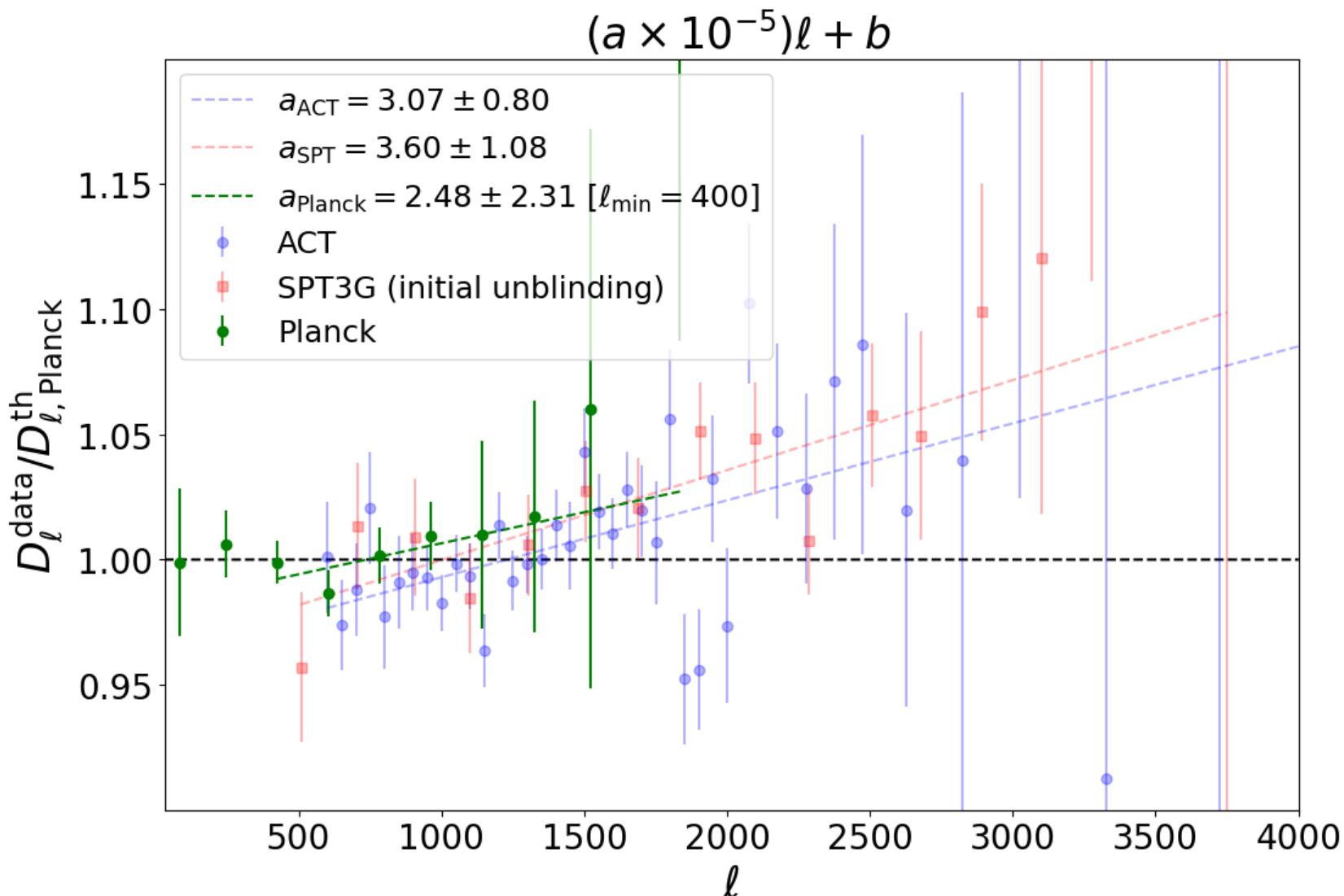
The mismatch between temperature and polarisation beam is attributed to depolarization of their beam side-lobes, **as far as I know** no physical model for this phenomenon has been demonstrated by the collaboration.

$$(a \times 10^{-5})\ell + b$$



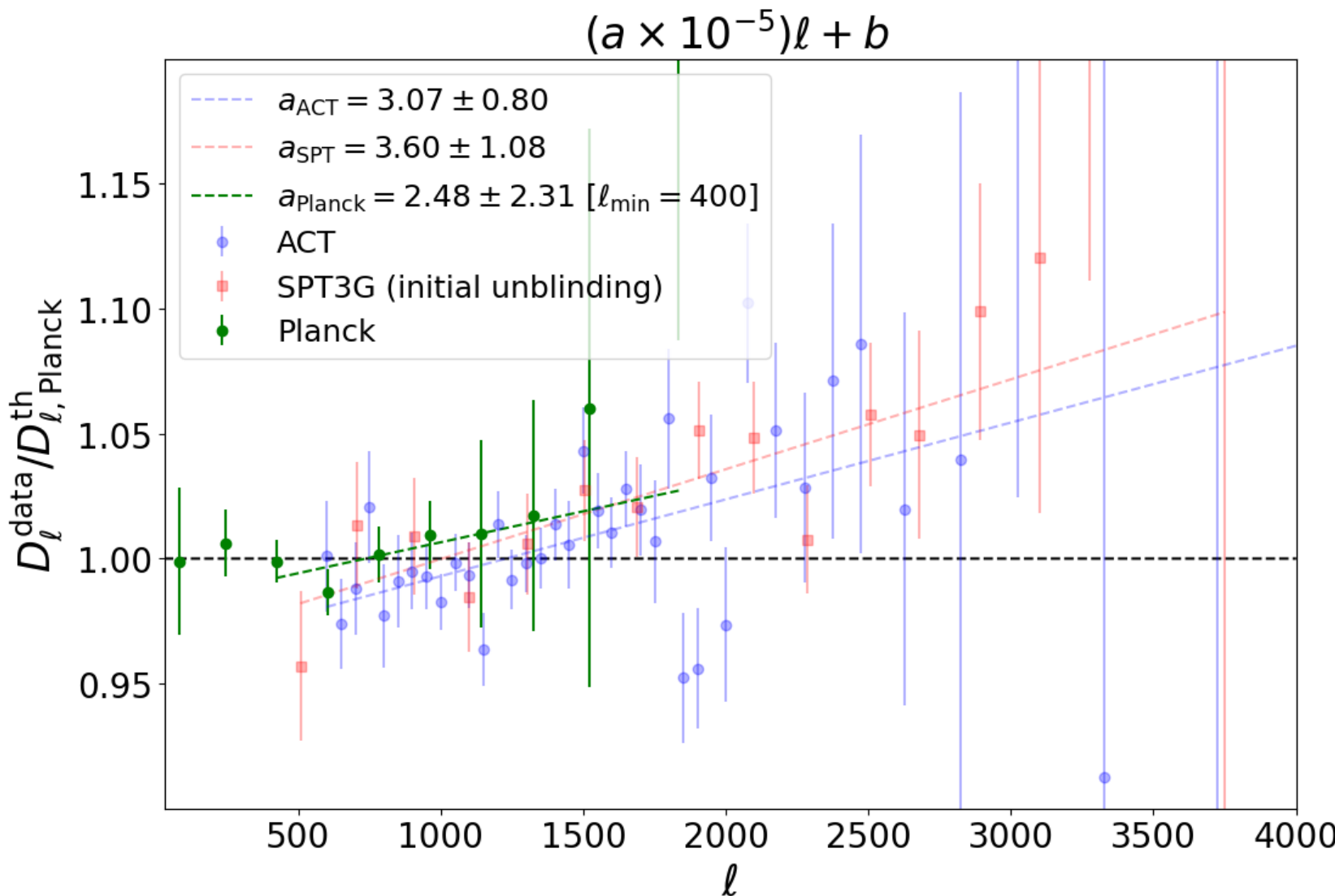
What are the options here ?:

- 1) SPT results were indeed affected by systematic.
- 2) SPT was seeing a small departure from Planck preferred cosmology in their high ell EE power spectra (that Planck couldn't measure !).



What are the options here ?:

- 1) SPT results were indeed affected by systematic.
- 2) SPT was seeing a small departure from Planck preferred cosmology in their high ell EE power spectra (that Planck couldn't measure !).



What are the options here ?:

- 1) SPT results were indeed affected by systematic.
- 2) SPT was seeing a small departure from Planck preferred cosmology in their high ell EE power spectra (that Planck couldn't measure !).

The prediction from Option 2 was that ACT would see it and this was the outcome. Option 1 is still possible but now requires a common systematic present in the two independent experiments.

Puzzles for the systematic interpretation

- > Both ACT and SPT sees it
- > ACT and SPT don't see evidence for variation with frequency.
- > ACT and SPT don't see evidence for it to vary as a function of the group of detectors they consider.

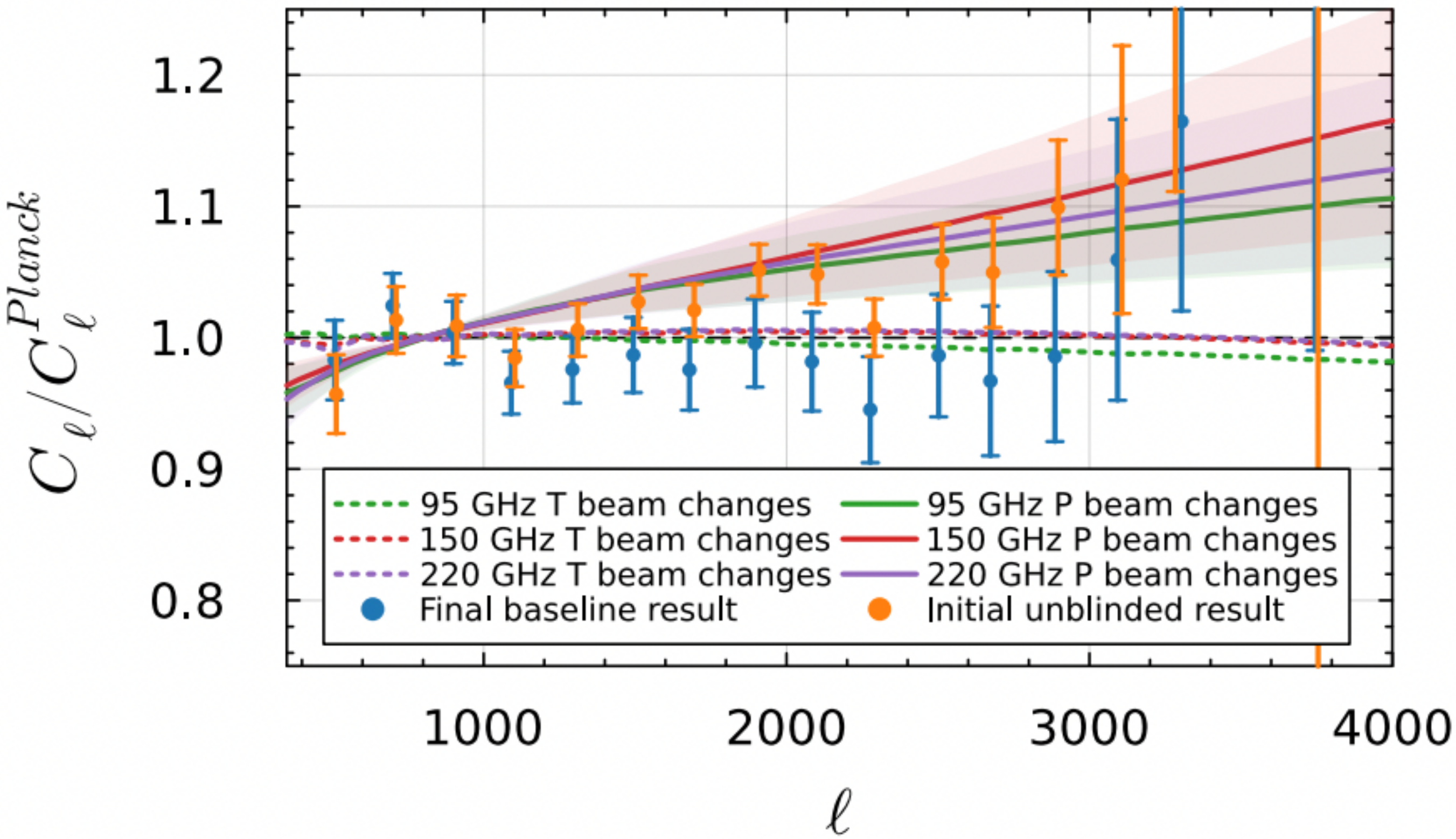
Best would be to prove the effect on polarized sources.

But, are they bright enough to measure SPT beam side-lobes ?

Other option would be to identify the physical driver for the side-lobes
And show from physical modeling that the degree of de-polarization is realistic (and that achromaticity is expected) ?

Puzzles for the sky signal interpretation

- > not sure there is any ?

EE 

Puzzles for the systematic interpretation

- > Both ACT and SPT sees it
- > ACT and SPT don't see evidence for variation with frequency.
- > ACT and SPT don't see evidence for it to vary as a function of the group of detectors they consider.

Best would be to prove the effect on polarized sources.

But, are they bright enough to measure SPT beam side-lobes ?

Other option would be to identify the physical driver for the side-lobes
And show from physical modeling that the degree of de-polarization is realistic (and that achromaticity is expected) ?

Puzzles for the sky signal interpretation

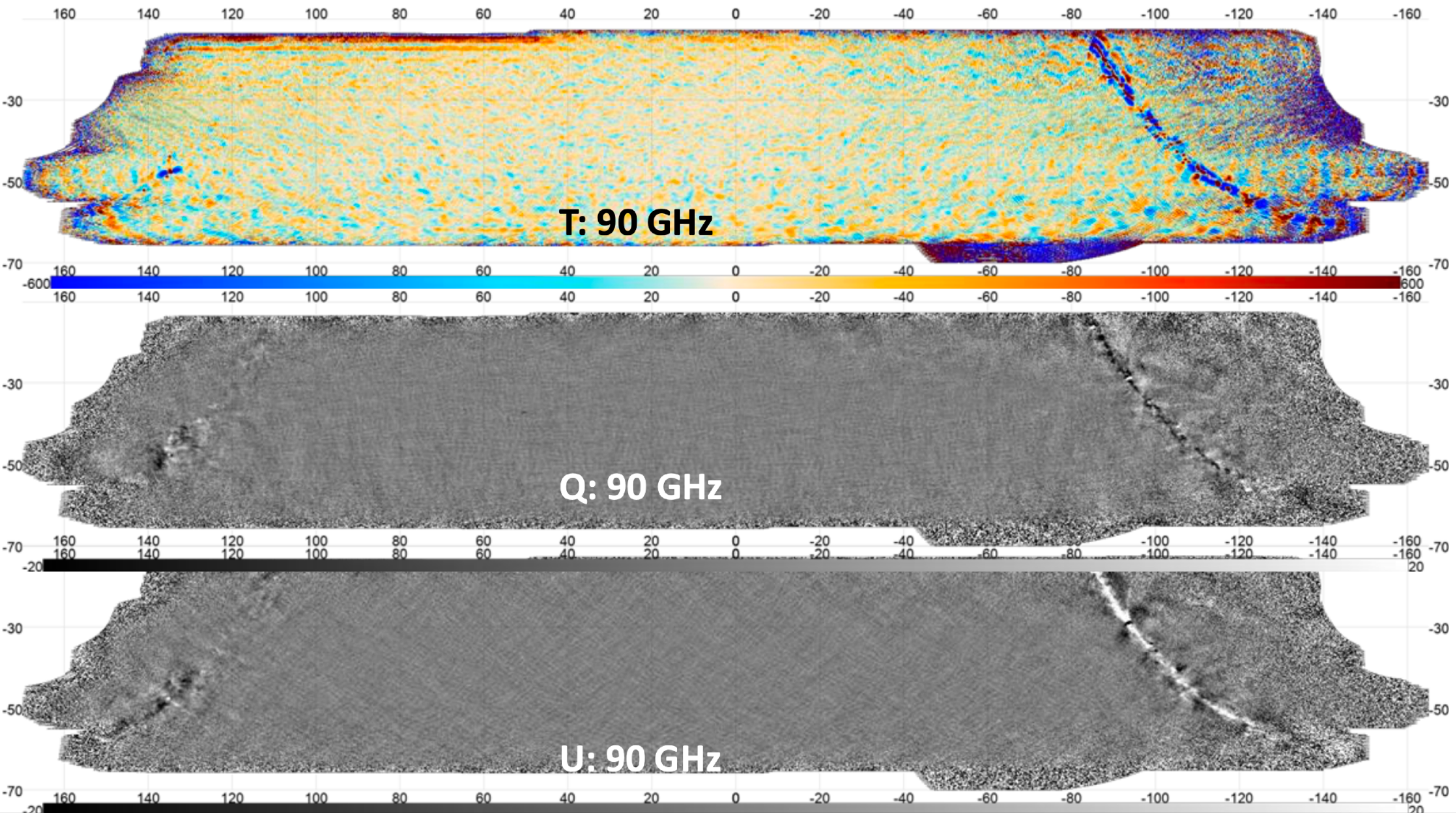
- > not sure there is any ?

A bright future for CMB observation from the Atacama desert

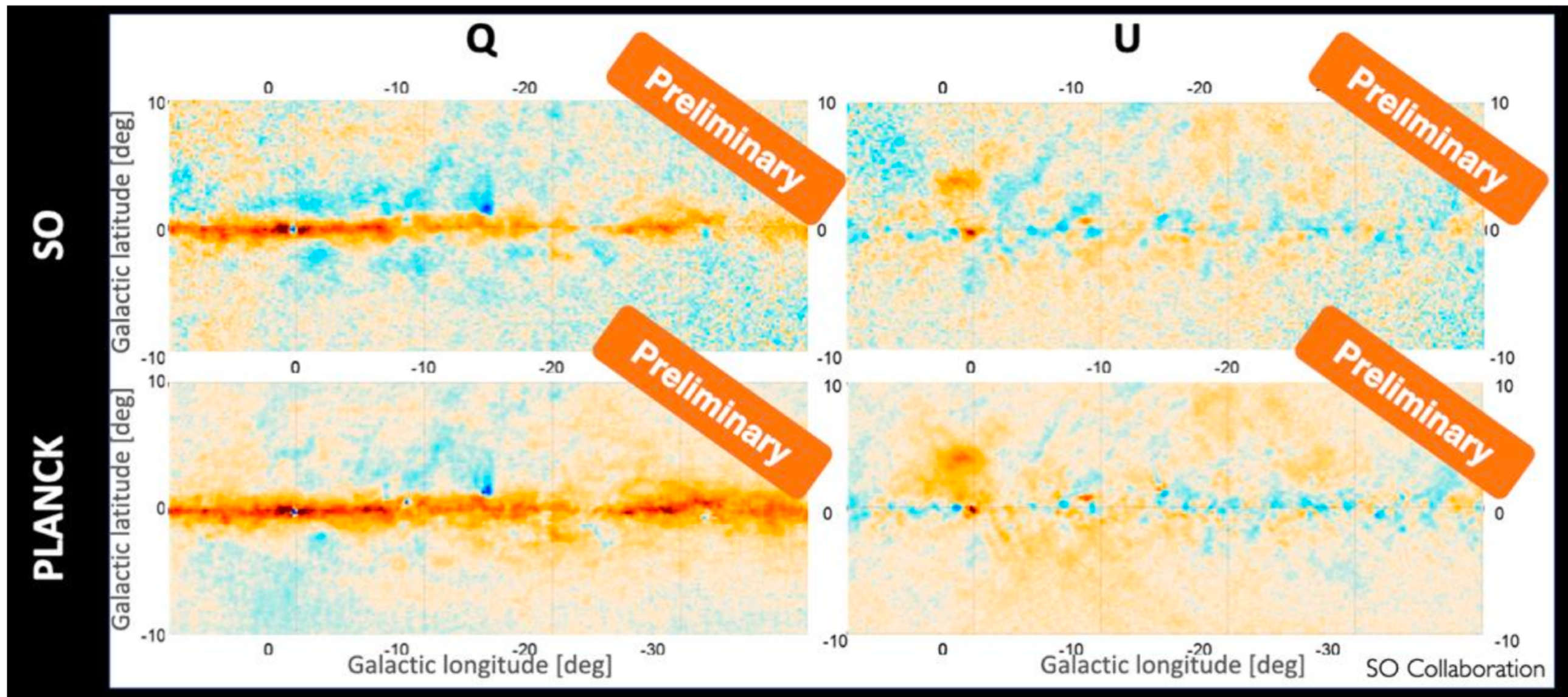




Preliminary SAT Maps: 90 GHz from one telescope



Preliminary SAT Maps

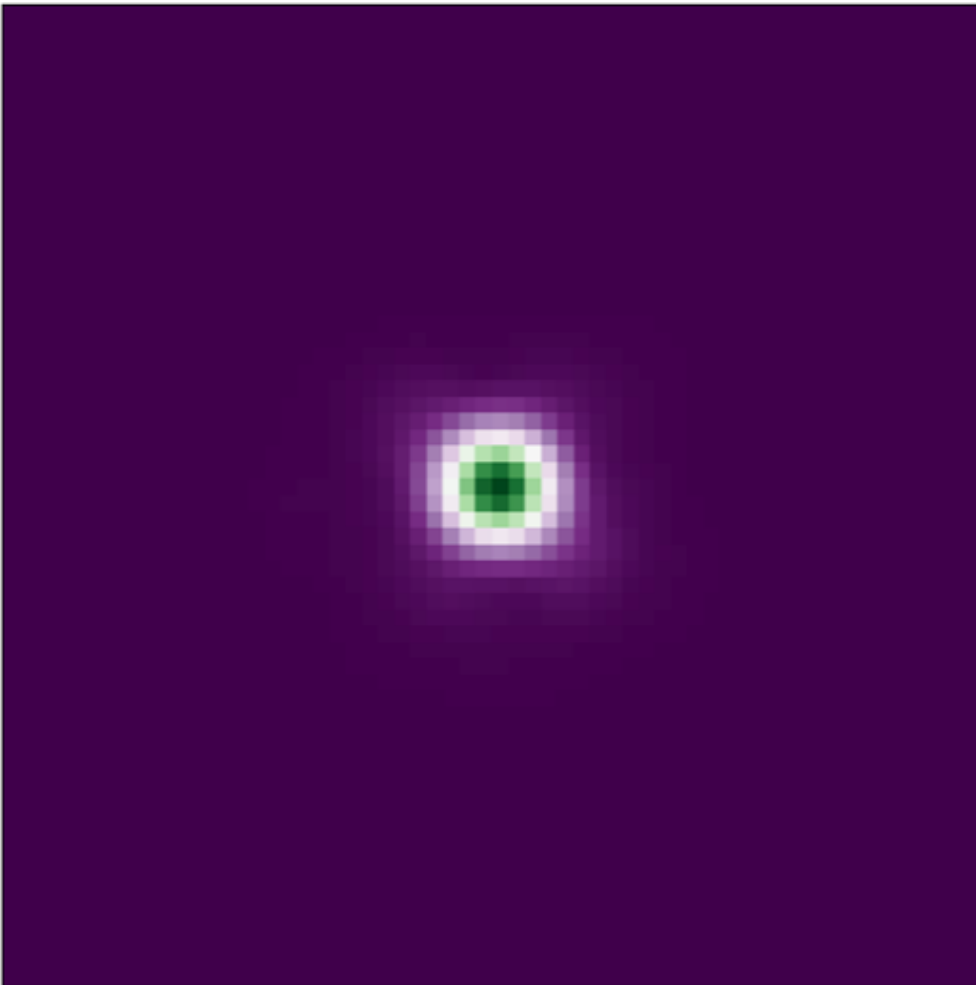


Polarized galaxy center maps in comparison with Planck
demonstrate instrument performance and larger scale recovery.



Each tube in the cryostat of the LAT is roughly equivalent to ACT

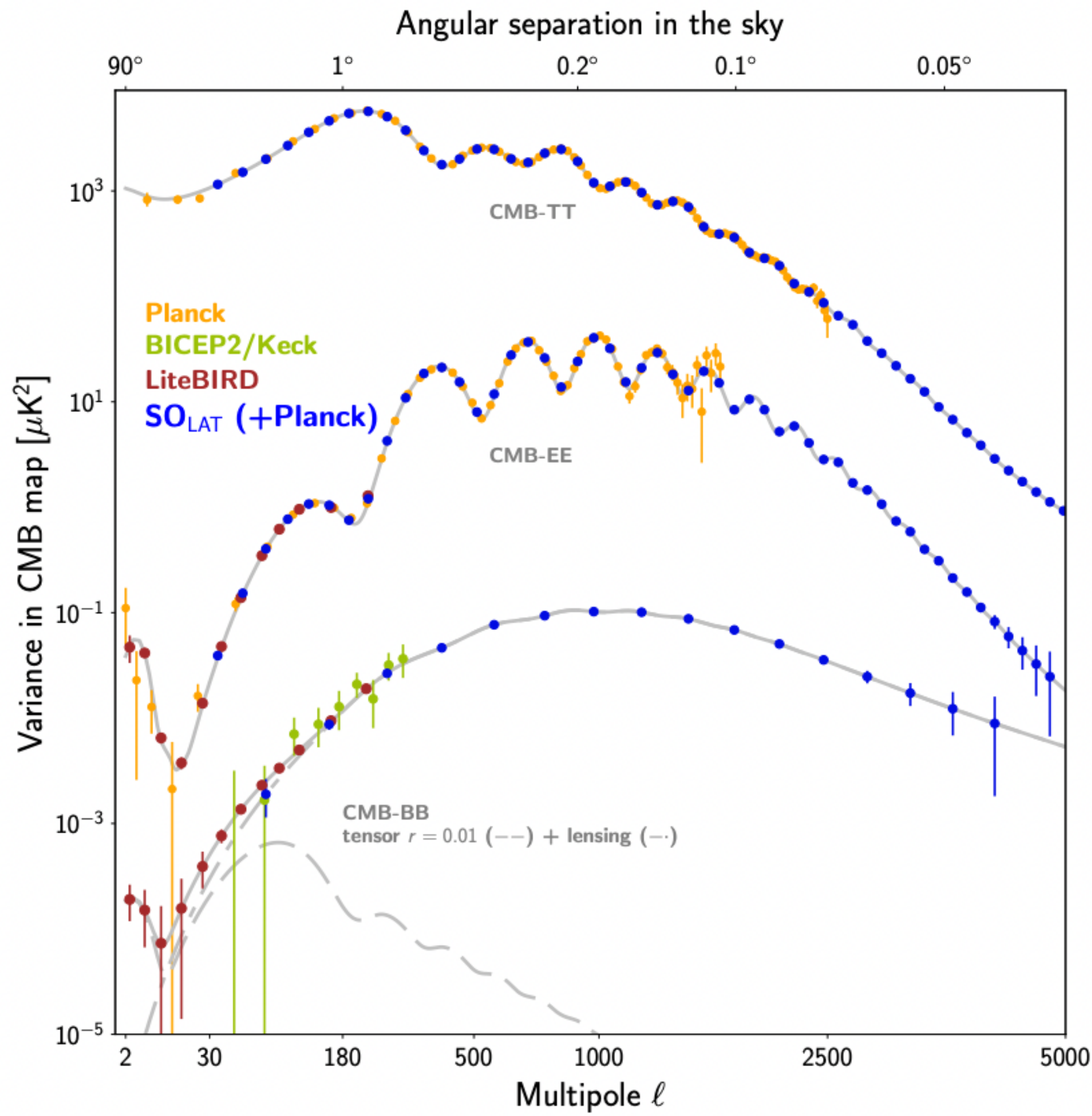
Large Aperture Telescope – First Light February 2025!



24,000 + Detectors on the Sky.

- Mirrors not yet aligned/focused.
- Signal to Noise of 4000+ per detector.
- 640 detectors used the Mars map.
- CMB maps are already being made.





- *ACT has released an unprecedented data set measuring the polarisation of the CMB over 40 % of the sky.*
- *We have released data and code, making our results entirely reproducible (and falsifiable).*
- *We are consistent with Planck in LCDM, but we do not find anomalous lensing amplitude or curvature. We don't have an hint for a model solving the H0 tension.*
- *Plank + ACT: P-ACT, a constraining data set exploiting the strengths of each survey*
- *Simons observatory: a bright an exciting future in CMB cosmology ahead of us !*

BACK UP

Data Combinations

We make use of several external datasets and combinations.

Planck	$\text{Planck}^{\text{TT/TE/EE}} + \text{Sroll2}$
ACT	$\text{ACT}^{\text{TT/TE/EE}} + \text{Sroll2}$
P-ACT	$\text{ACT}^{\text{TT/TE/EE}} + \text{Planck}_{\text{cut}}^{\text{TT/TE/EE}} + \text{Sroll2}$
W-ACT	$\text{ACT}^{\text{TT/TE/EE}} + \text{WMAP}^{\text{TT/TE/EE}} + \text{Sroll2}$

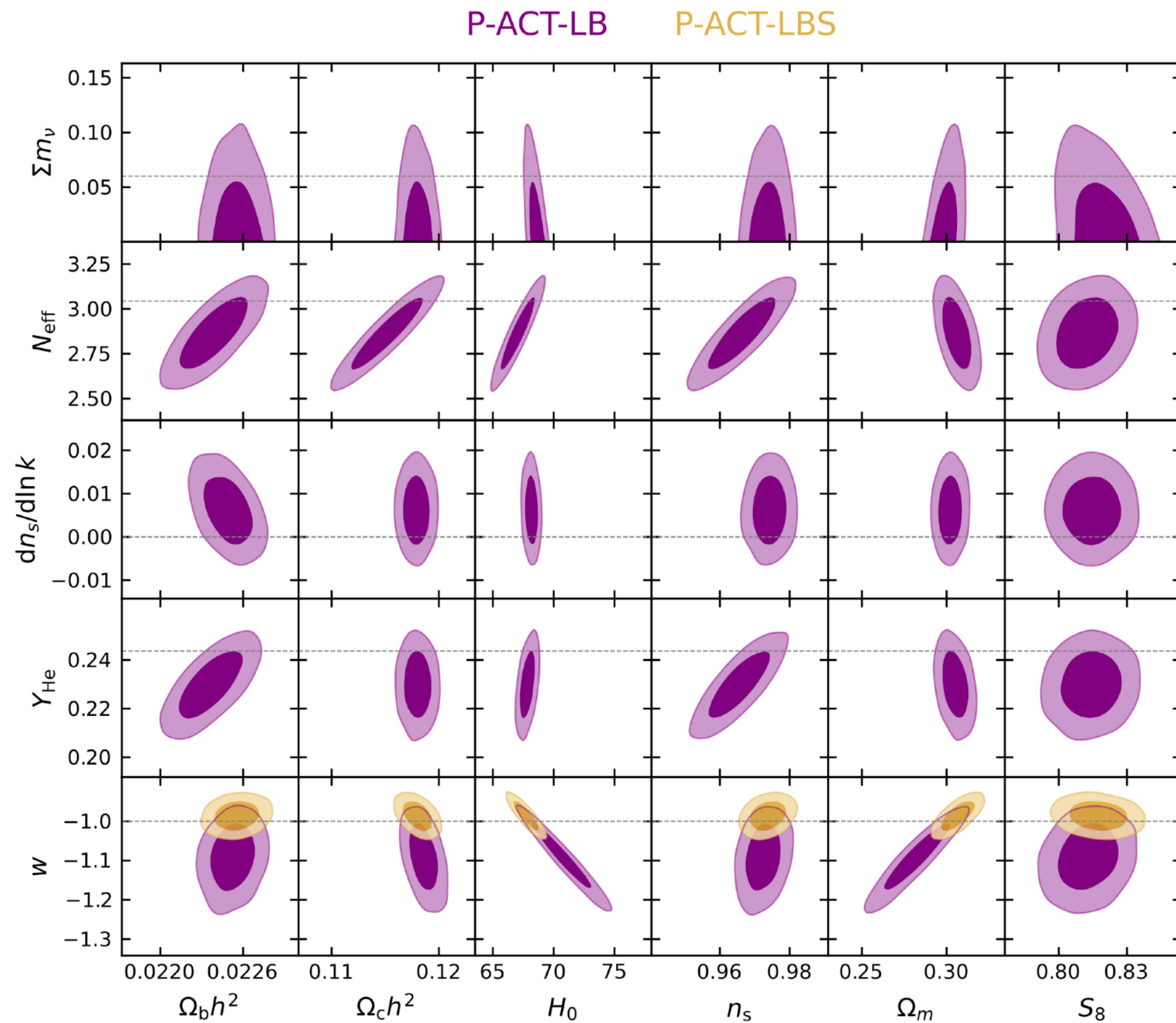
followed by

-LB	when adding CMB lensing and BAO
-LS	when adding CMB lensing and SNIa
-LBS	when adding CMB lensing, BAO, and SNIa

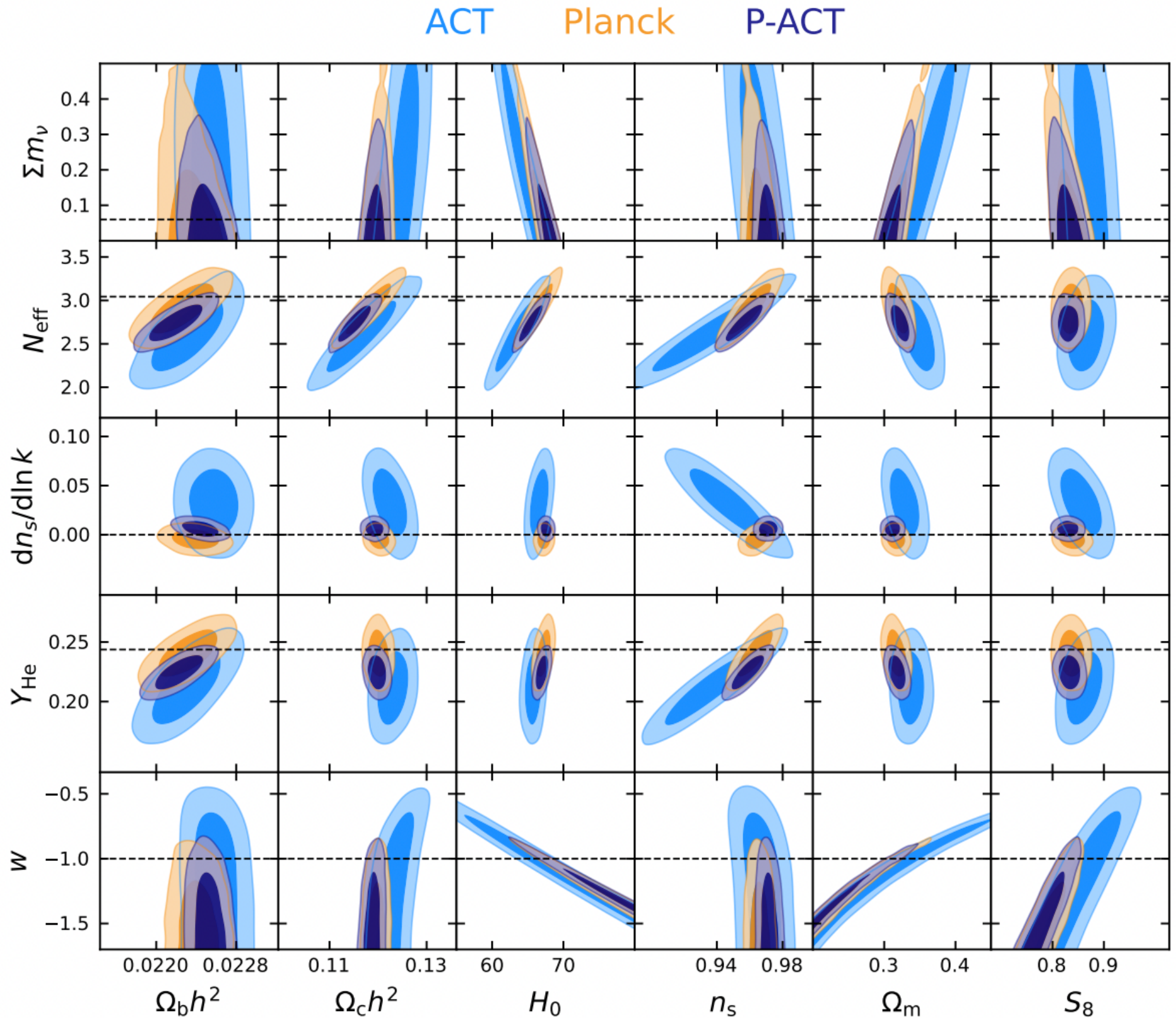
- Sroll2 uses low-E data from Planck
- P-ACT uses Planck cut at 1000/600/600, with full ACT and Sroll2
- CMB Lensing is from ACT DR6 and Planck PR4
- BAO measurements from DESI Y1 as baseline, BOSS/eBOSS BAO data are used as cross-check in some cases
- Type Ia Supernovae from Pantheon+

BEYOND LCDM models

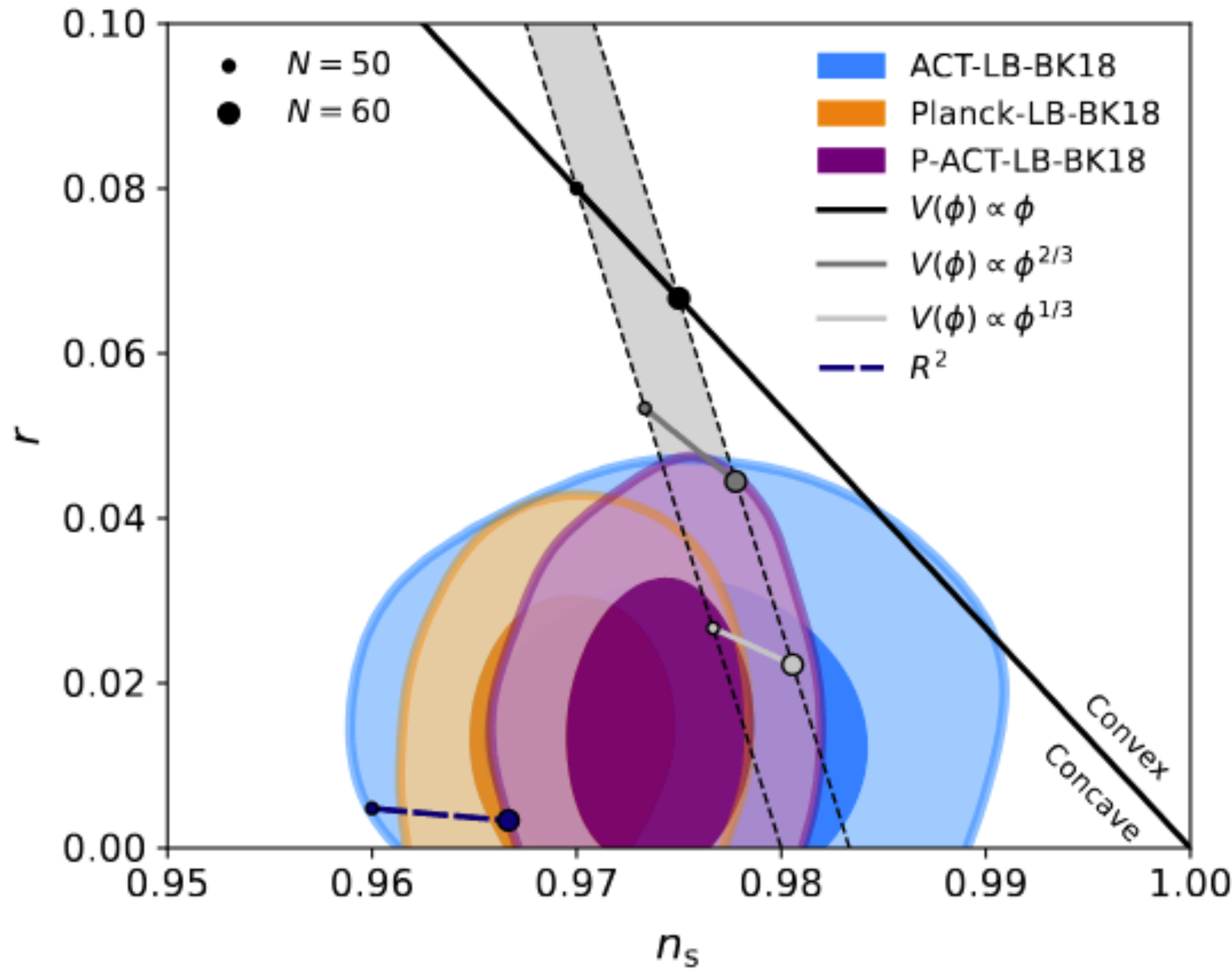
Exploration of extended cosmological models



Exploration of extended cosmological models



Primordial perturbations and inflation



A_{lens}

the ACT power spectrum data:

$$\begin{aligned} A_{\text{lens}} &= 1.007 \pm 0.057 \quad (\text{ACT}) \\ &= 1.08^{+0.10}_{-0.12} \quad (\text{ACT-TT}) \\ &= 1.24^{+0.18}_{-0.22} \quad (\text{ACT-TE}) \\ &= 0.89^{+0.10}_{-0.23} \quad (\text{ACT-EE}) \end{aligned}$$

$$A_{\text{lens}} = 1.043 \pm 0.049 \quad (\text{W-ACT}),$$

model prediction. The PR3 analysis found $A_{\text{lens}} > 1$ at the almost 3σ level (Planck Collaboration 2020d), with $A_{\text{lens}} = 1.180 \pm 0.065$. Analyses of the NPIPE data, using larger fractions of sky, found lower departures of only 1.7σ for the CamSpec likelihood, with $A_{\text{lens}} = 1.095 \pm 0.056$ (Rosenberg et al. 2022), or 0.75σ using the Hillipop likelihood, with $A_{\text{lens}} = 1.039 \pm 0.052$. (Tristram et al. 2024). No excess lensing was observed in the ACT DR4 data, with $A_{\text{lens}} = 1.01 \pm 0.11$ (Aiola et al. 2020).

of A_{lens} with the matter density. In the *Planck* PR3 data an oscillatory residual for TT in the range $1000 < \ell < 2000$ was identified as driving the preference for the enhanced lensing; we do not see evidence for this in the ACT data. For P-ACT we find $A_{\text{lens}} = 1.081 \pm 0.043$ which is consistent with e.g., Rosenberg et al. (2022).

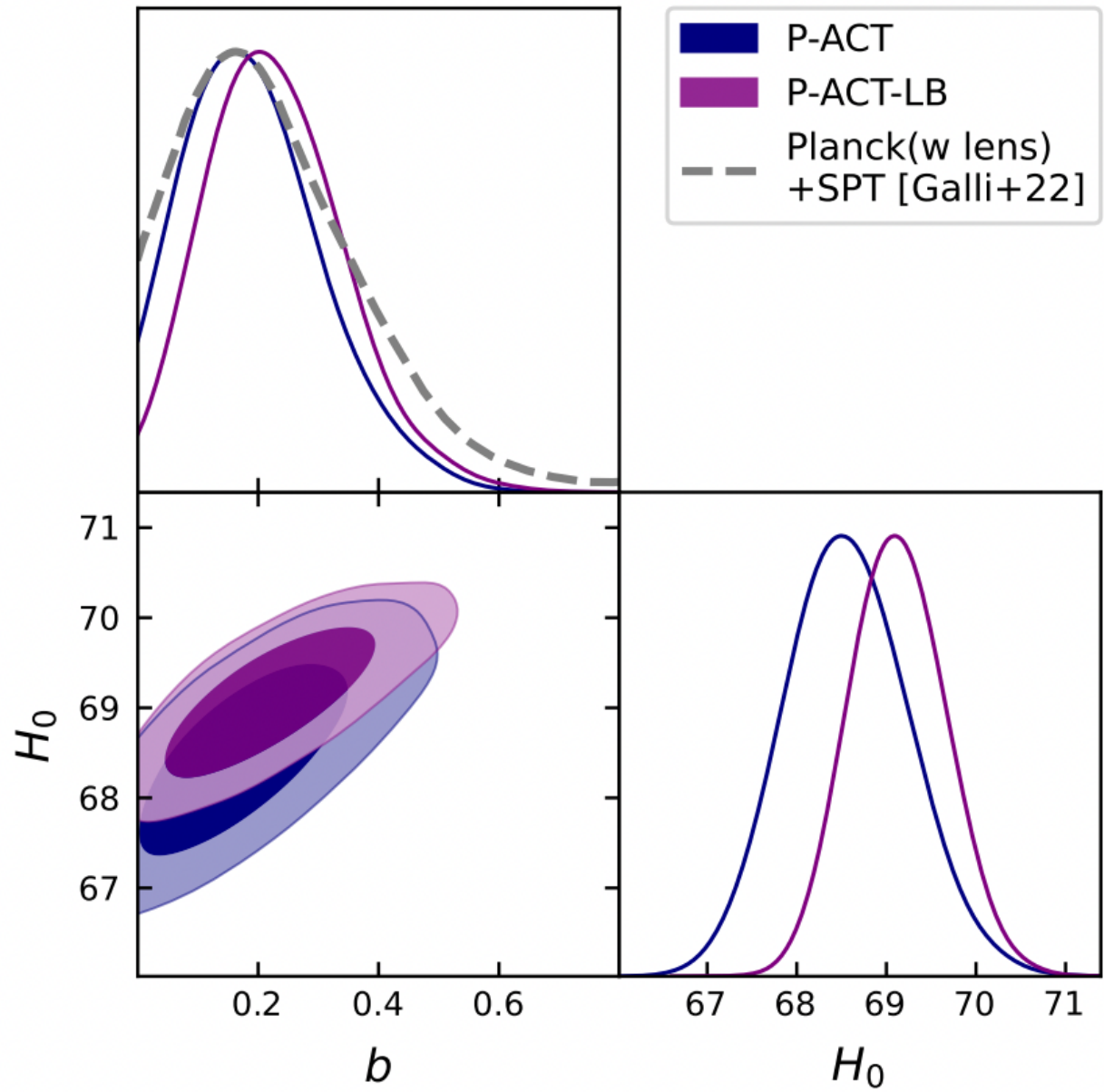
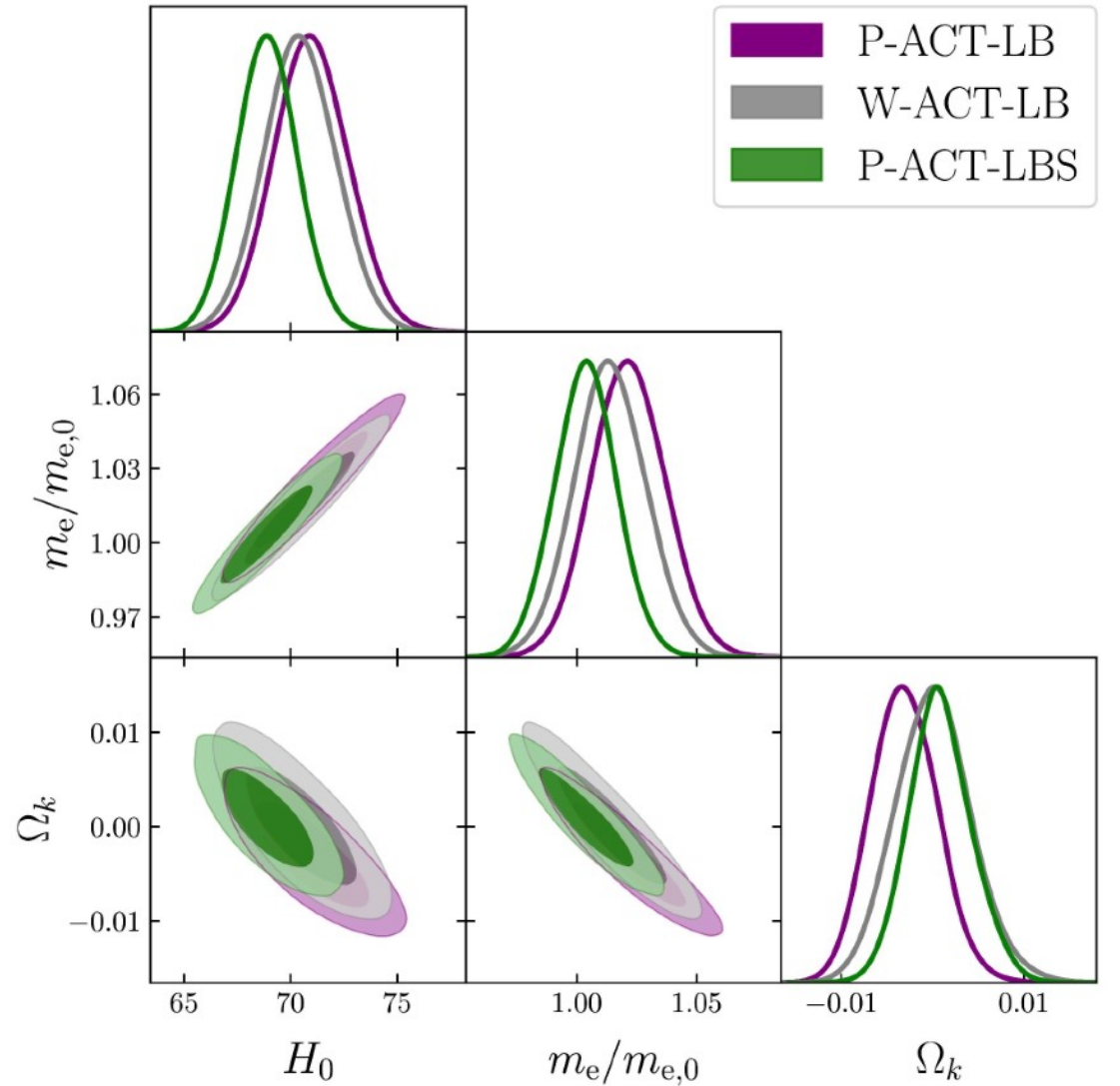


Figure 15. Constraints on the variance b of the small-scale baryon density distribution at recombination from P-ACT (navy) and P-ACT-LB (purple), compared with the latest results from *Planck* (including CMB lensing) combined with SPT small-scale polarization (gray dashed line). Primordial magnetic fields would induce baryon clumping on small scales, and hence $b > 0$. No evidence of clumping is seen in our analysis.

Varying m_e + curvature



Particle cosmology

No evidence for new light, relativistic species

Free-streaming:

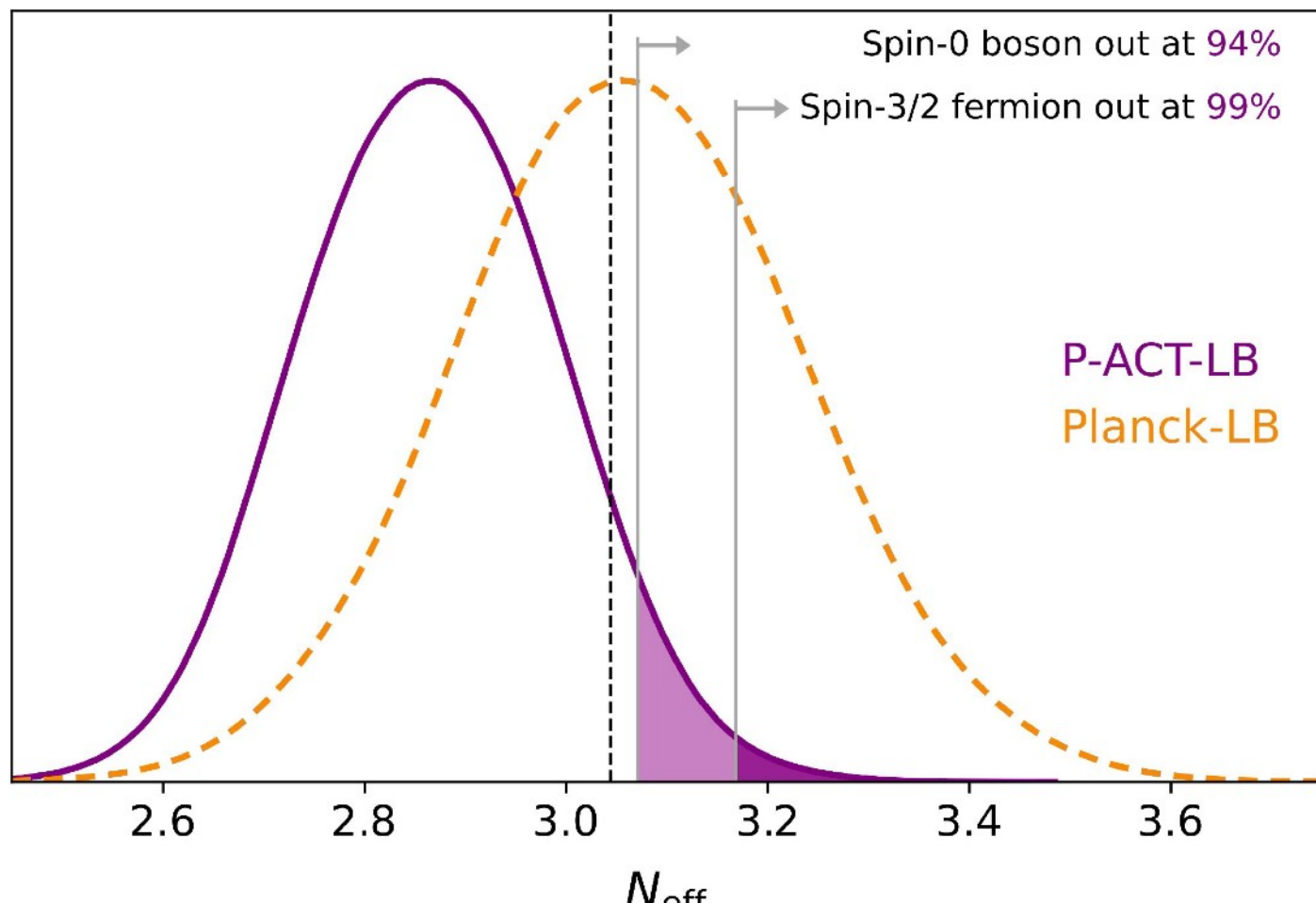
$$N_{\text{eff}} = 2.86 \pm 0.13 \text{ (68%, P-ACT-LB)}$$

$$N_{\text{eff}} = 2.89 \pm 0.11 \text{ (68%, P-ACT-LB-BBN)}$$

in the acoustic peaks ([Bashinsky & Seljak 2004](#)). Combining the *Planck* legacy CMB with *Planck* CMB lensing and BOSS BAO, the neutrino number is measured to be $N_{\text{eff}} = 2.99 \pm 0.17$ at 68% CL ([Planck Collaboration 2020c](#)), or $N_{\text{eff}} = 3.06 \pm 0.17$ at 68% CL when we evaluate this estimate using Planck-LB.

With the new ACT DR6 spectra we find $N_{\text{eff}} = 2.60^{+0.21}_{-0.29}$ at 68% CL, combining into

$$\begin{aligned} N_{\text{eff}} &= 2.73 \pm 0.14 \quad (68\%, \text{P-ACT}), \\ &= 2.86 \pm 0.13 \quad (68\%, \text{P-ACT-LB}), \end{aligned} \quad (30)$$



Particle cosmology

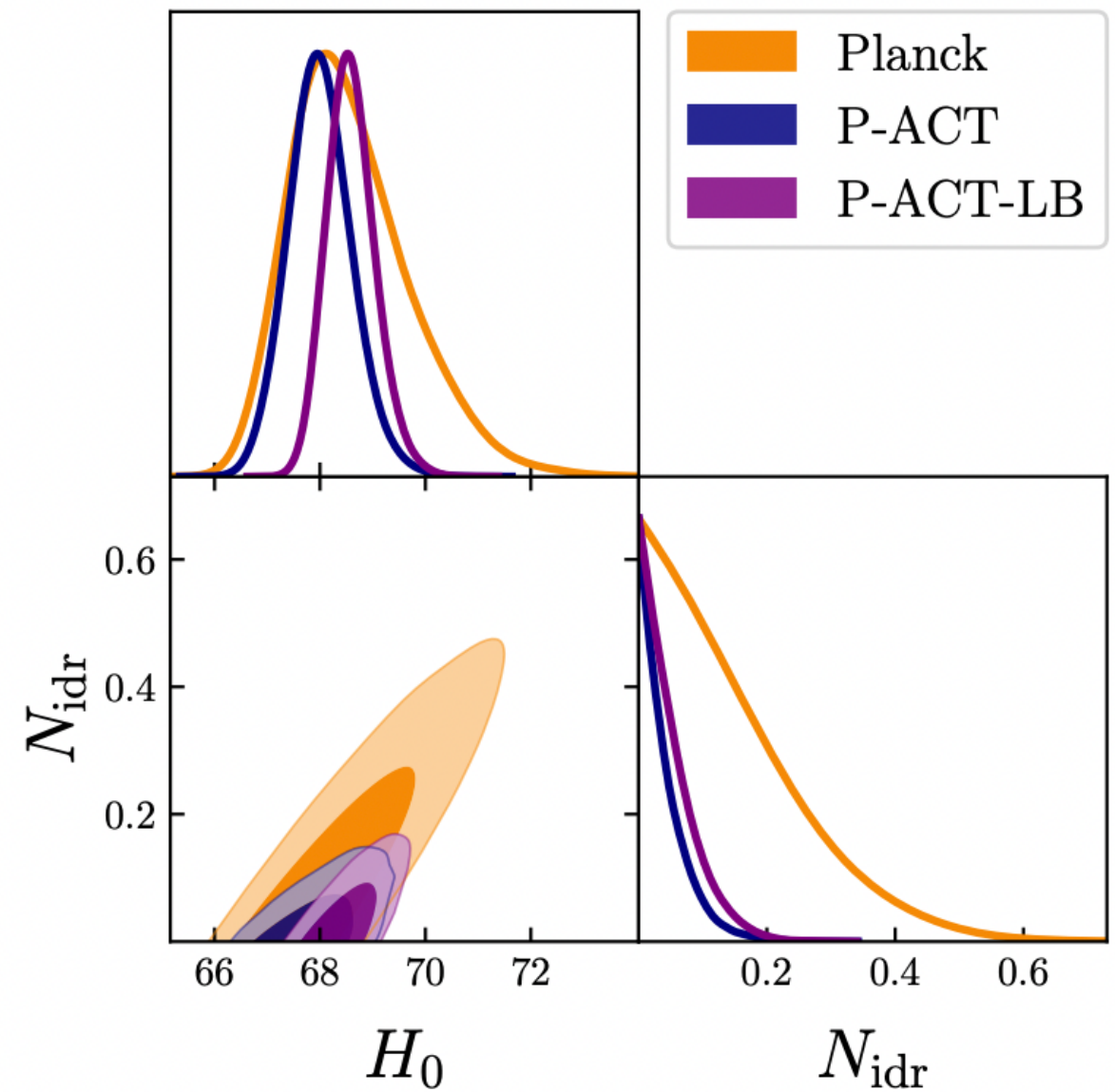
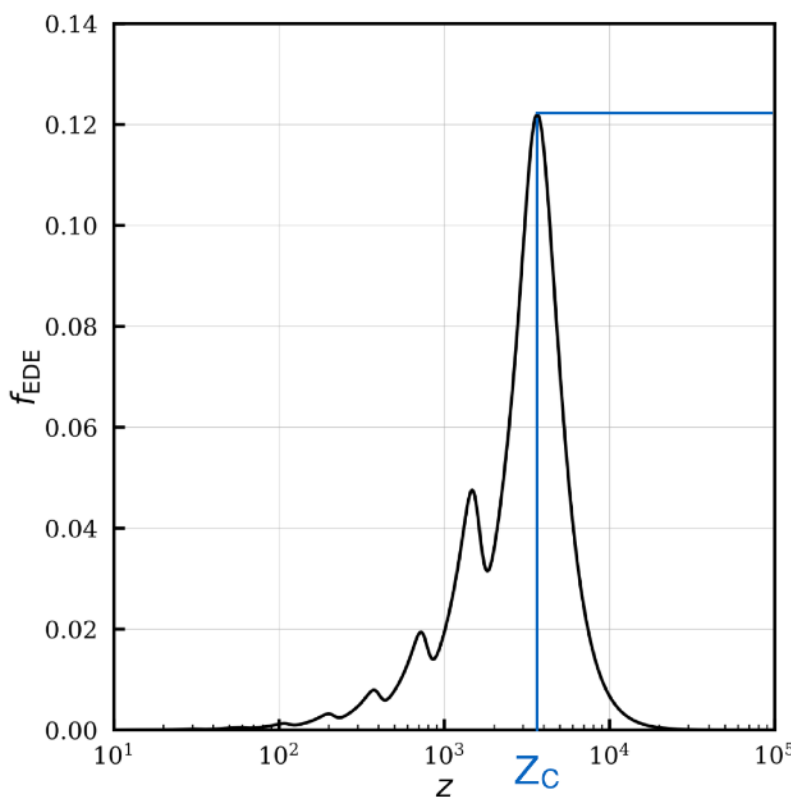


Figure 34. Constraints on the number of strongly self-interacting dark relativistic species, N_{idr} . The addition of ACT DR6 spectra improves the constraint from *Planck* by more than a factor of three (navy versus orange) and notably disfavors values of H_0 above 70 km/s/Mpc that are allowed by *Planck* alone. Inclusion of CMB lensing and DESI BAO data (purple) slightly weakens the SIDR upper limit due to small shifts in the best-fit model parameters, but nevertheless further tightens the H_0 posterior. These are the tightest bounds on SIDR obtained to date.

Pre- and modified recombination physics

No evidence for an early dark energy (EDE) component:

A mild hint (2-3 σ) of EDE was seen in ACT DR4 (Hill+2022); the new ACT DR6 spectra show that this was a statistical fluctuation.



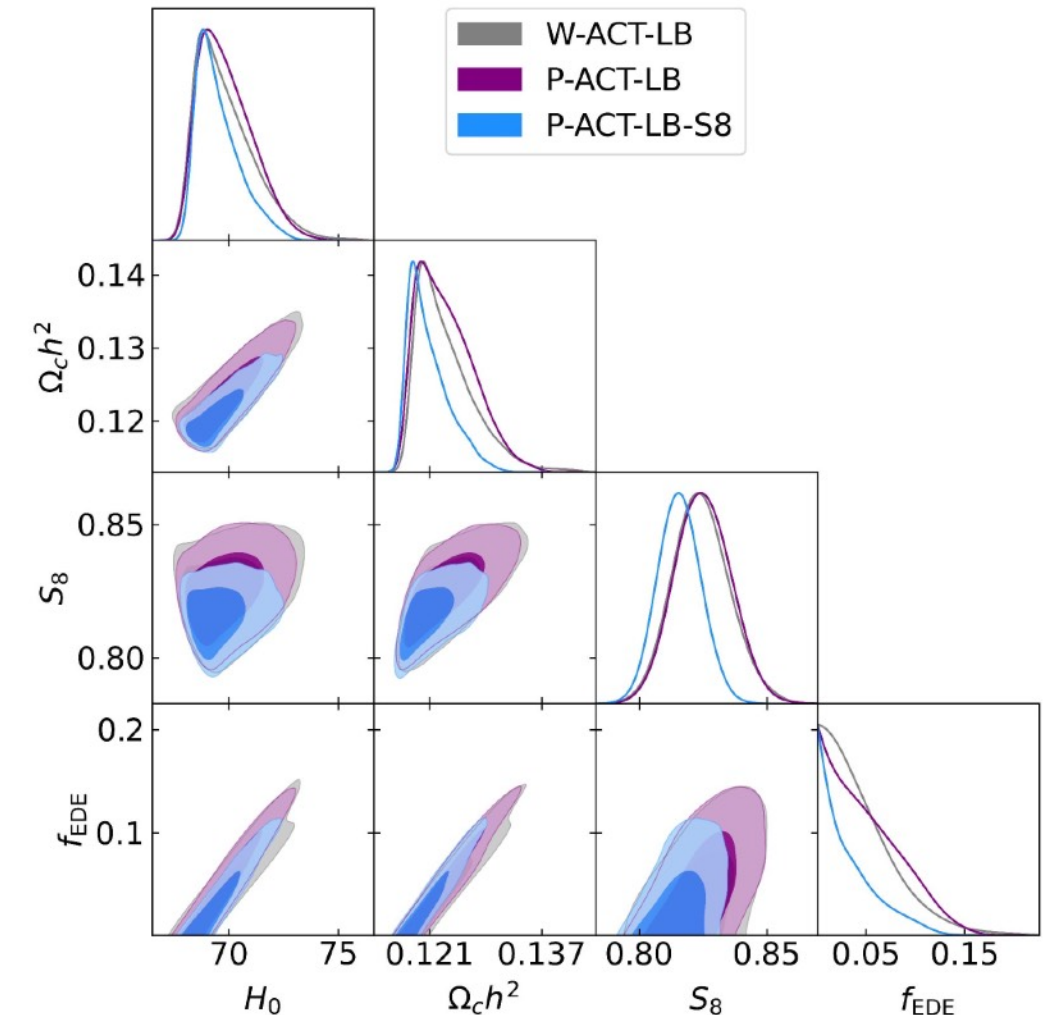
Maximal contribution:

$$f_{\text{EDE}}(z_c) \equiv (\rho_{\text{EDE}}/3M_{pl}^2 H^2)|_{z_c}$$

which occurs at redshift z_c

Final parameter: $\Theta_i = \phi_i/f$
(initial field displacement)

→ { f_{EDE} , z_c , Θ_i }



	$\Delta\chi^2$	Pref. in σ	$H_0^{(\text{EDE})}$	f_{EDE}	$\log_{10} z_c$
ACT	≈ 0.0	0.0	66.5	0.012	3.00
W-ACT	1.9	0.5	69.9	0.089	3.55
P-ACT	4.3	1.2	70.4	0.091	3.56
W-ACT-LB	2.9	0.8	70.2	0.070	3.52
P-ACT-LB	6.6	1.7	71.2	0.093	3.56

Table 2. The $\Delta\chi^2 = \chi^2_{\Lambda\text{CDM}} - \chi^2_{\text{EDE}}$ from the **MFLike** likelihood MAP points for the $n = 3$ EDE model compared to ΛCDM for each dataset combination, and preference (in units of σ) for EDE over ΛCDM using the likelihood-ratio test statistic. The values for H_0 , f_{EDE} , and $\log_{10} z_c$ in the MAP EDE model are also reported. The data show no significant preference for non-zero EDE. For ACT alone, the MAP χ^2 for EDE is indistinguishable from that for ΛCDM within our numerical precision, indicating that adding EDE parameters does not improve the fit at all in this case.

Neutrinos

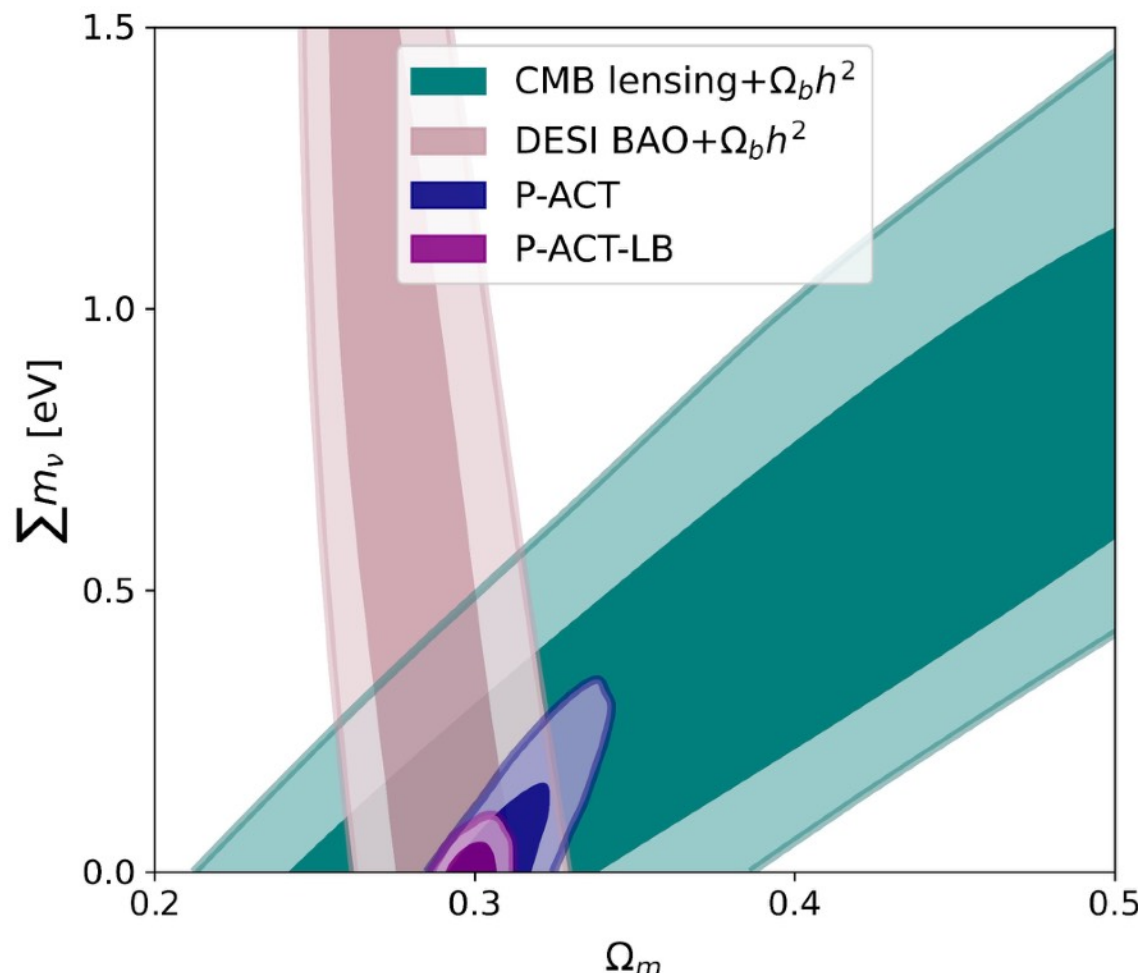
We find no evidence for non-zero neutrino masses:

$$\sum m_\nu < 0.082 \text{ eV} \quad (95\%, \text{P-ACT-LB})$$

$$\sum m_\nu < 0.083 \text{ eV} \quad (95\%, \text{W-ACT-LB})$$

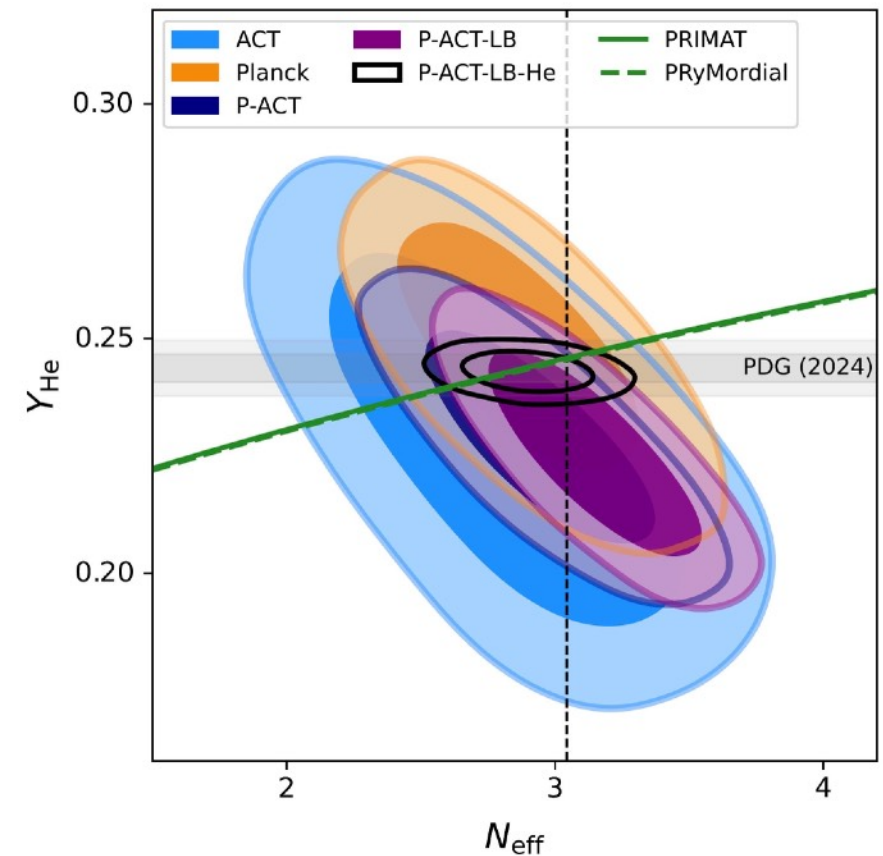
with significant contribution from DESI BAO

$$\sum m_\nu < 0.13 \text{ eV} \quad (95\%, \text{P-ACT-LB}_{\text{BOSS}})$$

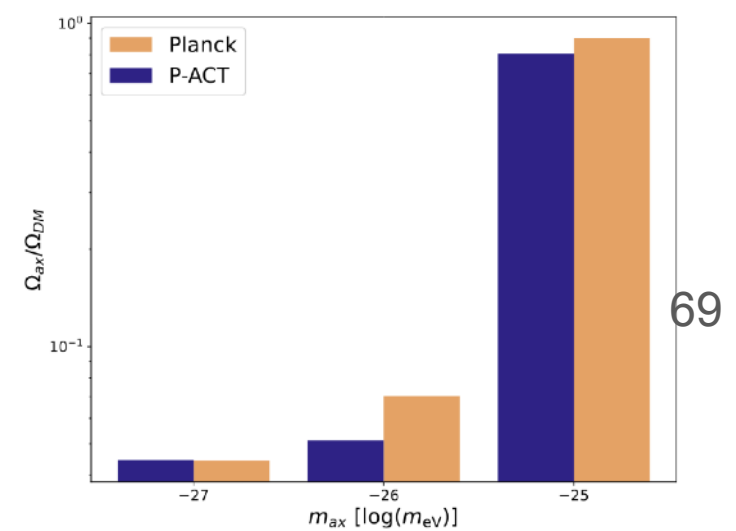
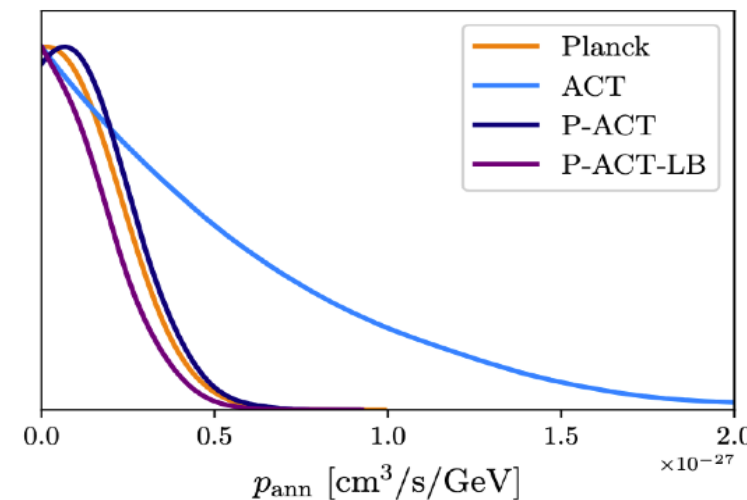
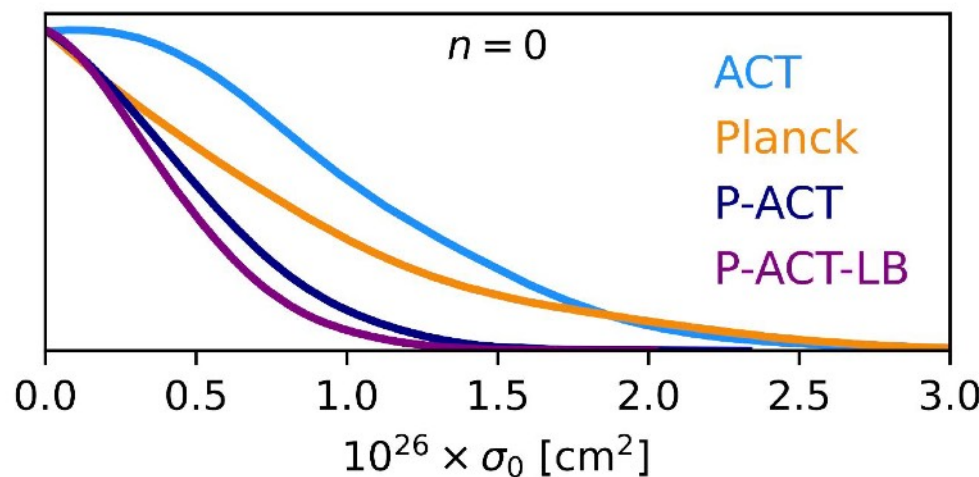


Particle astrophysics

We also find the abundances of primordial elements to be consistent with standard BBN.



We find dark matter to follow the standard CDM paradigm, with no evidence for scattering with baryons, self-annihilation, contribution from axion-like particles, or scattering off a dark radiation component.



Late-time physics: dark energy

From primary CMB data, we find no evidence for non-standard dark energy; hints of non-standard evolution are driven by low-redshift data and consistent with previous analyses of DESI and SNIa data.

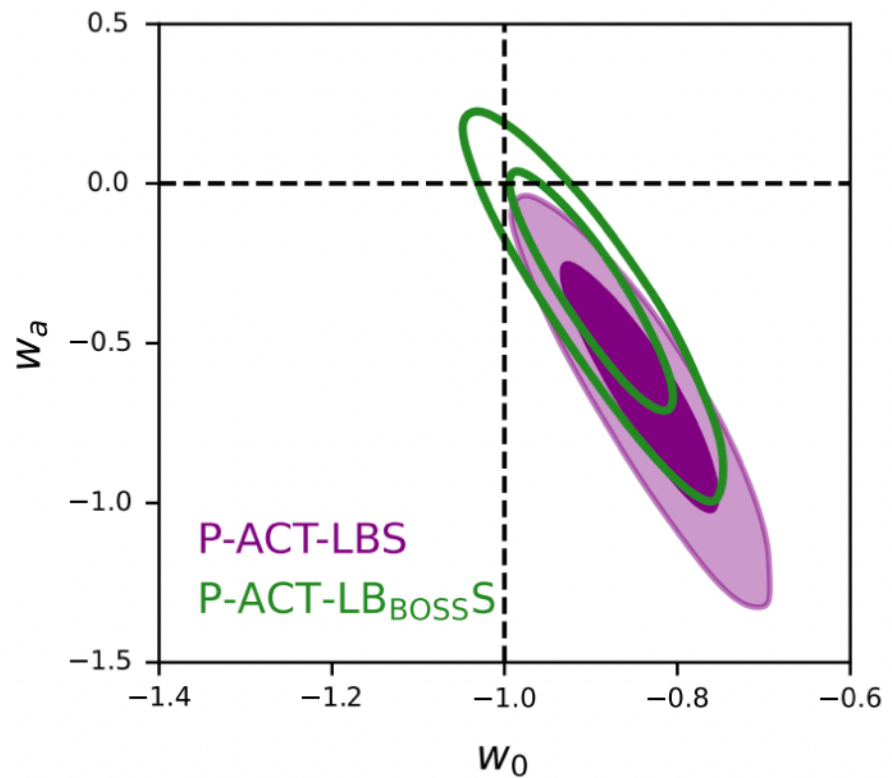


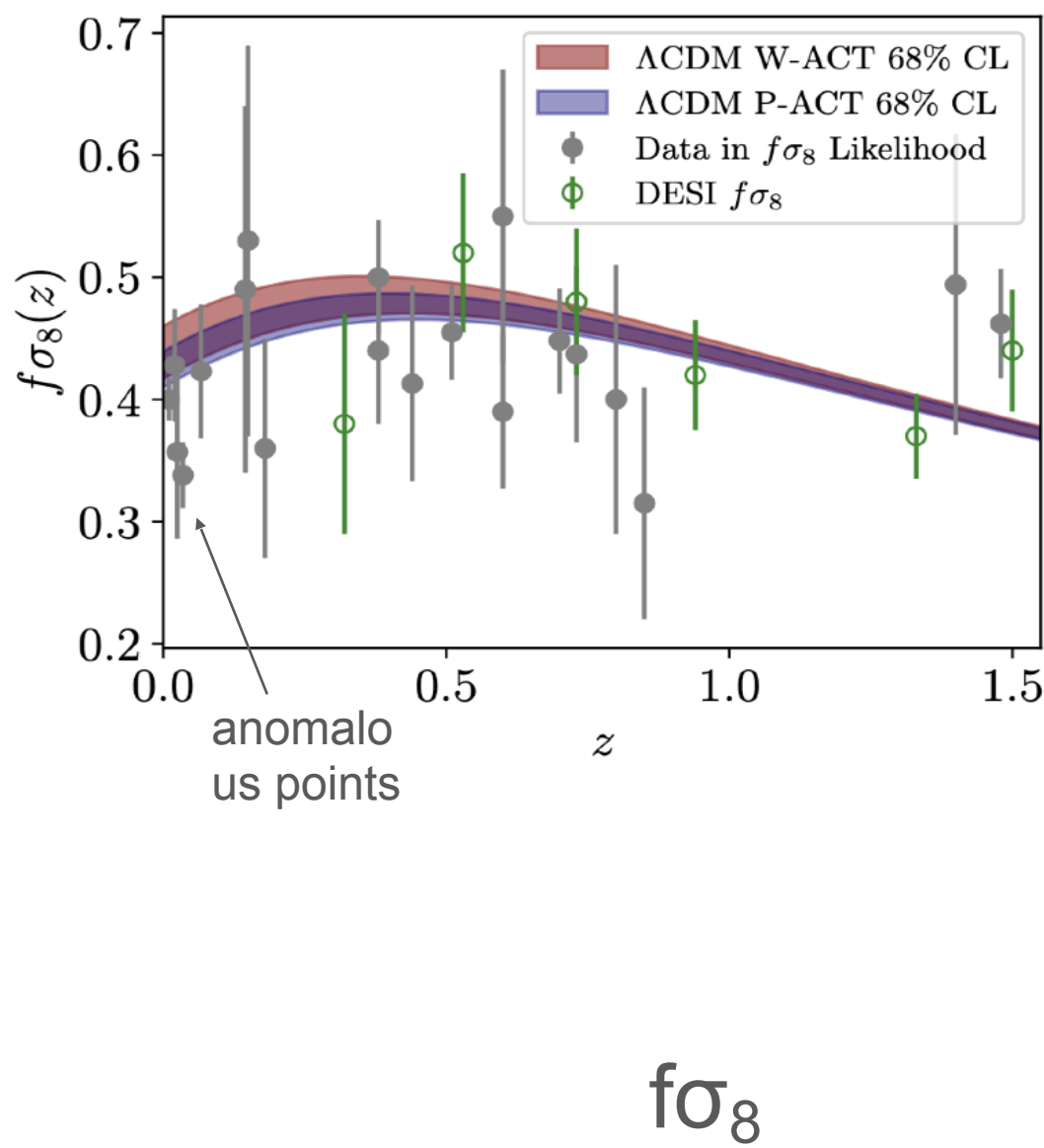
Figure 37. Constraints on the dark energy equation of state parameters, varying both today's value, w_0 , and its time variation, w_a . Similar to other studies, we find that DESI drives a preference for time-varying dark energy (compared to the dashed Λ CDM line), which is relaxed when considering BOSS BAO instead (green contours). The CMB contribution to this measurement is sub-dominant, apart from breaking parameter degeneracies, with Planck, W-ACT, and P-ACT giving similar results.

P-ACT-LBS consistent with Λ at 2.2σ
[P-LBS (in)consistent with Λ at 2.5σ
(DESI+2024)]

$$\left. \begin{array}{l} w_0 = -0.837 \pm 0.061 \\ w_a = -0.66^{+0.27}_{-0.24} \end{array} \right\} (68\%, \text{P-ACT-LBS})$$

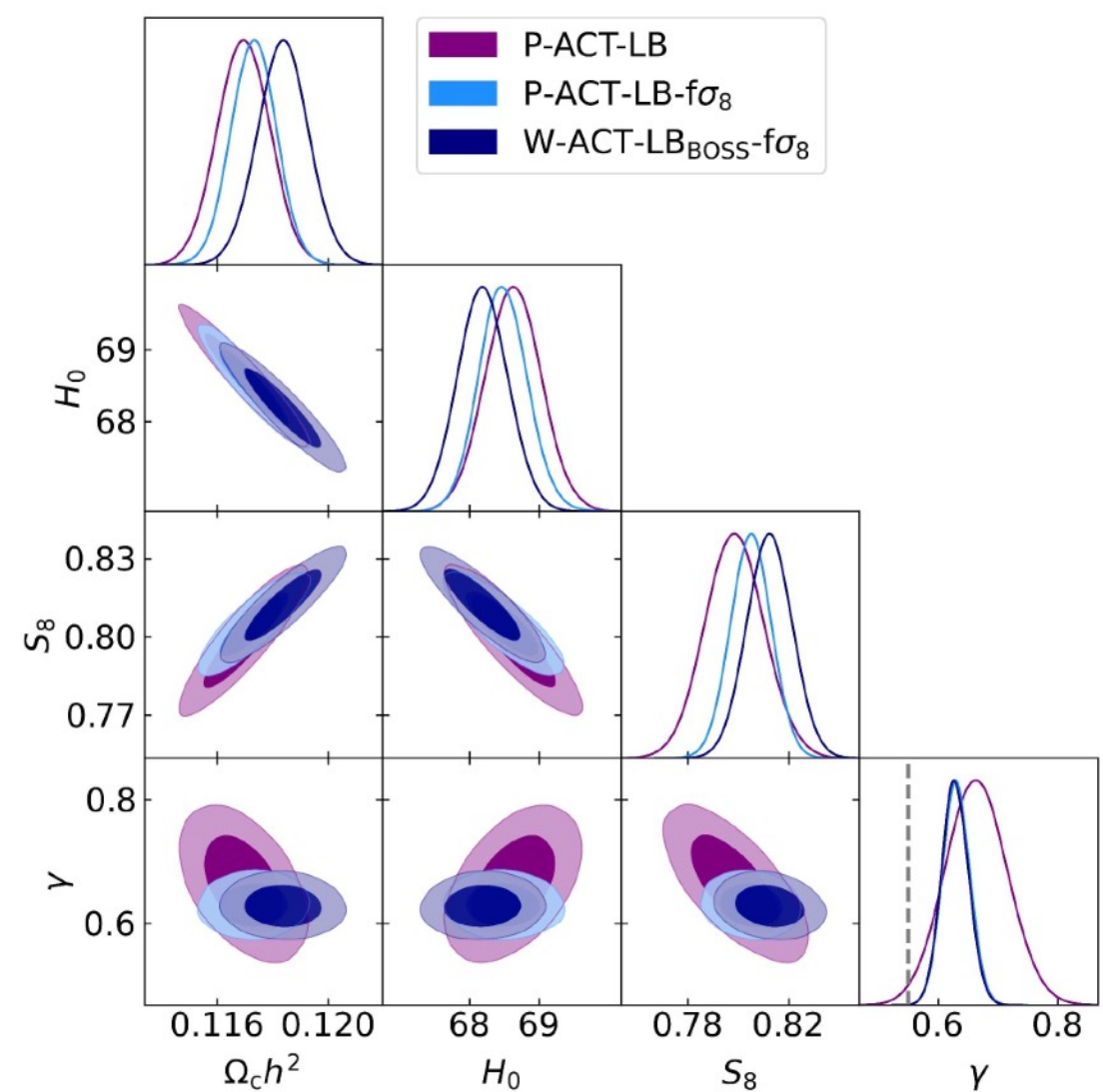
Late-time physics: modified growth

We also see no evidence of modified growth, e.g., due to beyond-GR gravity (modulo two slightly outlying $f\sigma_8$ measurements at very low redshifts).



$$f(a) = \Omega_m^\gamma(a)$$

$$\left. \begin{array}{l} \gamma = 0.663 \pm 0.052 \\ S_8 = 0.799 \pm 0.012 \end{array} \right\} (68\%, \text{P-ACT-LB})$$



Modified recombination control point

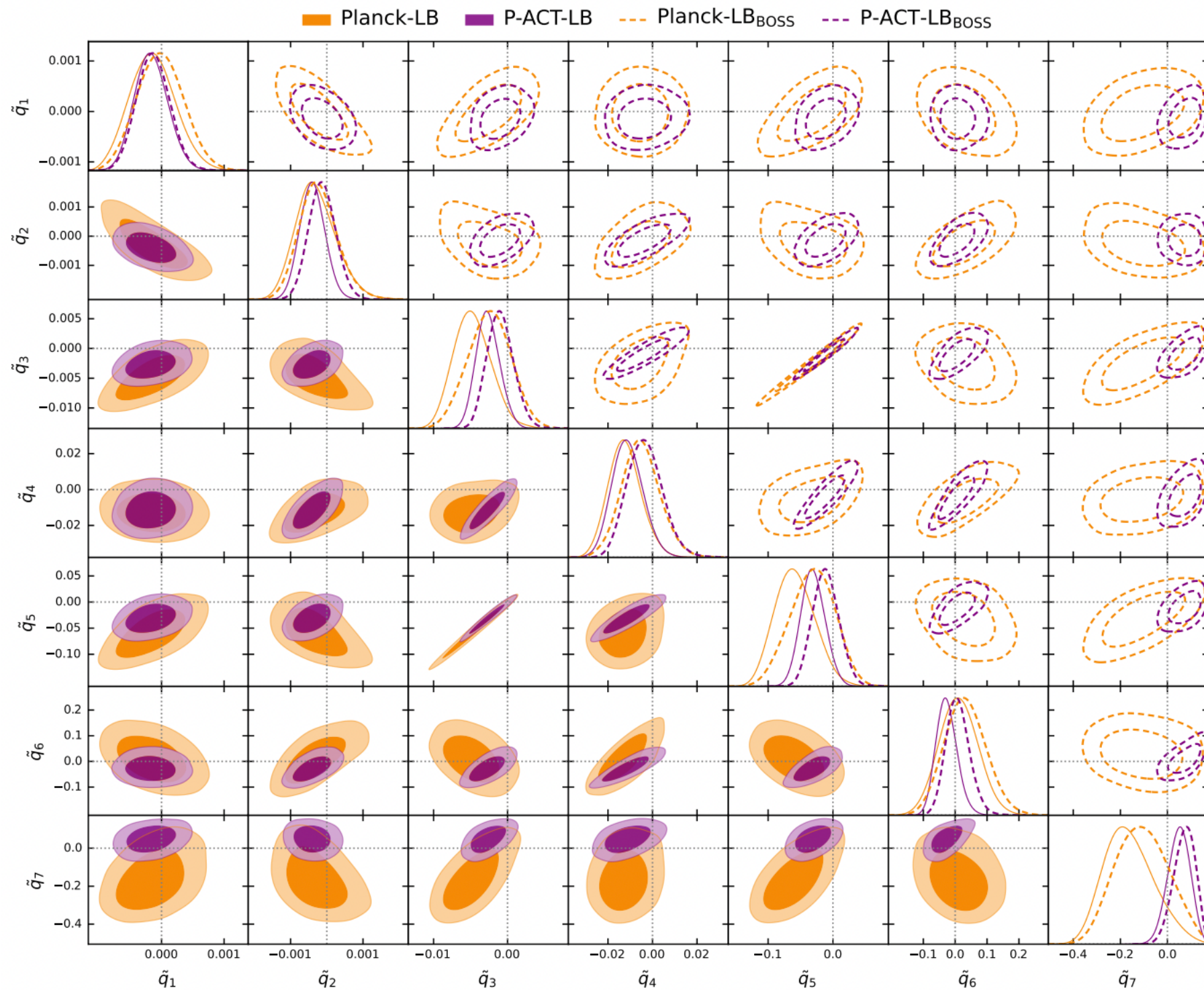
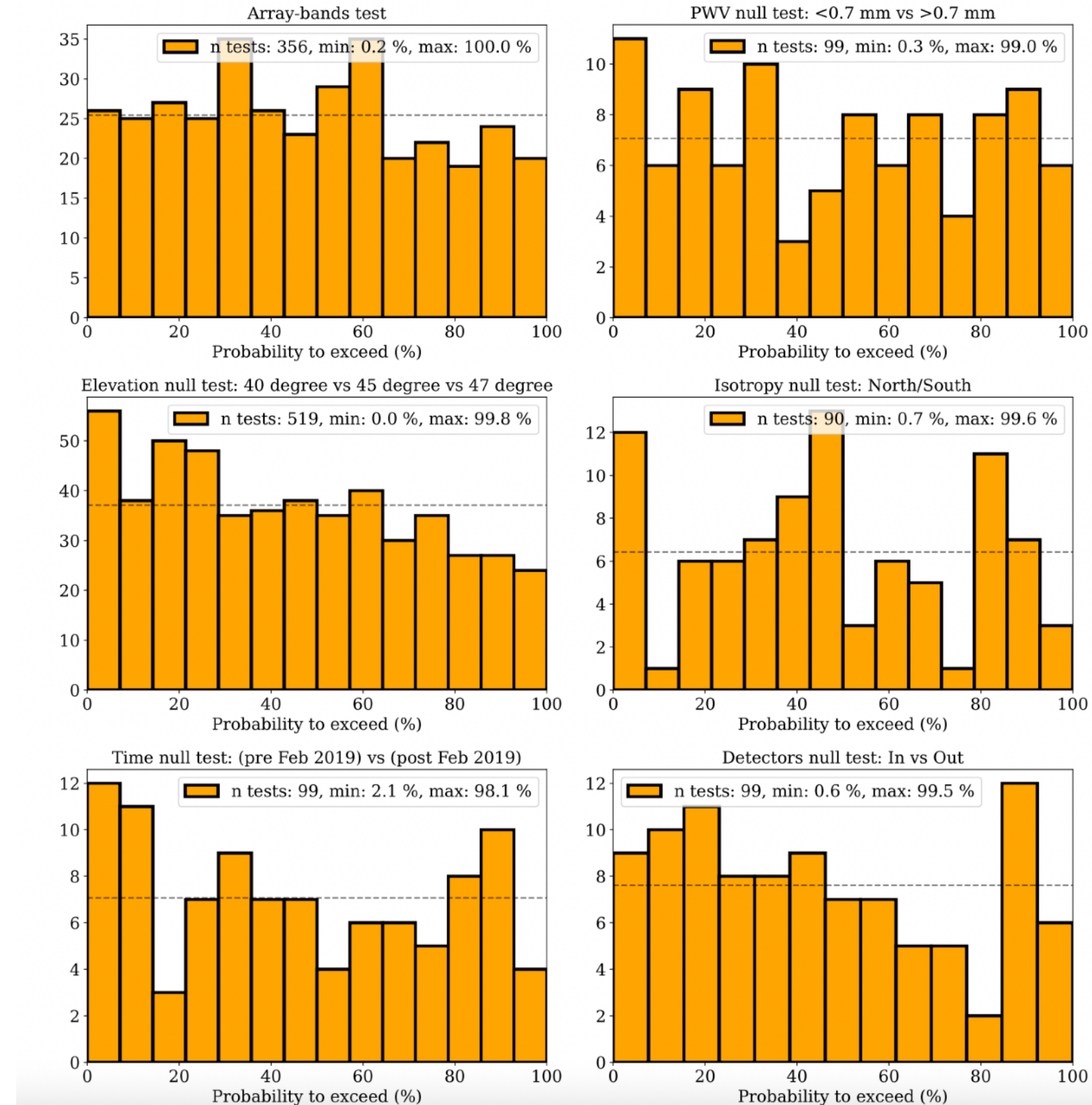


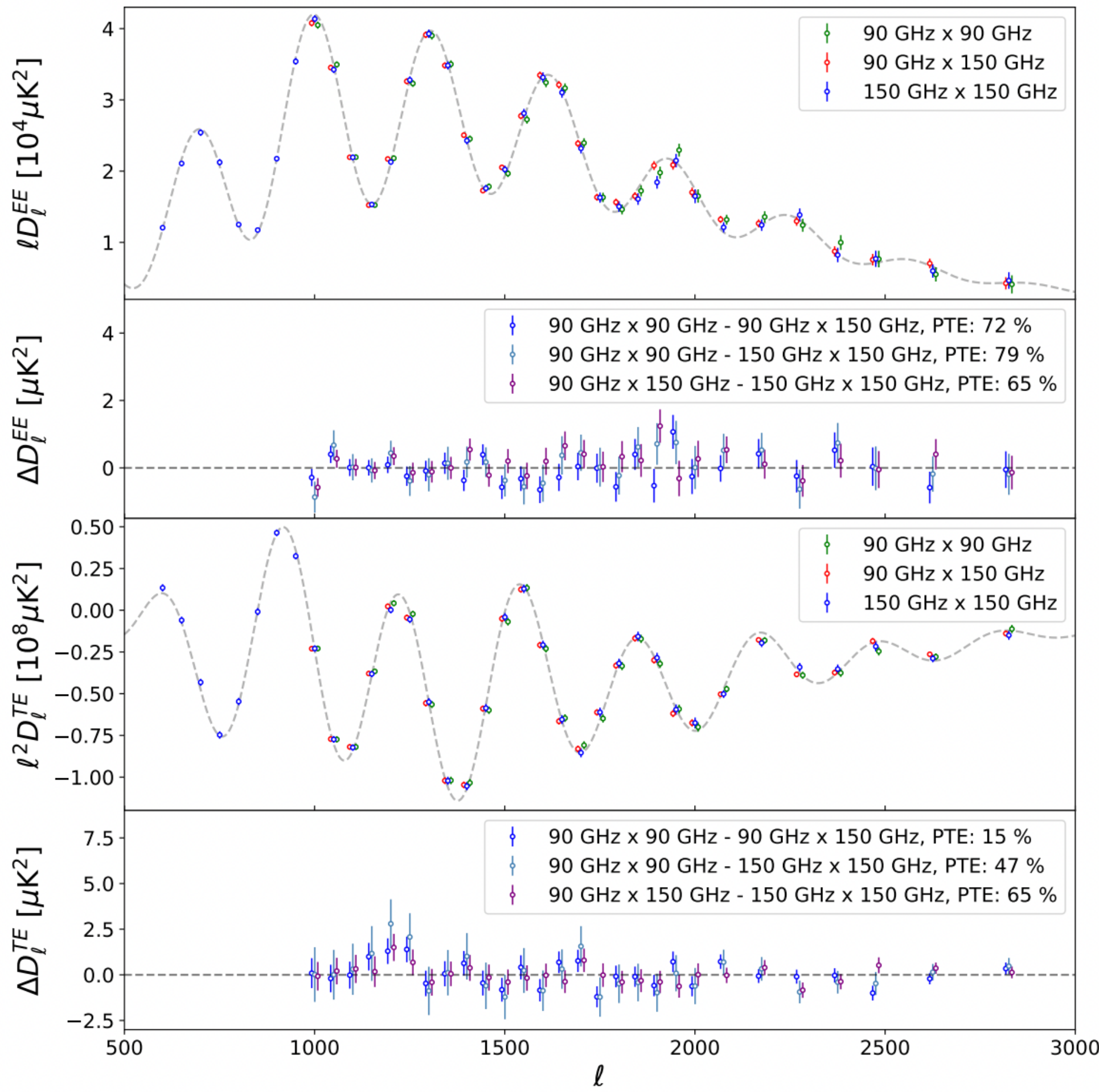
Figure 55. Marginalized parameter posteriors for the control points varied in the `ModRec` scenario analyzed in §5.5. The bottom (top) panels use DESI (BOSS) BAO. The dotted gray lines indicate the standard recombination scenario ($\tilde{q}_i = 0$).

DR6 data set test

We have done around 2000 null tests on the data, we checked that the results do not depends on

- array bands
- weather conditions
- scan elevation
- sky location
- time of observation
- detectors positions





Non-Gaussian and Systematic Error Budget

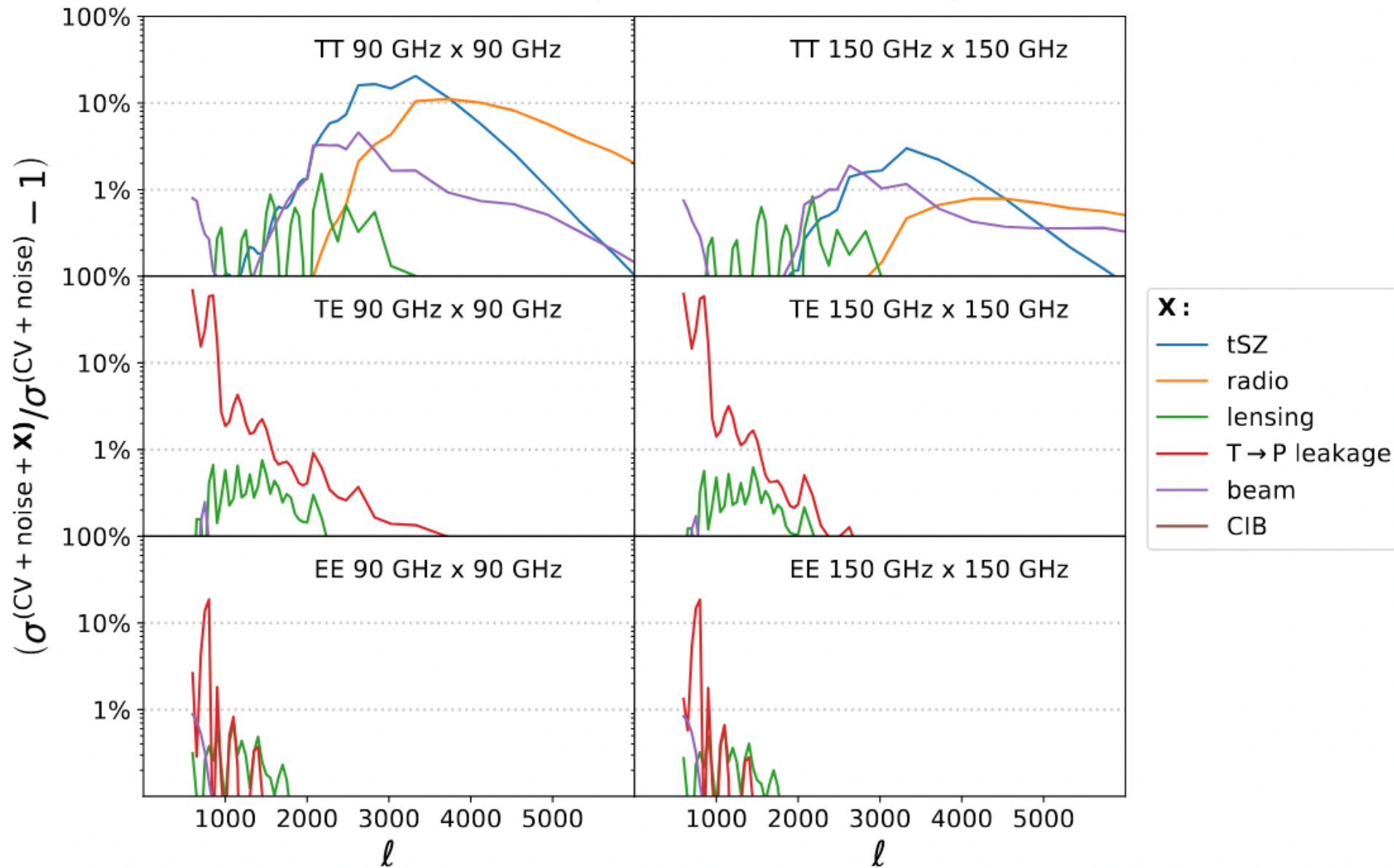


Figure 4. Relative contributions of additional error terms compared to cosmic variance and noise. The contributions to σ_{TT} are shown in the top panel for 90 GHz (left) and 150 GHz (right). For f090, uncertainties from non-Gaussian tSZ and non-Gaussian radio sources are important on small scales. The contribution from unclustered CIB non-Gaussianity is smaller than 0.1% and not visible in the figure. The middle panel shows the contributions to σ_{TE} , where uncertainties in the measurement of the leakage beam are a significant source of uncertainty on large scales. The bottom panel highlights that these uncertainties only mildly affect σ_{EE} , reaching up to 15% at $\ell = 800$. In addition to increasing errors, the additional covariance contributions also result in nonzero off-diagonal correlations.

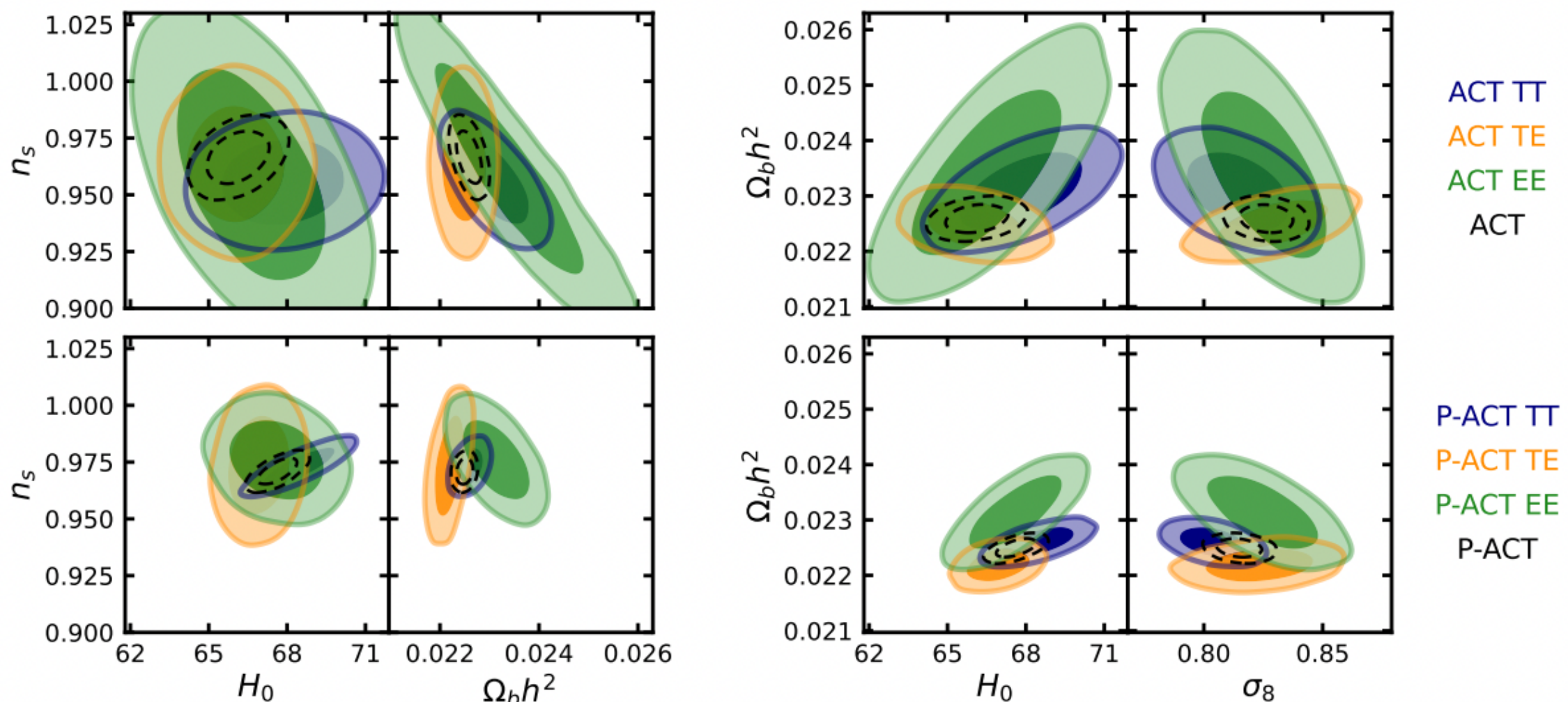


Figure 14. Cosmological parameter distributions estimated from TT, TE or EE from ACT (top) and P-ACT (bottom), including the optical depth prior. Black dashed contours correspond to the distributions estimated from TT, TE, and EE simultaneously, again for ACT (top) and P-ACT (bottom). A prior on the ACT polarization efficiencies, derived from the joint T+E fit, is imposed for the ACT (top) results. For ACT, the TE data provide the tightest constraints on the baryon density, cold dark matter density and the Hubble constant, while the TT data best measure the spectral index. The EE-only constraints are now competitive with those from TT and TE. There is less foreground contamination in the TE and EE spectra than TT; the consistent results add confidence in the model.

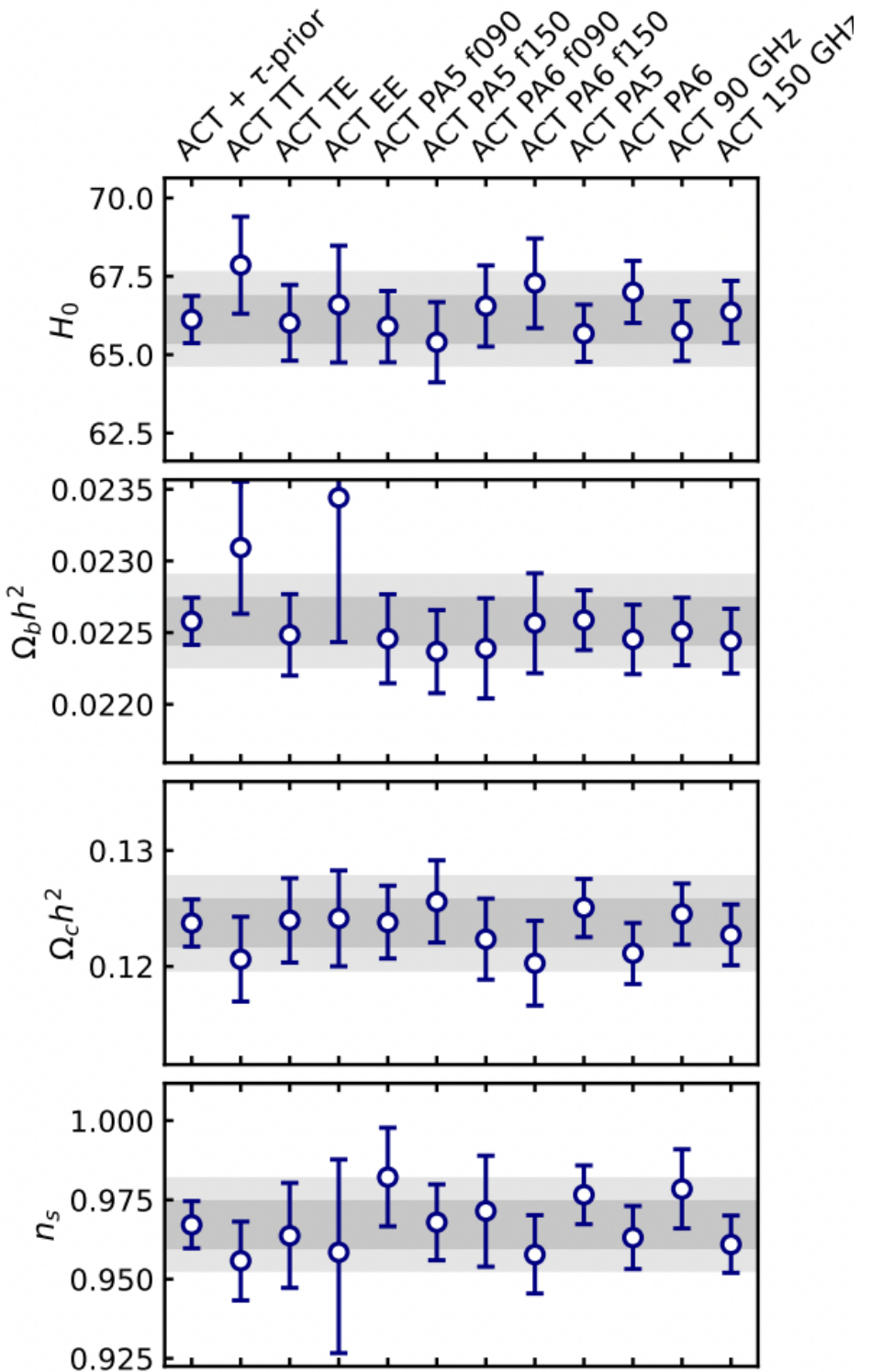


Figure 13. 1D marginalized 68% confidence levels (CL) on cosmological parameters estimated from subsets of the ACT DR6 dataset. The baryon and CDM densities are best measured by the TE spectrum, and the spectral index by the TT spectrum. The different arrays and frequencies give consistent results. All the results shown here use the same optical depth prior. The shaded band shows the 68% and 95% CL on the baseline ACT results.

Breakdown of goodness-of-fit for P-ACT

TT:

- ACT: 566.05/601
- Planck: 89.05/114

TE:

- ACT: 651.77/644
- Planck: 67.82/69

EE:

- ACT: 392.19/406
- Planck: 68.93/69

	ACT	Planck	W-ACT	P-ACT	P-ACT-LB
Parameter					
Sampled					
$10^4\theta_{\text{MC}}$	104.056 ± 0.031 ...	104.088 ± 0.031 ...	104.066 ± 0.029 ...	104.073 ± 0.025 ...	104.086 ± 0.025 ...
$10^2\Omega_b h^2$	2.259 ± 0.017	2.237 ± 0.015	2.263 ± 0.012	2.250 ± 0.011	2.256 ± 0.011
$10^2\Omega_c h^2$	12.38 ± 0.21	12.00 ± 0.14	12.20 ± 0.18	11.93 ± 0.12	11.79 ± 0.09
$\log(10^{10}A_s)$	3.053 ± 0.013	$3.054^{+0.012}_{-0.013}$	$3.057^{+0.010}_{-0.012}$	3.056 ± 0.013	$3.060^{+0.011}_{-0.012}$
n_s	0.9666 ± 0.0077 ...	0.9651 ± 0.0044 ...	0.9660 ± 0.0046 ...	0.9709 ± 0.0038 ...	0.9743 ± 0.0034 ...
τ [%]	$5.62^{+0.53}_{-0.63}$	$5.90^{+0.55}_{-0.65}$	$5.71^{+0.54}_{-0.64}$	$6.03^{+0.55}_{-0.65}$	$6.32^{+0.55}_{-0.66}$
Derived					
H_0 [km/s/Mpc]	66.11 ± 0.79	67.31 ± 0.61	66.78 ± 0.68	67.62 ± 0.50	68.22 ± 0.36
Ω_m [%]	33.7 ± 1.3	31.58 ± 0.85	32.6 ± 1.1	31.16 ± 0.71	30.32 ± 0.48
Ω_b [%]	5.17 ± 0.12	4.937 ± 0.070	5.075 ± 0.098	4.920 ± 0.063	4.847 ± 0.044
Ω_c [%]	28.3 ± 1.2	26.50 ± 0.78	27.37 ± 0.96	26.10 ± 0.65	25.34 ± 0.44
Ω_Λ [%]	66.3 ± 1.3	68.41 ± 0.85	67.4 ± 1.1	68.83 ± 0.71	69.67 ± 0.48
$10^2\Omega_m h^2$	14.70 ± 0.21	14.31 ± 0.13	14.53 ± 0.18	14.25 ± 0.12	14.11 ± 0.08
$n_s - 1$ [%]	-3.34 ± 0.77	-3.49 ± 0.44	-3.40 ± 0.46	-2.91 ± 0.38	-2.57 ± 0.34
σ_8	0.8263 ± 0.0074 ...	0.8151 ± 0.0066 ...	0.8221 ± 0.0070 ...	0.8149 ± 0.0063 ...	0.8126 ± 0.0046 ...
S_8	0.875 ± 0.023	0.836 ± 0.016	0.857 ± 0.020	0.830 ± 0.014	0.8169 ± 0.0087
Age [Gyr]	13.801 ± 0.023	13.800 ± 0.024	13.788 ± 0.019	13.789 ± 0.018	13.772 ± 0.015
$10^4\theta_\star$	104.075 ± 0.031 ...	104.109 ± 0.031 ...	104.085 ± 0.029 ...	104.094 ± 0.025 ...	104.107 ± 0.025 ...
10^4Y_{He}	2459.50 ± 0.71	2458.55 ± 0.64	2459.66 ± 0.51	2459.10 ± 0.48	2459.37 ± 0.46
$10^{10}\eta_b$	6.185 ± 0.046	6.124 ± 0.041	6.196 ± 0.033	6.159 ± 0.030	6.177 ± 0.029
z_{reio}	$7.88^{+0.54}_{-0.61}$	$8.15^{+0.55}_{-0.62}$	$7.93^{+0.54}_{-0.61}$	8.23 ± 0.59	$8.47^{+0.54}_{-0.61}$
τ_{rec} [Mpc]	593.6 ± 3.1	599.5 ± 2.0	596.2 ± 2.6	600.4 ± 1.8	602.4 ± 1.3
z_\star	1089.96 ± 0.30	1089.92 ± 0.29	1089.75 ± 0.24	1089.68 ± 0.21	1089.47 ± 0.18
$r_{s,\star}$ [Mpc]	143.32 ± 0.54	144.43 ± 0.31	143.74 ± 0.45	144.53 ± 0.29	144.85 ± 0.22
z_d	1060.72 ± 0.39	1059.94 ± 0.29	1060.67 ± 0.28	1060.17 ± 0.23	1060.21 ± 0.23
r_d [Mpc]	145.88 ± 0.56	147.09 ± 0.30	146.30 ± 0.46	147.14 ± 0.29	147.45 ± 0.23
$-2\ln\mathcal{L}_{\text{posterior}}^{\text{MAP}}$	1929.71	996.82	3934.93	2180.49	2216.71
χ^2_{MFLike}	$1590.91(1651)$	$1592.20(1651)$	$1597.72(1651)$	$1598.13(1651)$
$\chi^2_{\text{Planck-high}\ell}$	$583.16(613)$	$221.51(252)$	$221.02(252)$
$\chi^2_{\text{Planck-lowT}}$	$23.45(28)$	$22.46(28)$	$22.11(28)$
χ^2_{WMAP}	$2017.02(1945)$
χ^2_{CMBlens}	$19.63(19)$
$\chi^2_{\text{DESI-BAO}}$	$15.48(12)$

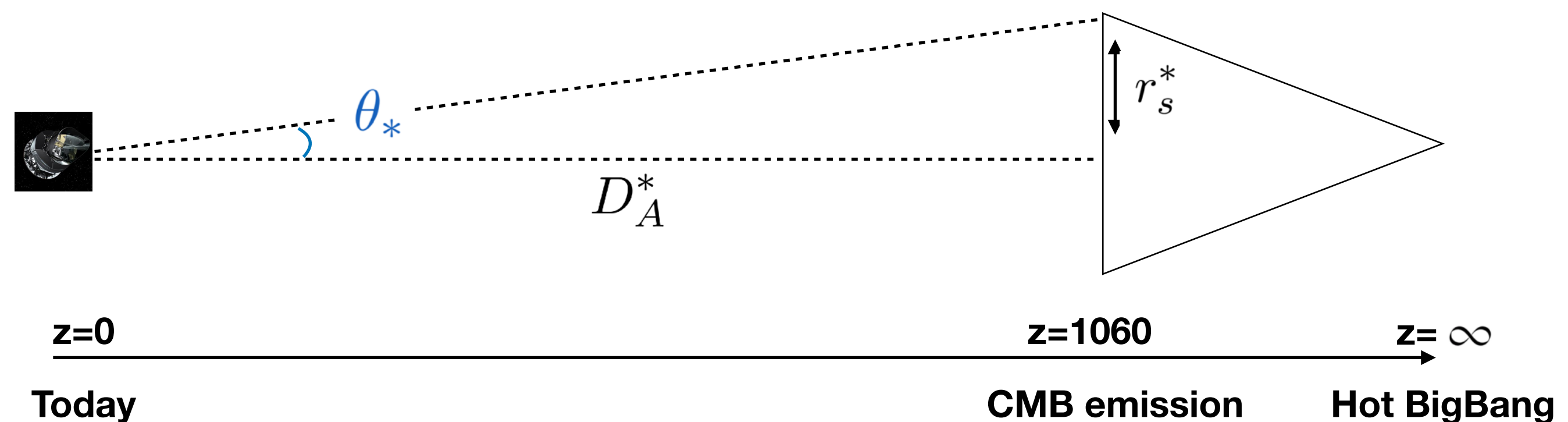
Table 5. Marginalized constraints on the Λ CDM sampled and derived parameters from the ACT data (including the *Planck* Sroll2 large-scale EE data to constrain the optical depth), and its combination with *WMAP* (W-ACT), $\ell < 1000$ *Planck* data (P-ACT), and CMB lensing from ACT and Planck and BAO data from DESI Y1 (P-ACT-LB). Parameter definitions are given in Appendix G.1. The goodness of fit of the best-fitting model, with maximum posterior probability, is reported for the different datasets along with the total maximum a posteriori (MAP) value that includes contributions from the Sroll2 likelihood and informative priors. Numbers in parentheses indicate the number of data points used in the respective χ^2 calculations. For comparison, constraints are shown from the *Planck* PR3 ([Planck Collaboration 2020d](#)) TT/TE/EE data that we rerun with the Sroll2 large-scale polarization data for consistency. Parameter constraints using the *Planck* NPIPE maps in [Rosenberg et al. \(2022\)](#) and [Tristram et al. \(2024\)](#) are typically 10-20% tighter, with comparable errors to our P-ACT combination.

Measuring H_0 from the CMB

Measuring the Hubble constant using the CMB

The angular size of the sound horizon is given as the ratio of the physical size of the sound horizon and the diameter angular distance of the last scattering surface

$$\theta_* = r_s^*/D_A^*$$



Measuring the Hubble constant using the CMB

The angular size of the sound horizon is given as the ratio of the physical size of the sound horizon and the diameter angular distance of the last scattering surface

$$\theta_* = r_s^*/D_A^*$$

r_s^* is fully determined by the cosmological parameters we have measured

We know r_s^* and θ_* this gives us D_A^*

$$D_A^* = c \int_0^{z^*} \frac{dz}{H(z)}$$

$$r_s^* = \int_0^{t^*} \frac{dt}{a(t)} c_s(t) = \int_{z^*}^{\infty} \frac{dz}{H(z)} c_s(z)$$

$$c_s(z) = c \sqrt{\frac{1}{3 [1 + 3\rho_b^0/4\rho_\gamma^0(1+z)^{-1}]}}$$

$$\left. \frac{3H^2(z)}{8\pi G} \right|_{\text{high } z} = [\rho_{\text{rad}}^0(1+z)^4 + (\rho_b^0 + \rho_{\text{CDM}}^0)(1+z)^3]$$

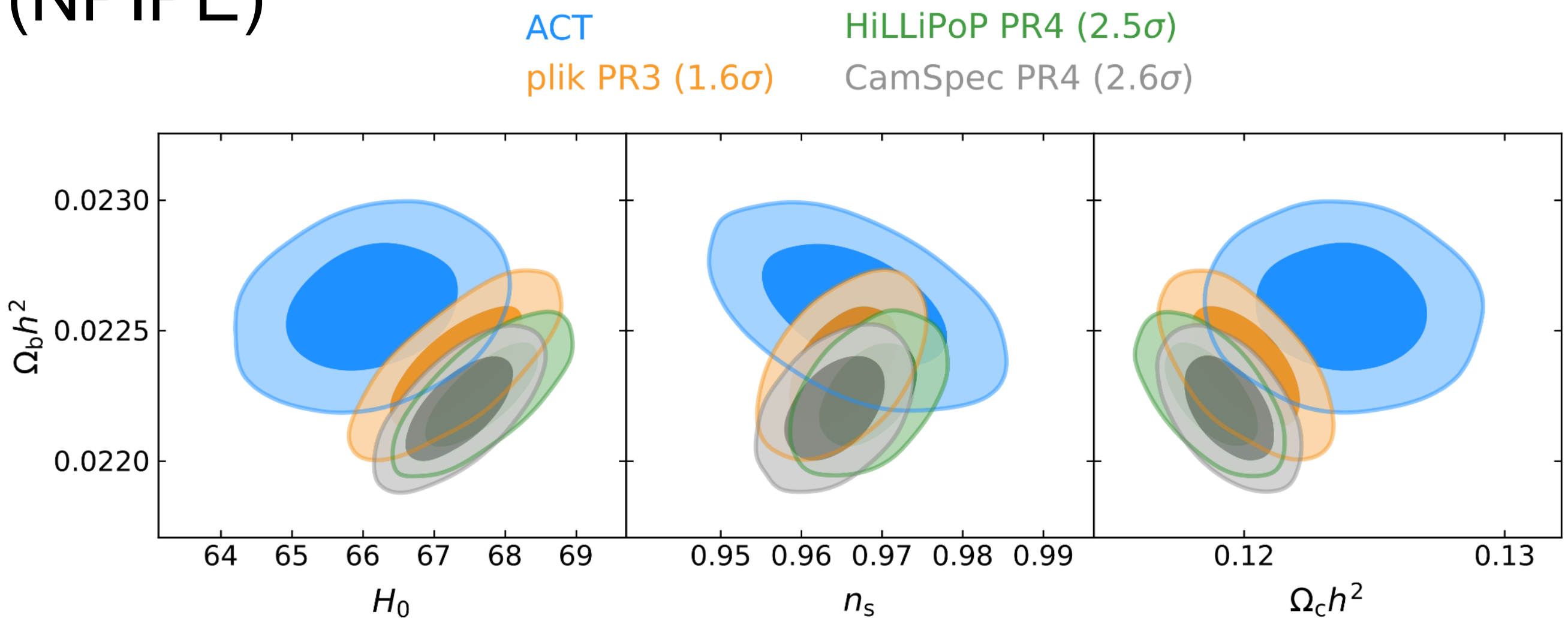
$$\left. \frac{3H^2(z)}{8\pi G} \right|_{\text{low } z} = [(\rho_b^0 + \rho_{\text{CDM}}^0)(1+z)^3 + \rho_\Lambda]$$

Which gives us ρ_Λ

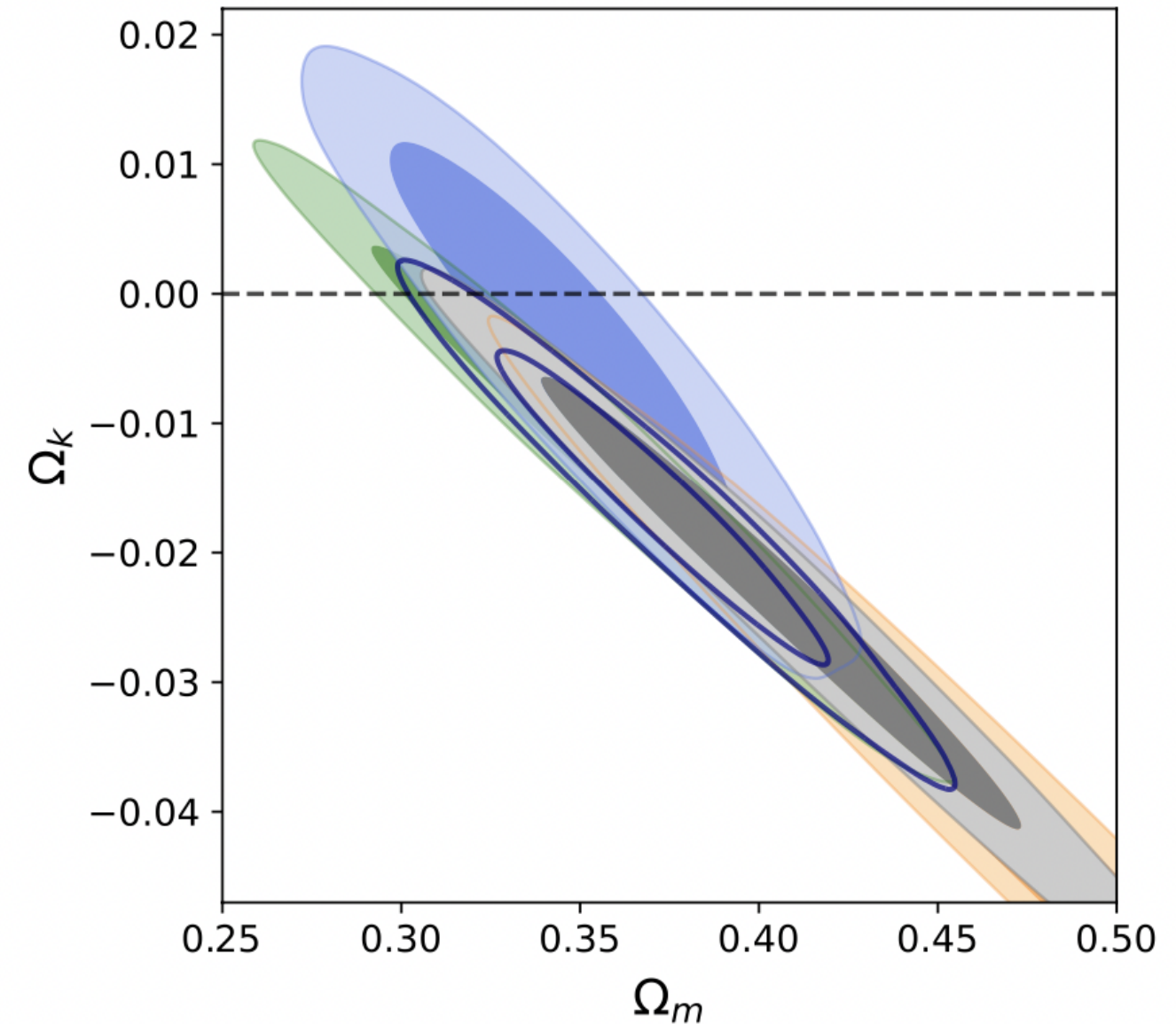
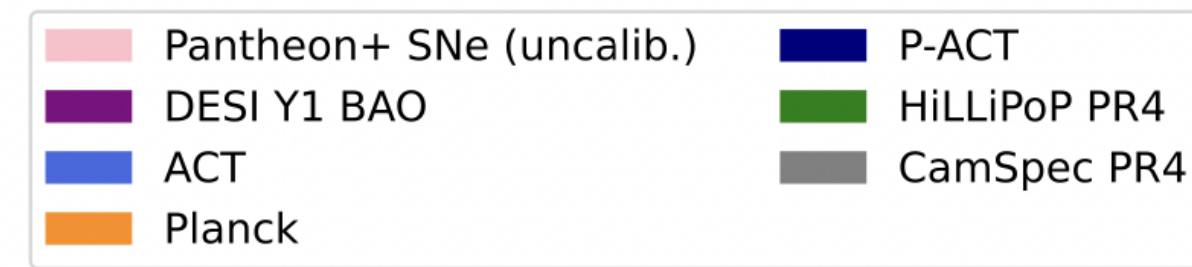
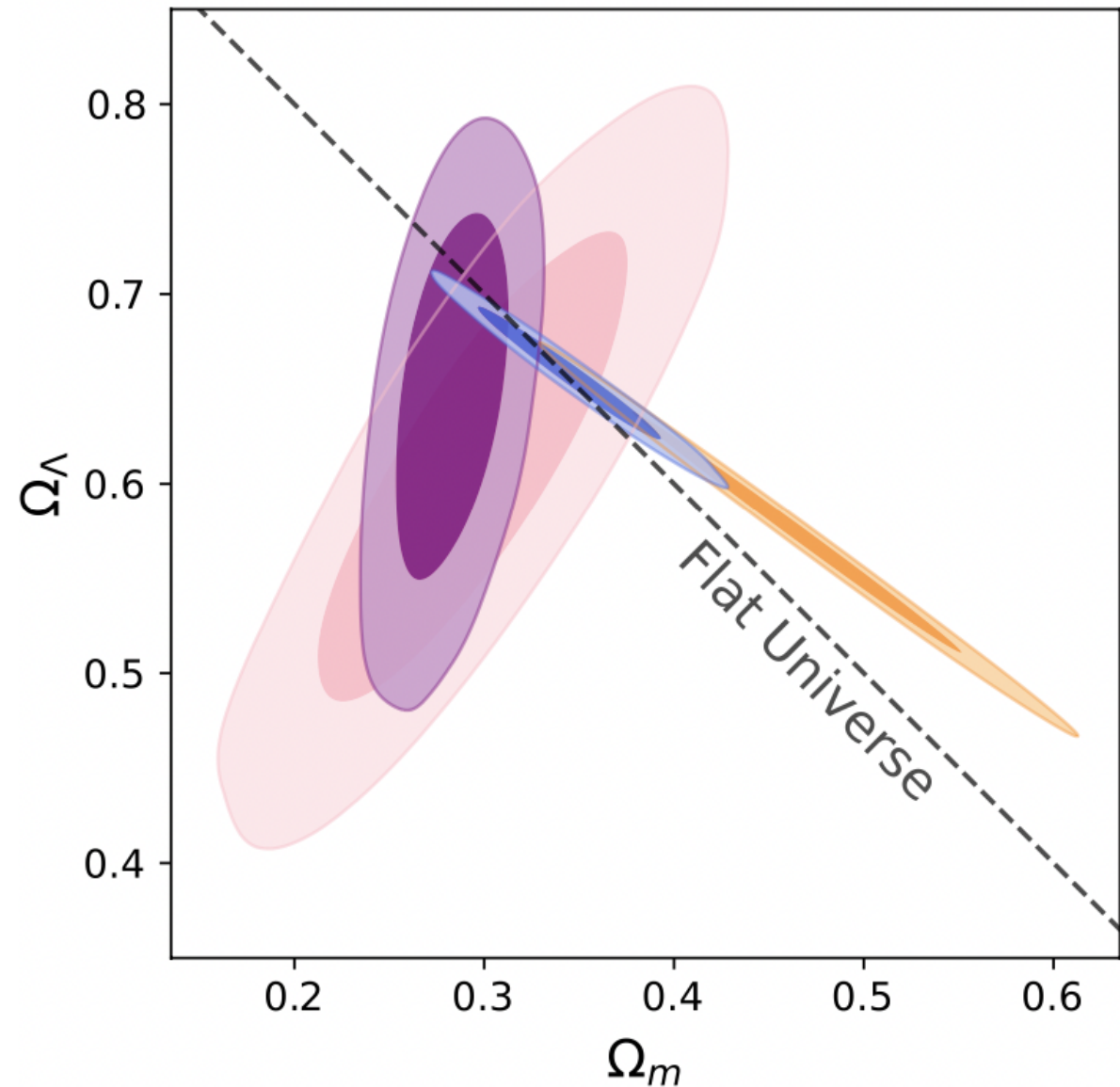
Once ρ_Λ known, we get H_0

PR3 and PR4

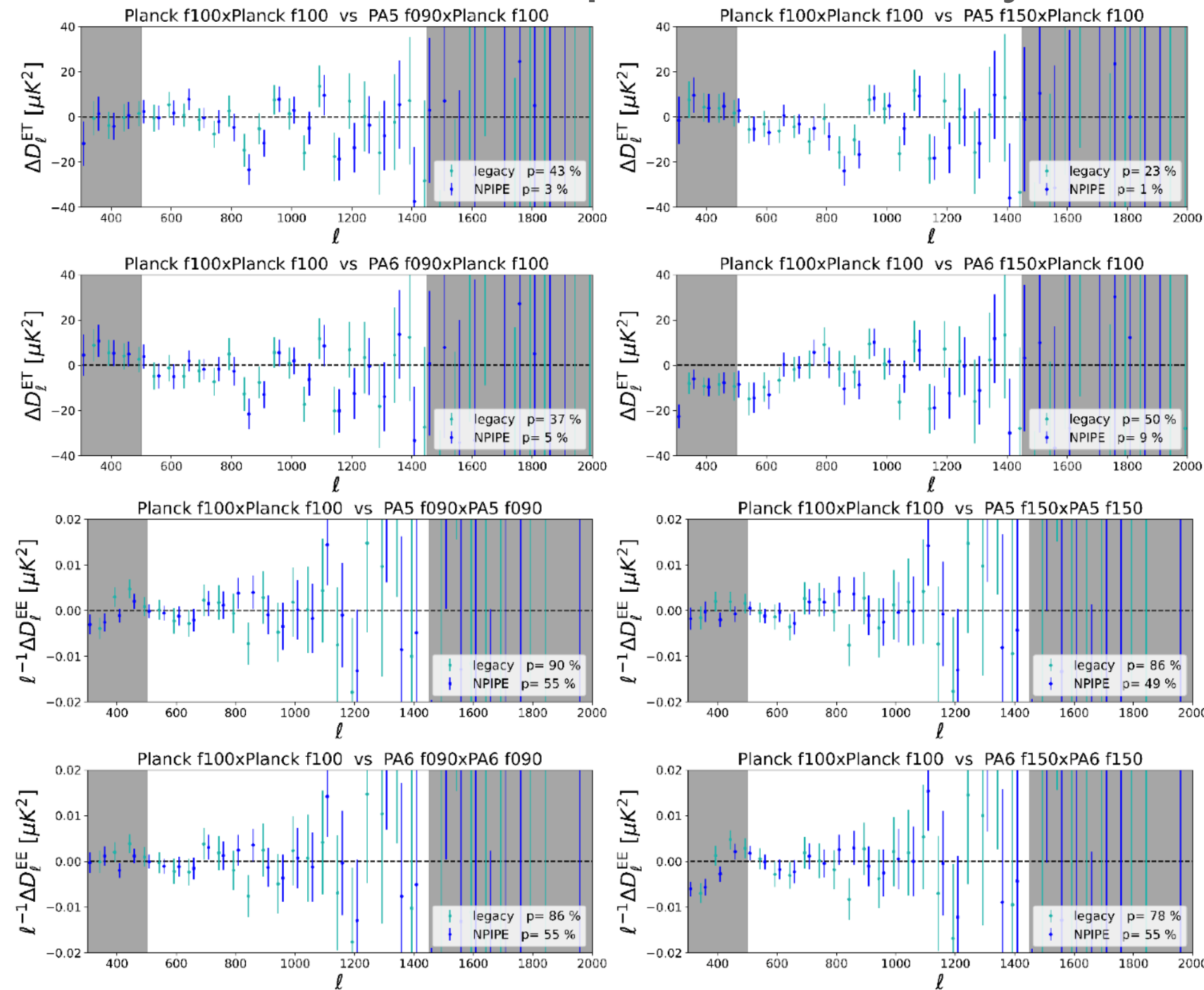
Comparison with Planck PR4 (NPIPE)



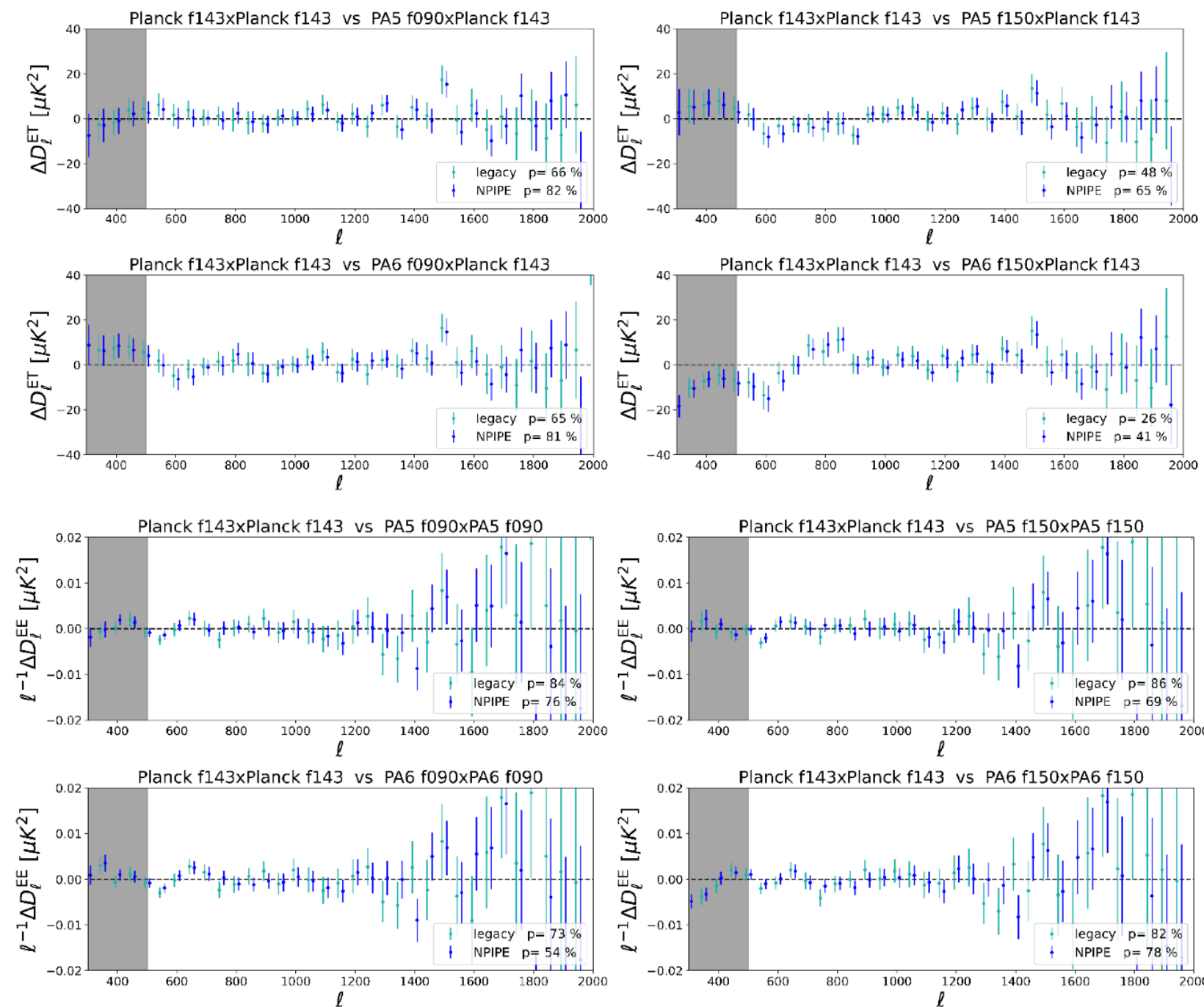
HiLLiPoP/NPIPE, curvature



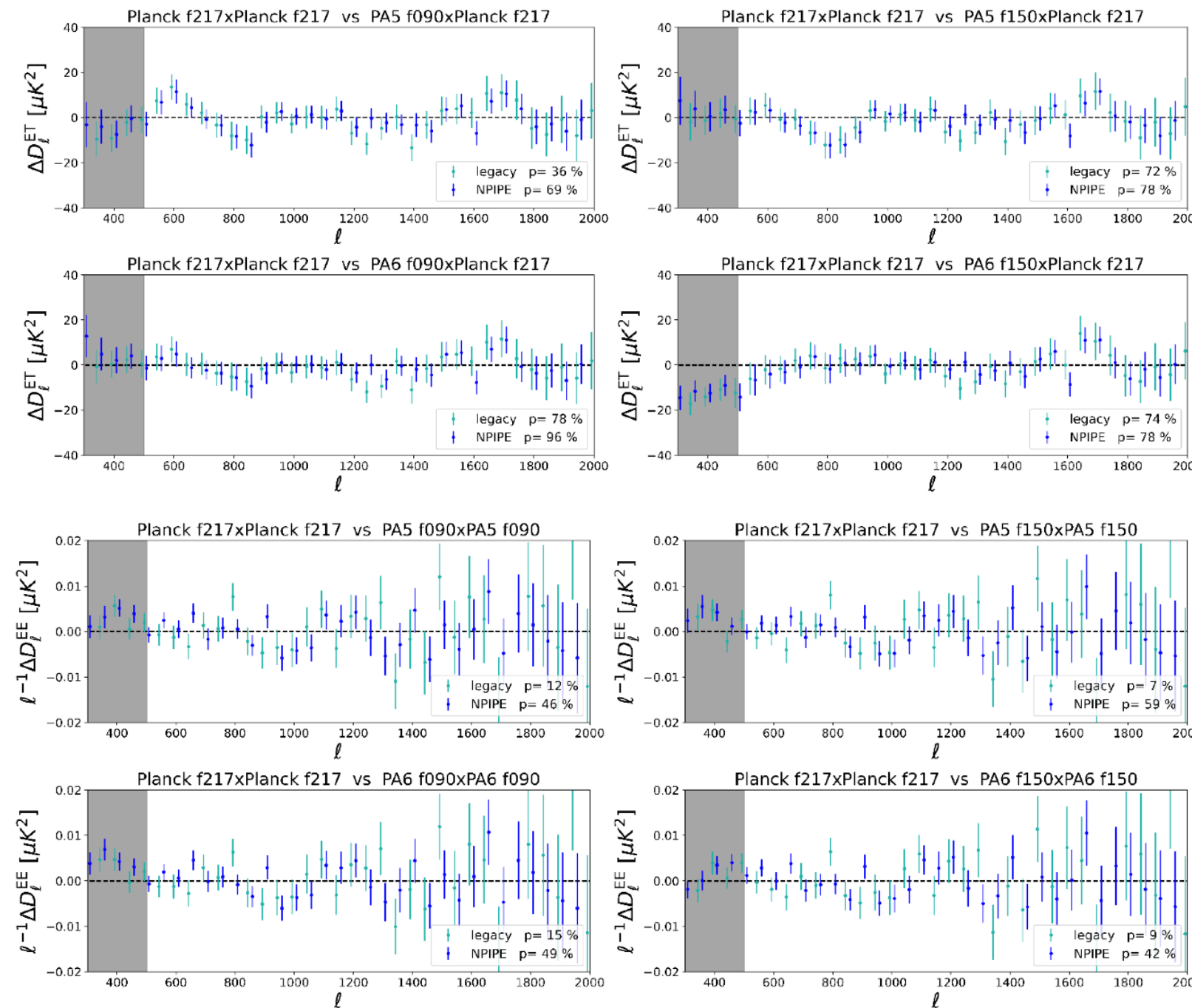
ACT and Planck on the same patch of the sky



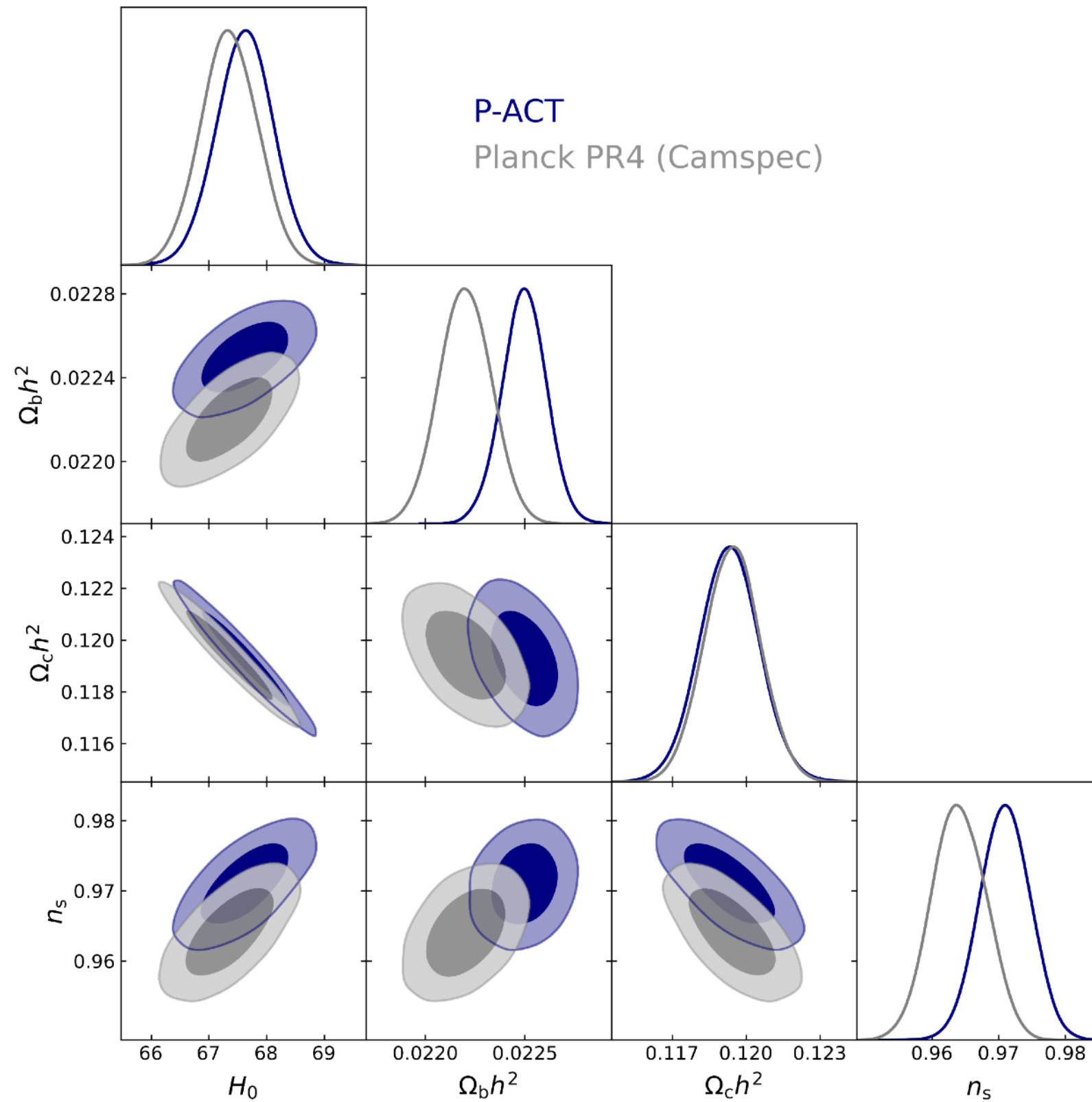
ACT and Planck on the same patch of the sky



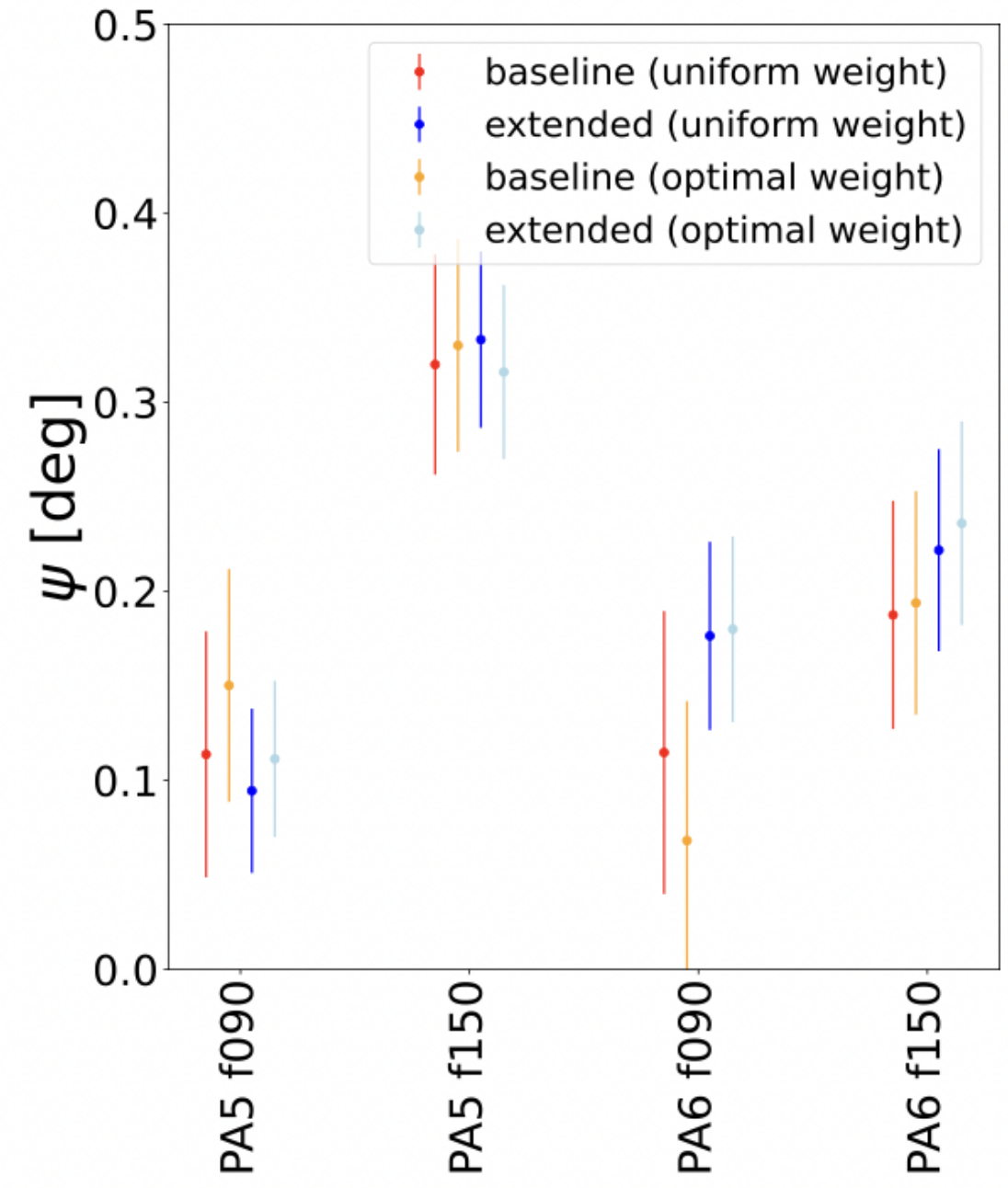
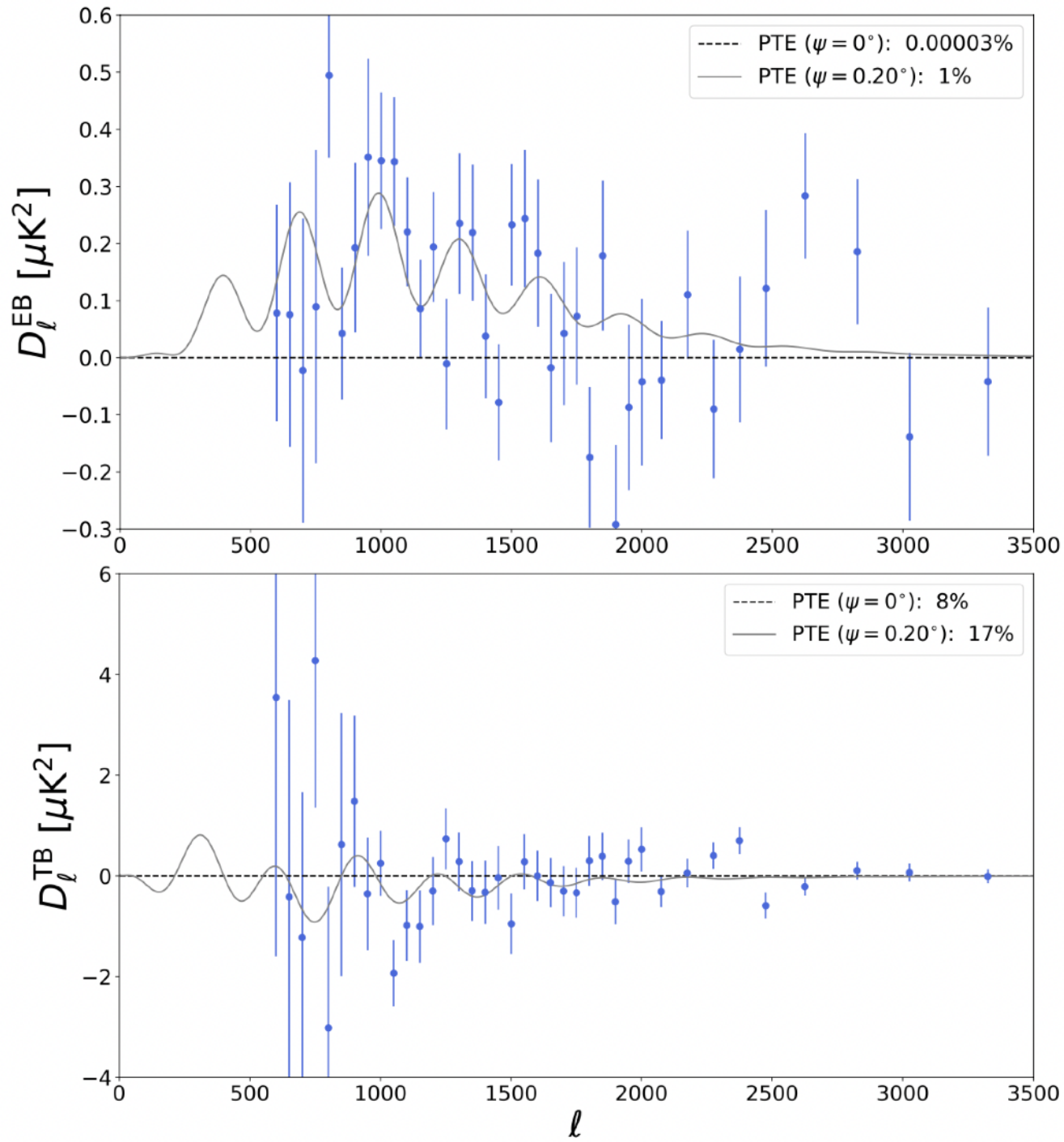
ACT and Planck on the same patch of the sky



Comparison with Planck PR4 (NPIPE)

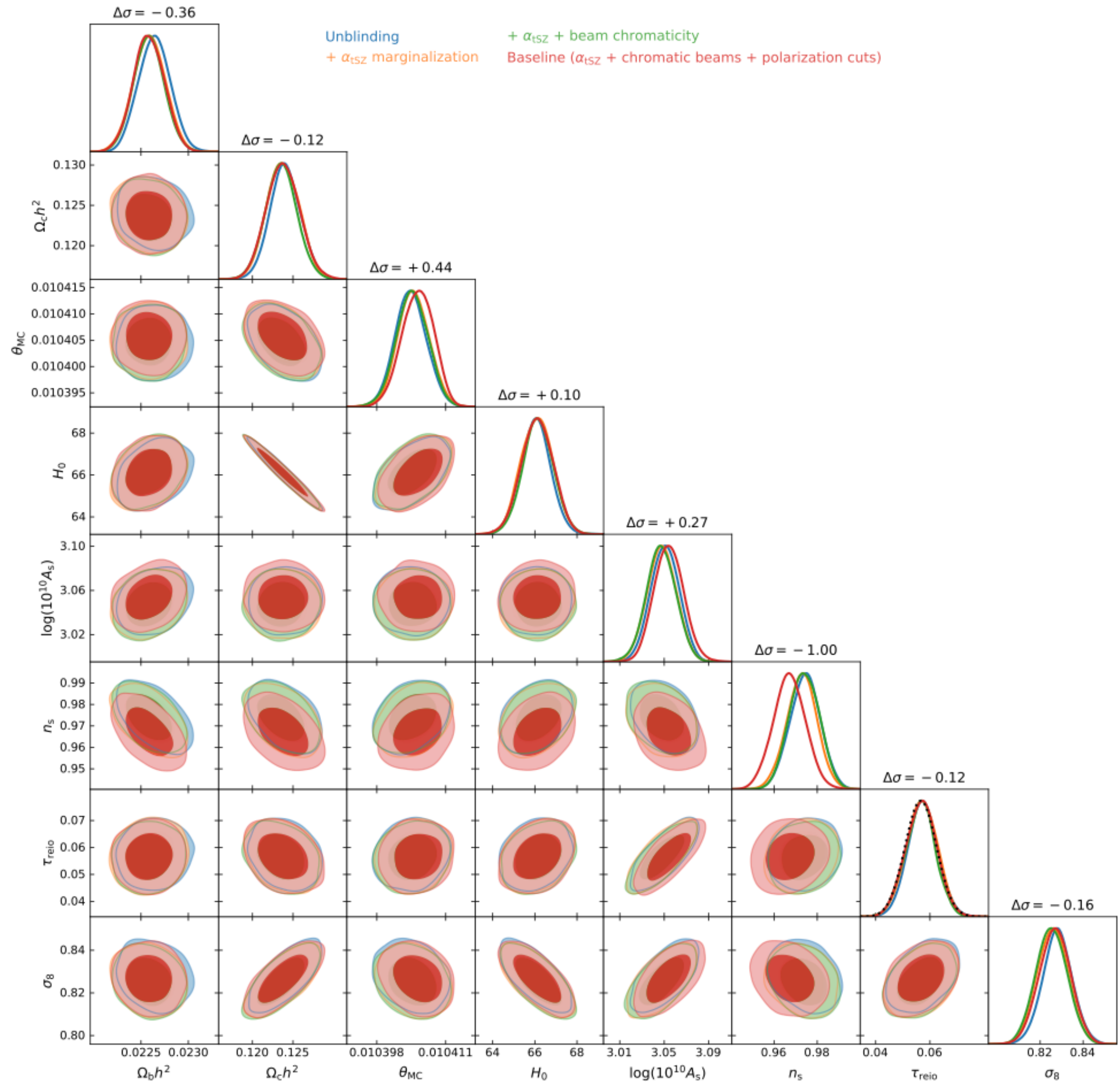


Birefringence

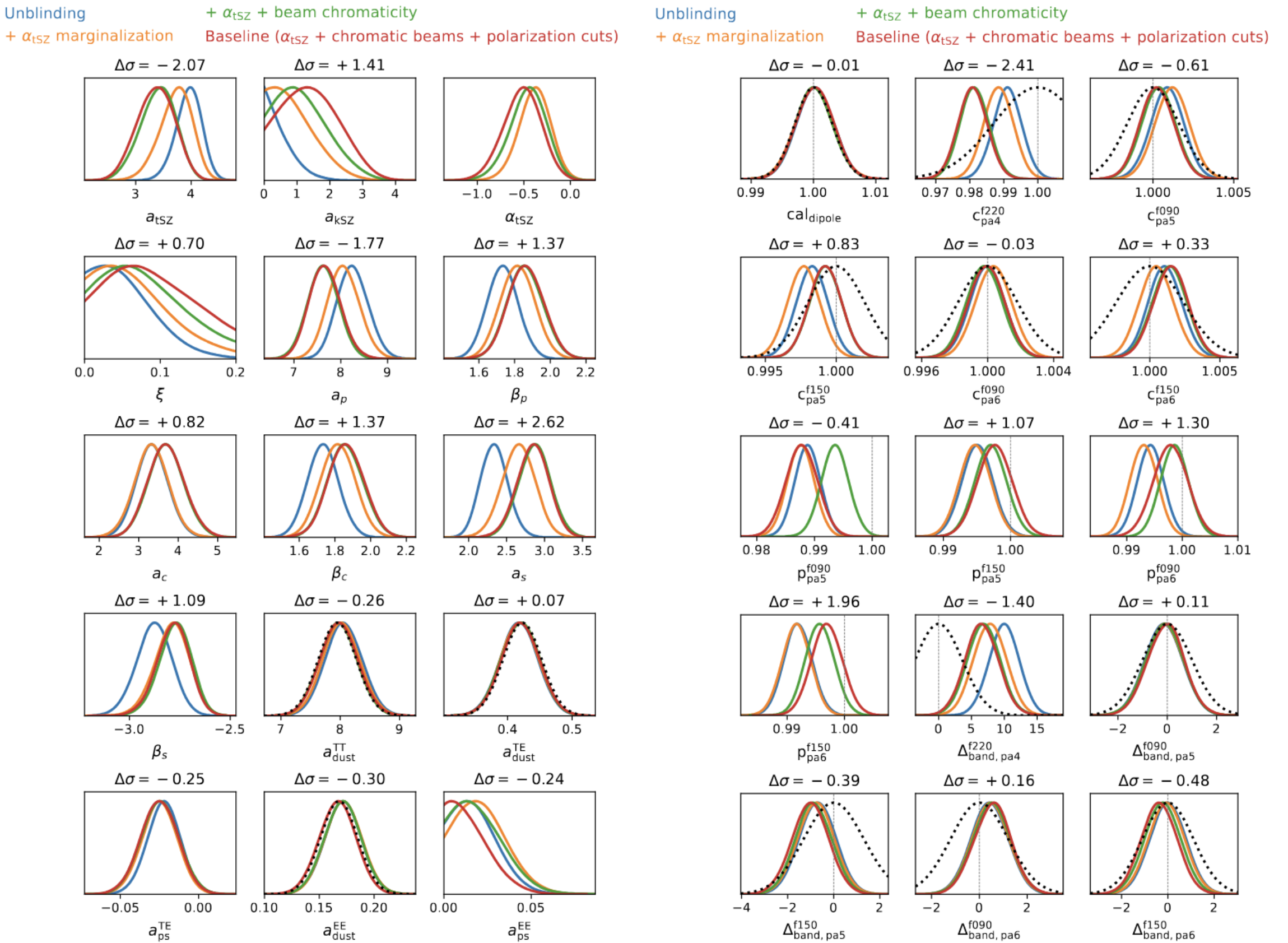


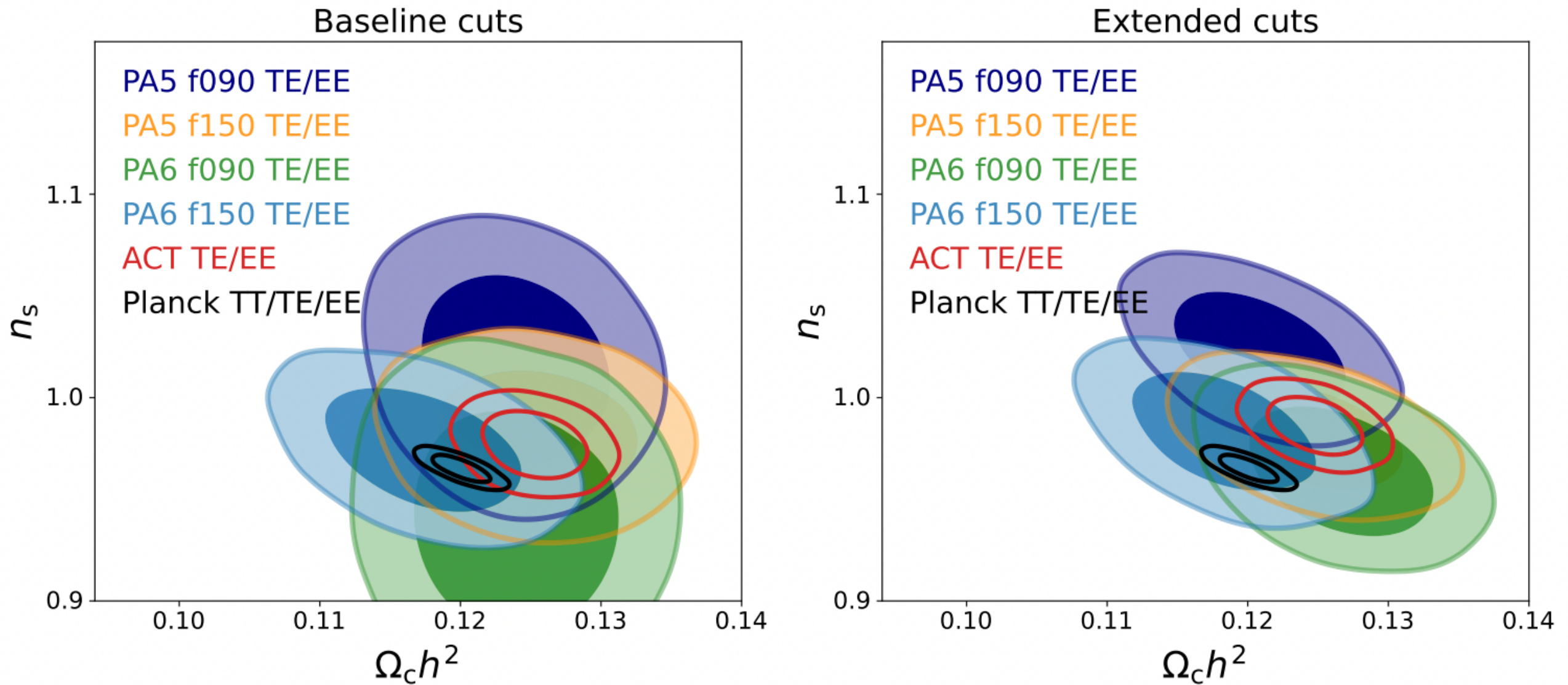
Post unblinding

Cosmo



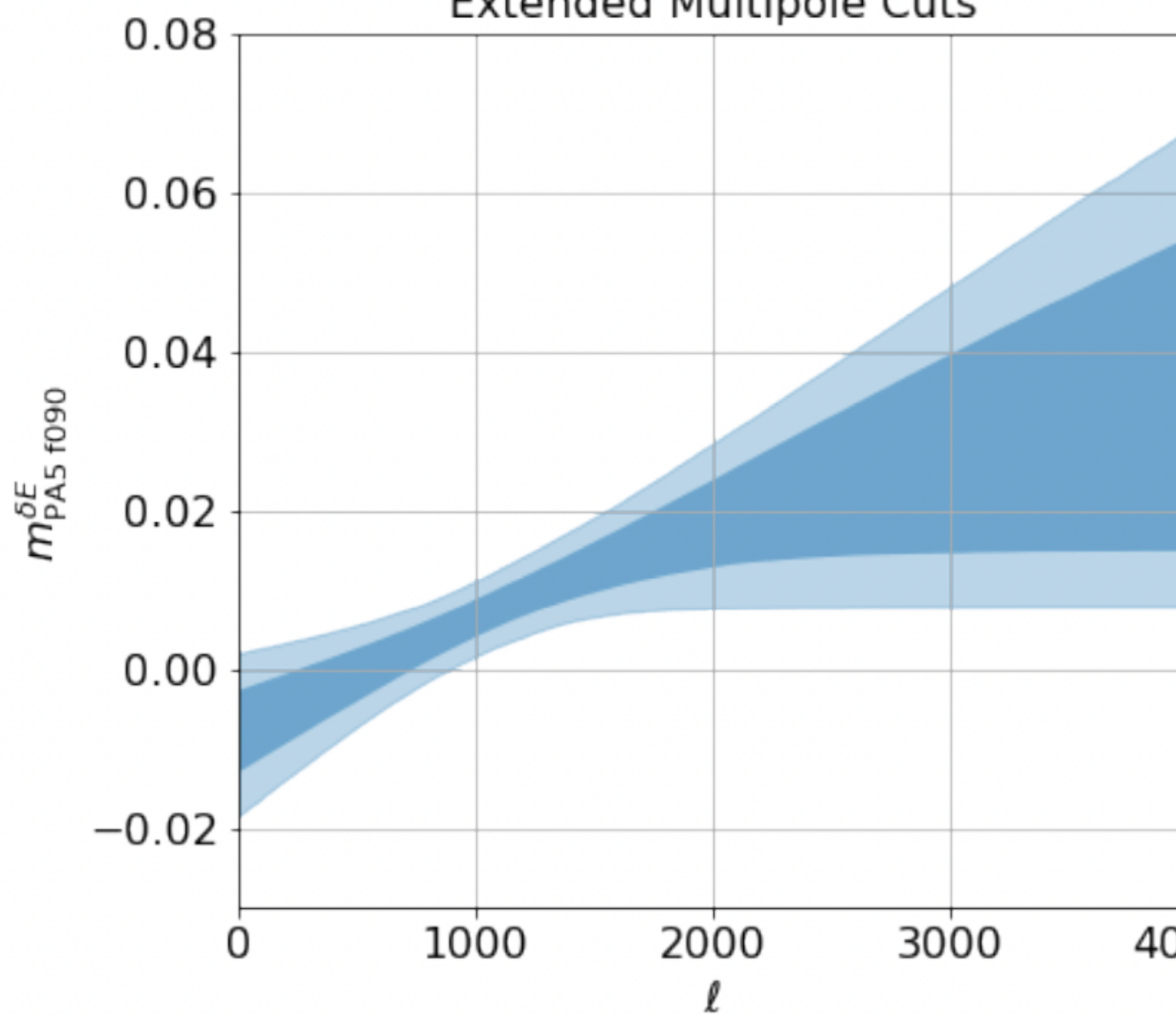
Astrophysical foregrounds and instrument parameters



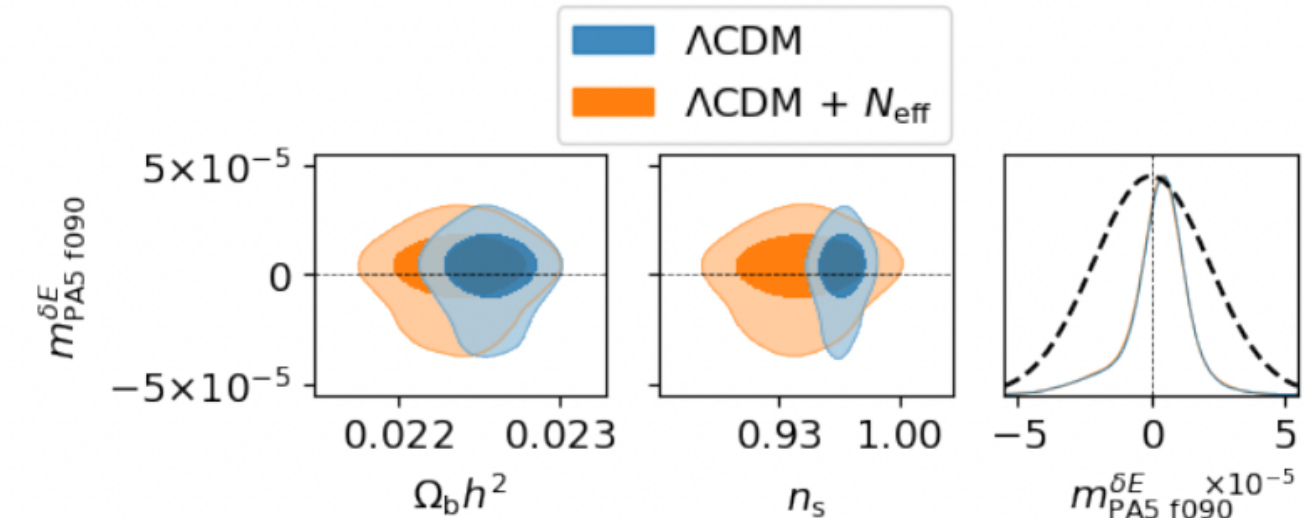
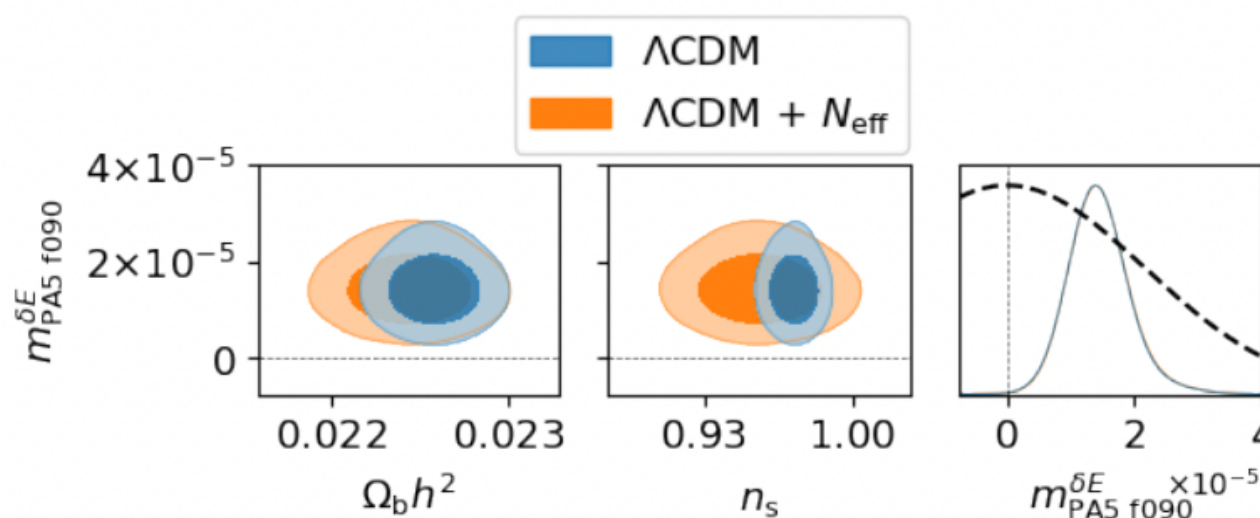
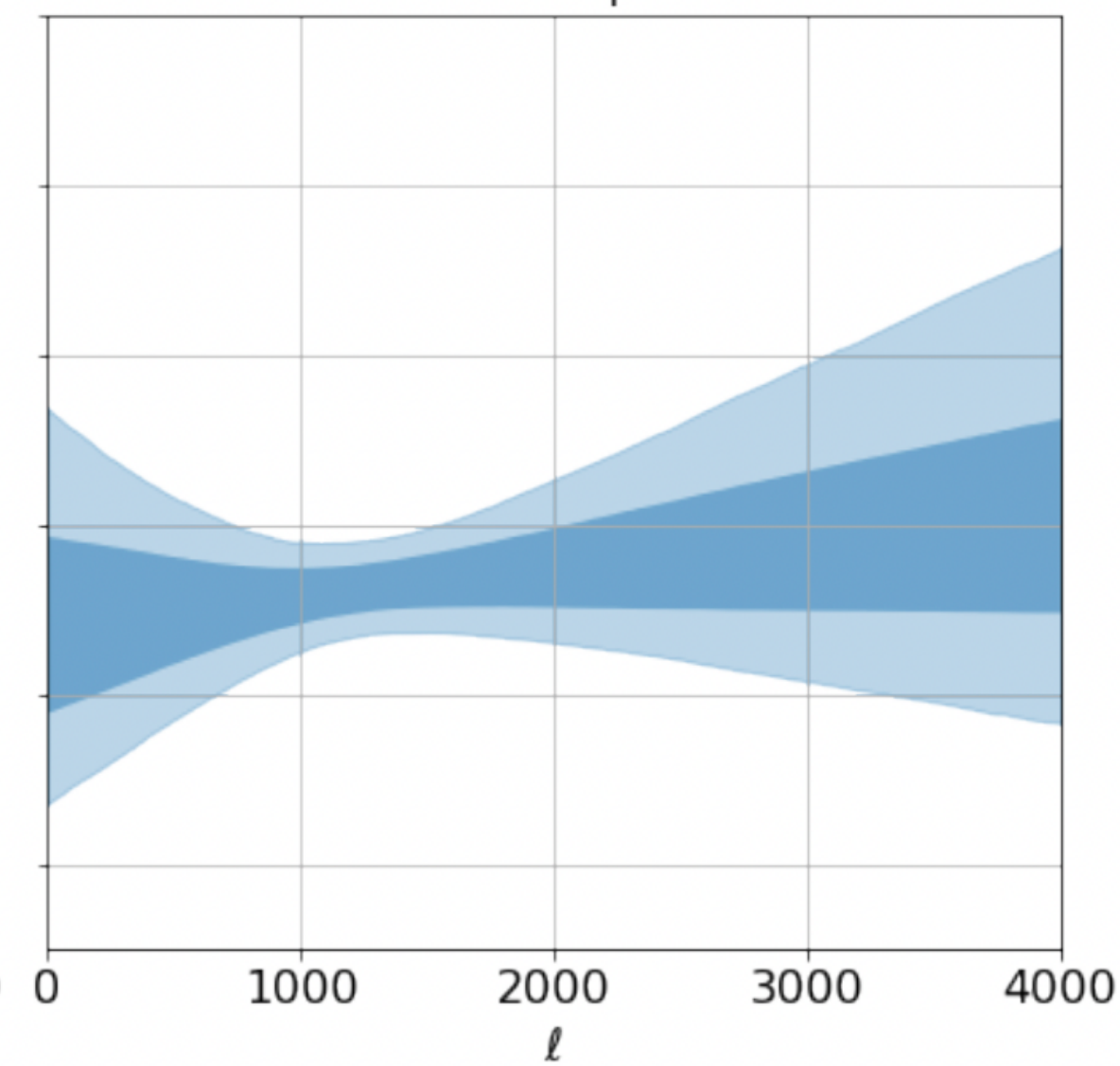


PA5 f090 Relative Multiplicative Systematic

Extended Multipole Cuts



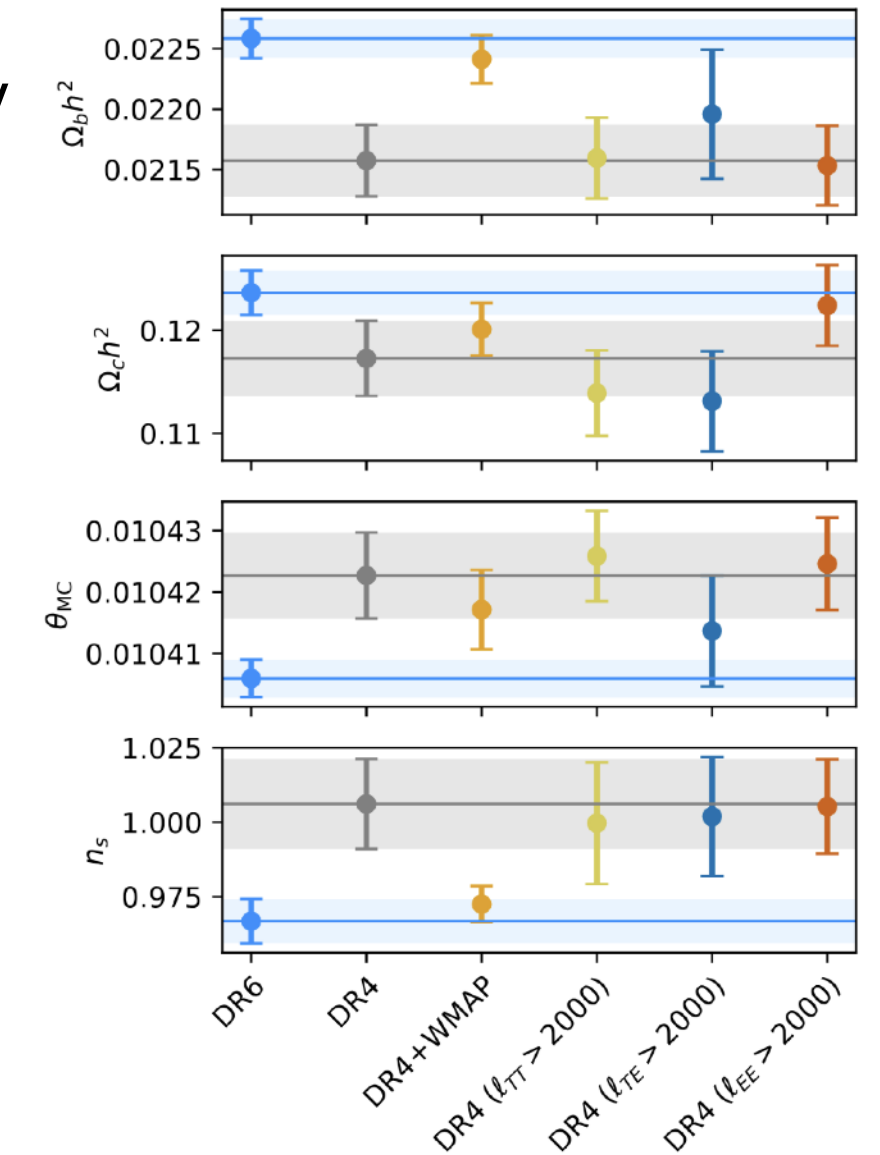
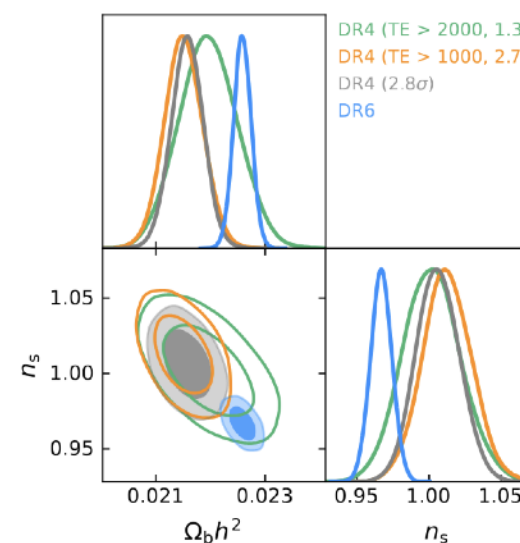
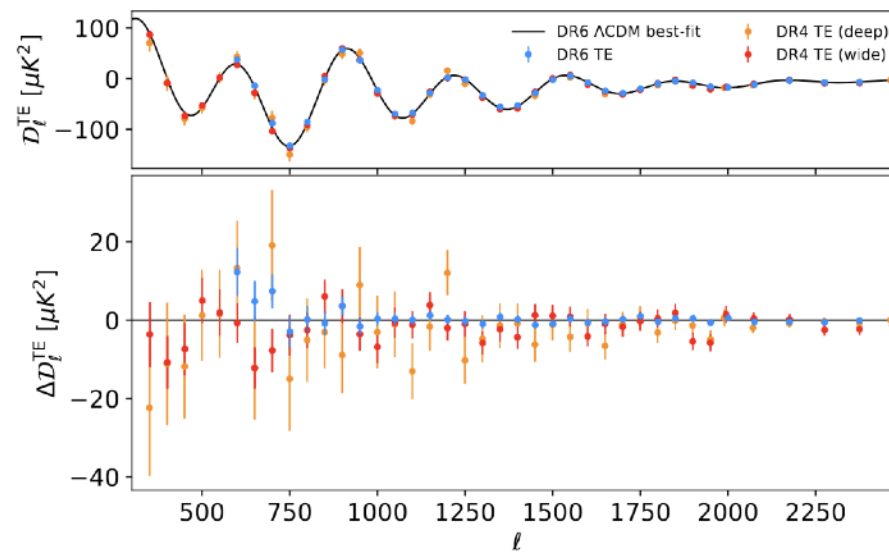
Baseline Multipole Cuts



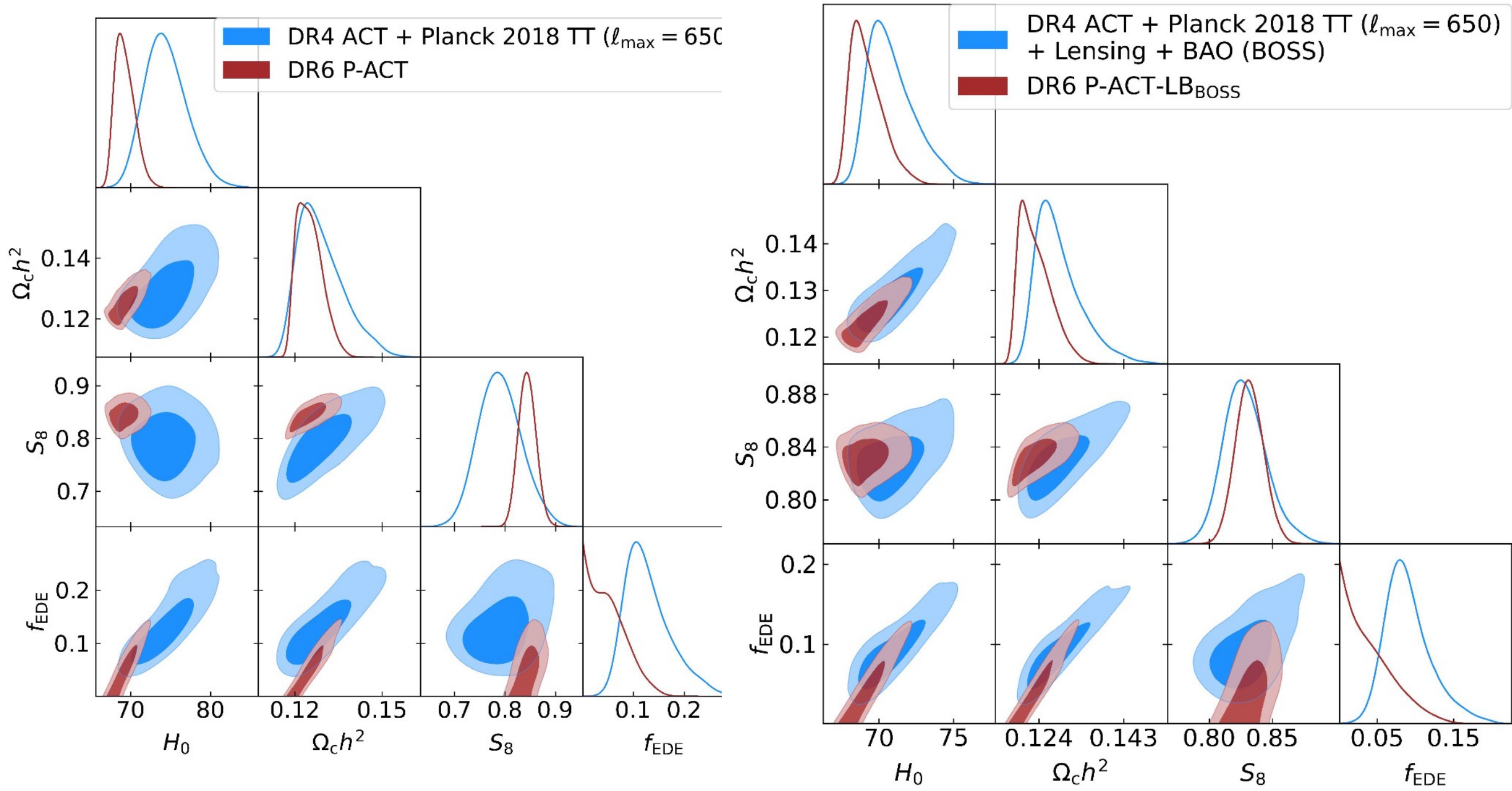
DR6 vs DR4

DR6 vs DR4 cosmology

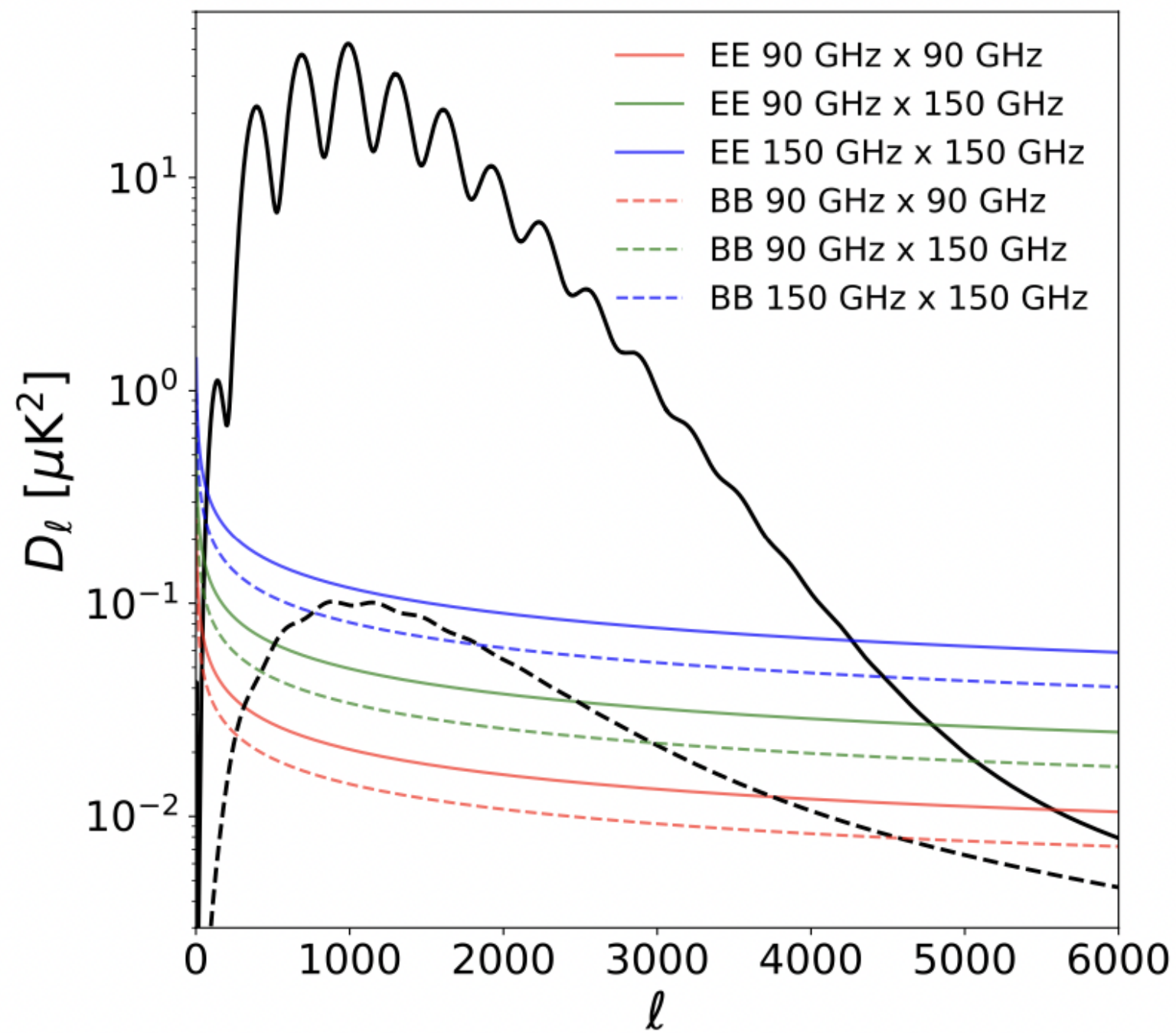
- very good agreement between DR6 and DR4 baseline result obtained from ACT+WMAP
- some differences with DR4 ACT-alone cosmology
- mainly driven by TE data at multipoles < 2000 (where residuals are mostly negative, disfavoring the DR6 LCDM cosmology)
- we speculate beam leakage modelling might be playing a role



Pre- and modified recombination physics: DR4 vs. DR6 EDE constraints



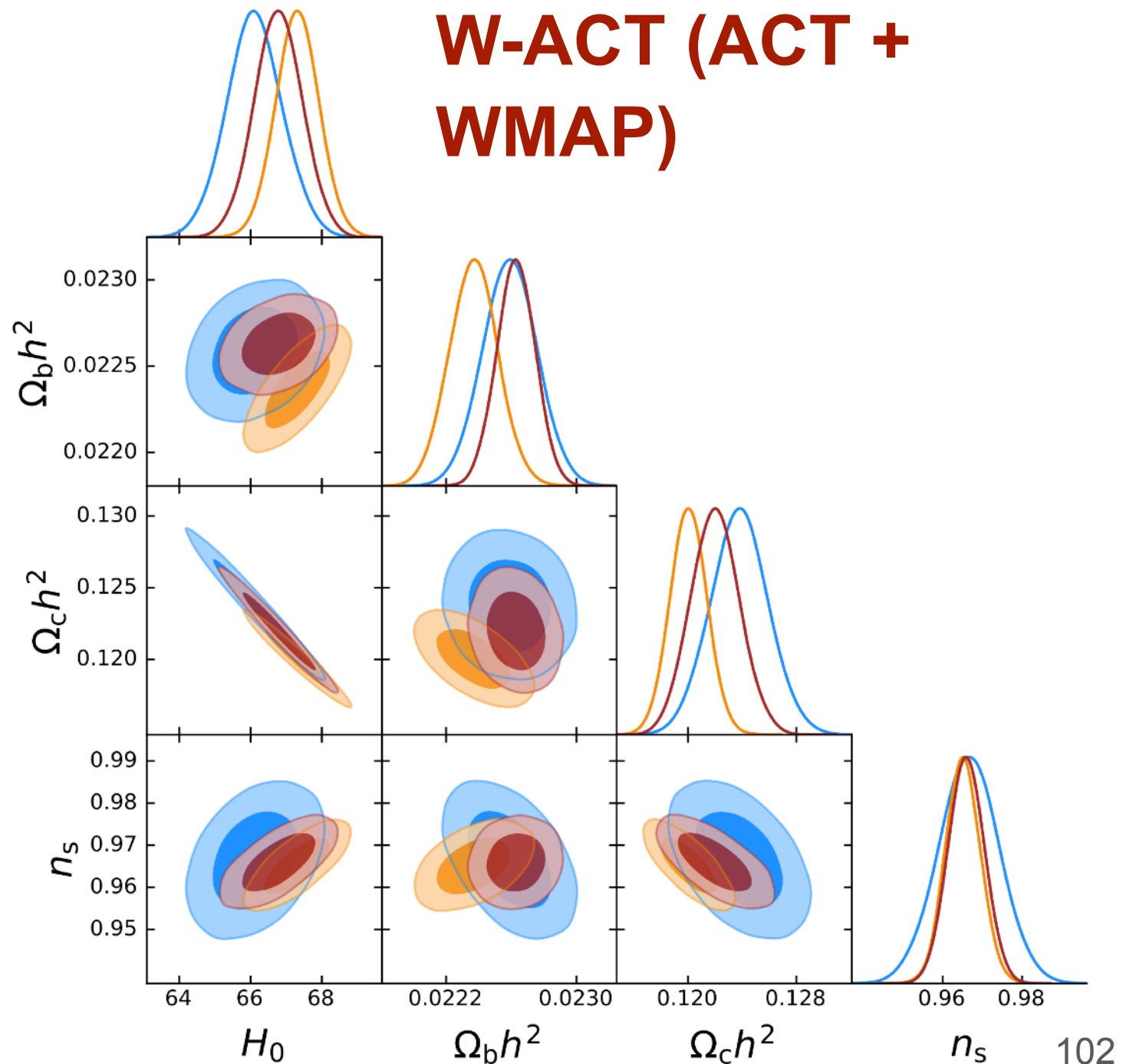
Dust in the DR6 patch



Independent constraints from ACT & WMAP

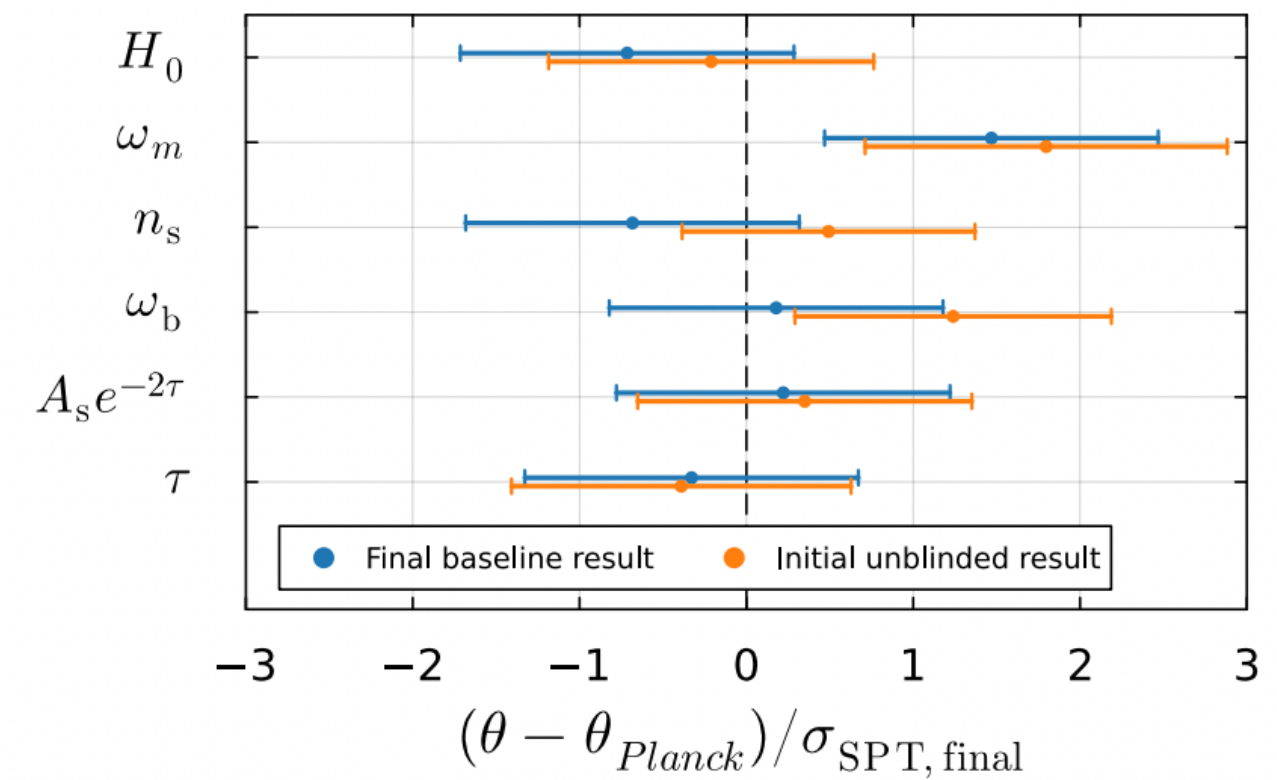
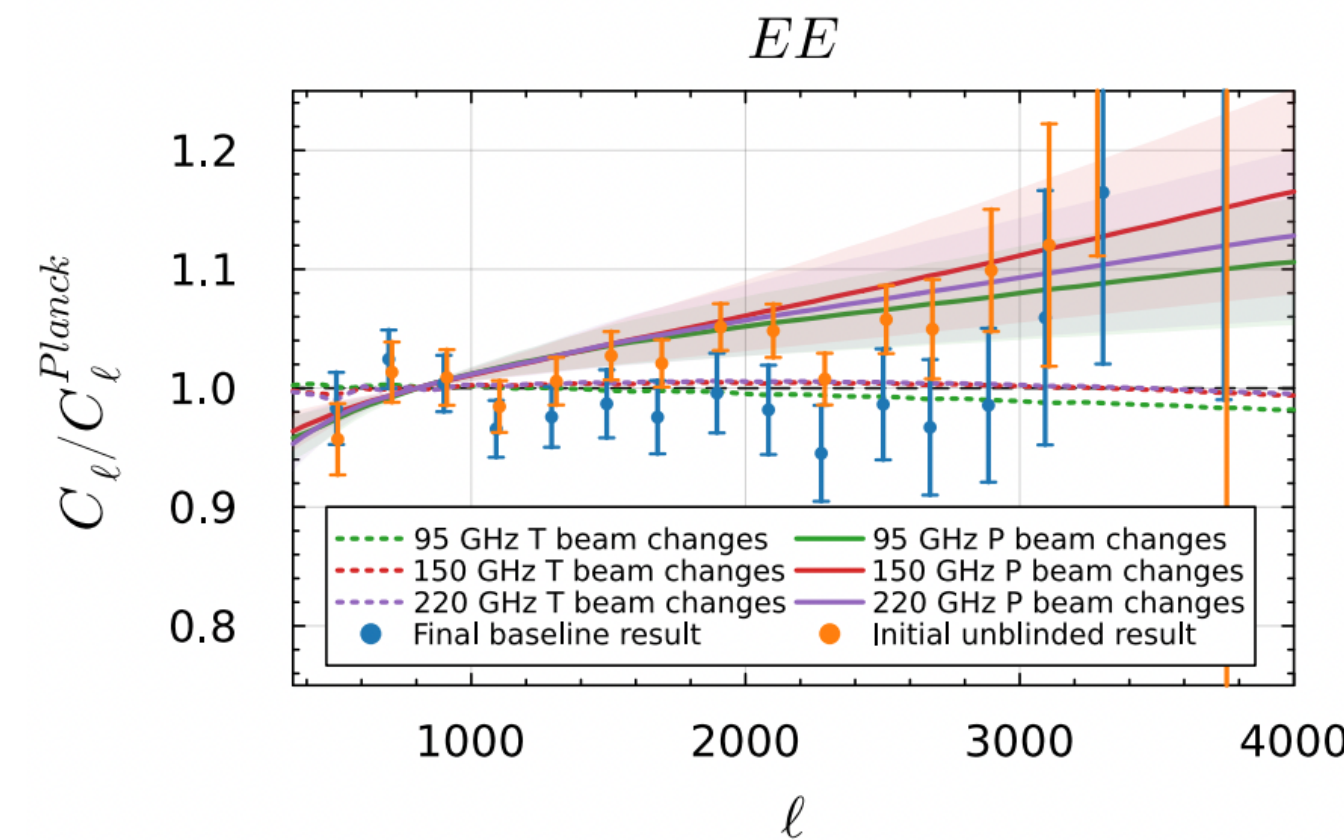
- Cosmological constraints from ACT DR6 and Planck are consistent (1.6σ)
- ACT + WMAP provides an independent and competitive dataset with e.g.
 $\Omega_b h^2 = 0.02263 \pm 0.00012$
 $H_0 = 66.78 \pm 0.68 \text{ km/s/} Mpc$

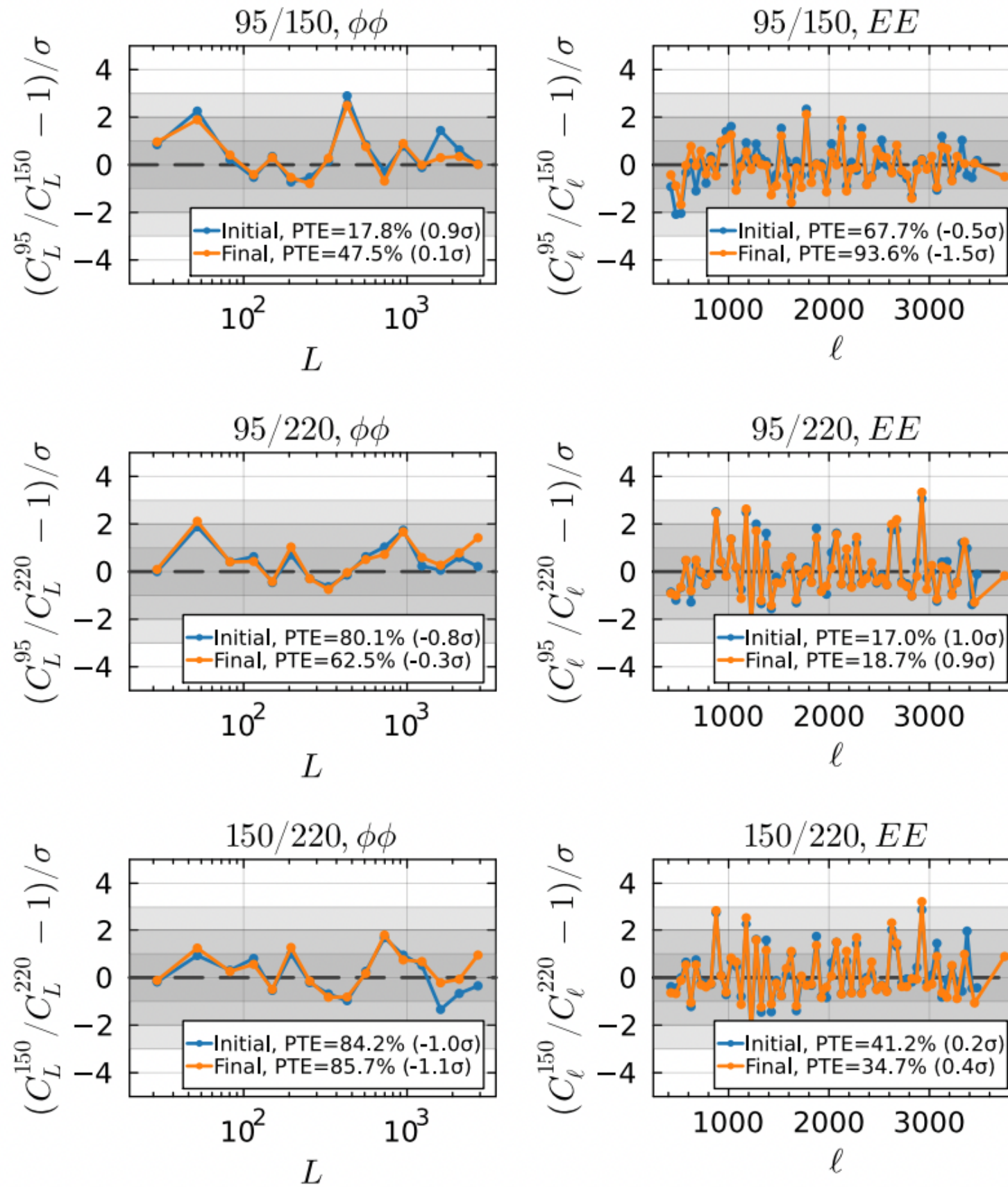
ACT
Planck PR3
W-ACT (ACT + WMAP)



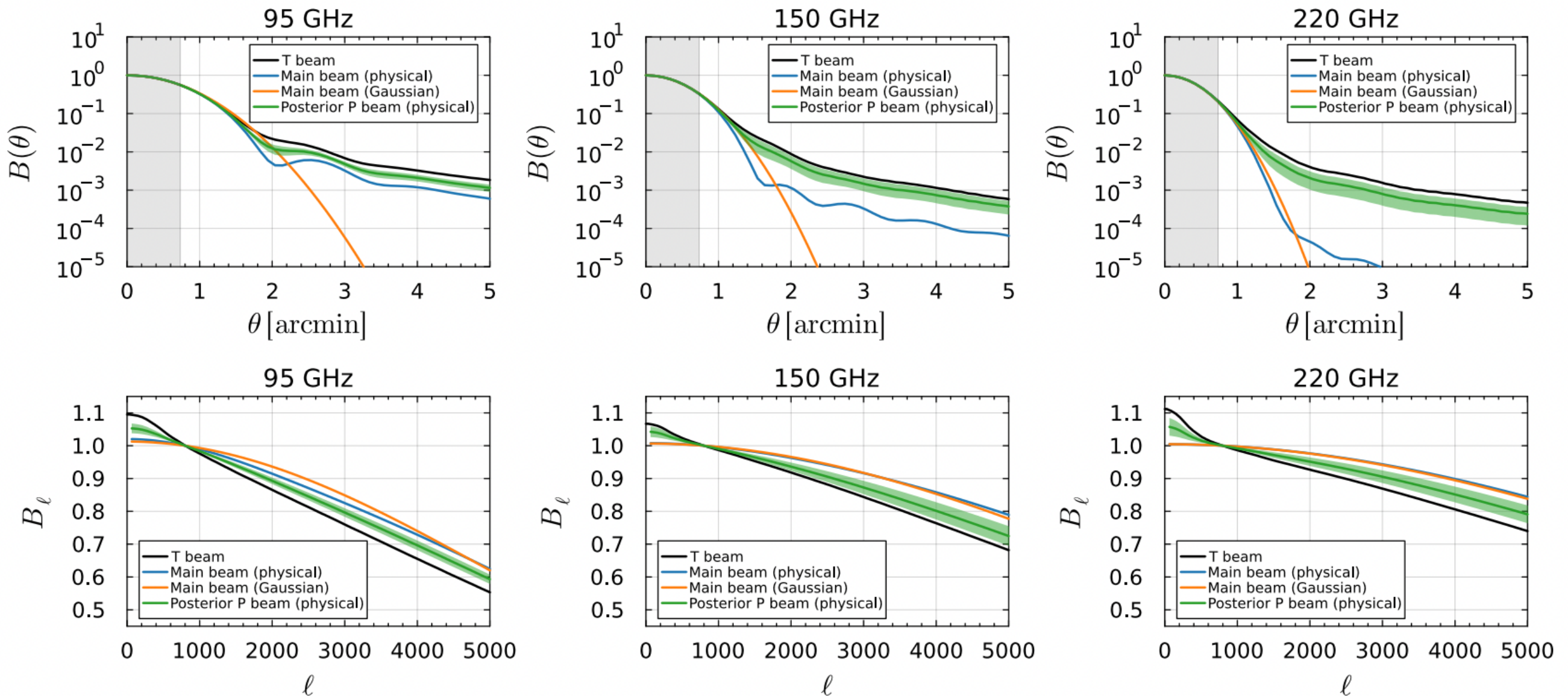
SPT post unblinding

[https://arxiv.org/pdf/2411.06000](https://arxiv.org/pdf/2411.06000.pdf) / SPT3G





<https://arxiv.org/pdf/2411.06000.pdf> / SPT3G



Posterior

	95 GHz	150 GHz	220 GHz
A_{cal}^1	0.8977 ± 0.0074	0.9276 ± 0.0074	0.8612 ± 0.0084
A_{cal}^2	0.8928 ± 0.0072	0.9133 ± 0.0071	0.864 ± 0.0079
A_{cal}^3	0.8861 ± 0.0073	0.9399 ± 0.0075	0.849 ± 0.0083
A_{cal}^4	0.8775 ± 0.008	0.9272 ± 0.0081	0.8405 ± 0.0097
$100 \epsilon_Q^1$	0.291 ± 0.025	0.319 ± 0.021	0.492 ± 0.059
$100 \epsilon_Q^2$	0.402 ± 0.024	0.39 ± 0.022	0.418 ± 0.06
$100 \epsilon_Q^3$	0.555 ± 0.025	0.838 ± 0.021	2.096 ± 0.066
$100 \epsilon_Q^4$	0.603 ± 0.033	0.912 ± 0.03	2.221 ± 0.084
$100 \epsilon_U^1$	0.584 ± 0.027	0.74 ± 0.025	0.735 ± 0.064
$100 \epsilon_U^2$	0.648 ± 0.025	0.748 ± 0.023	0.642 ± 0.058
$100 \epsilon_U^3$	0.851 ± 0.027	1.238 ± 0.023	1.33 ± 0.063
$100 \epsilon_U^4$	0.83 ± 0.035	1.174 ± 0.03	1.121 ± 0.092
$\psi_{\text{pol}} [\circ]$	0.393 ± 0.024	0.419 ± 0.021	-0.188 ± 0.079
β_{pol}	0.44 ± 0.20	0.60 ± 0.28	0.51 ± 0.26

Polar efficiencies

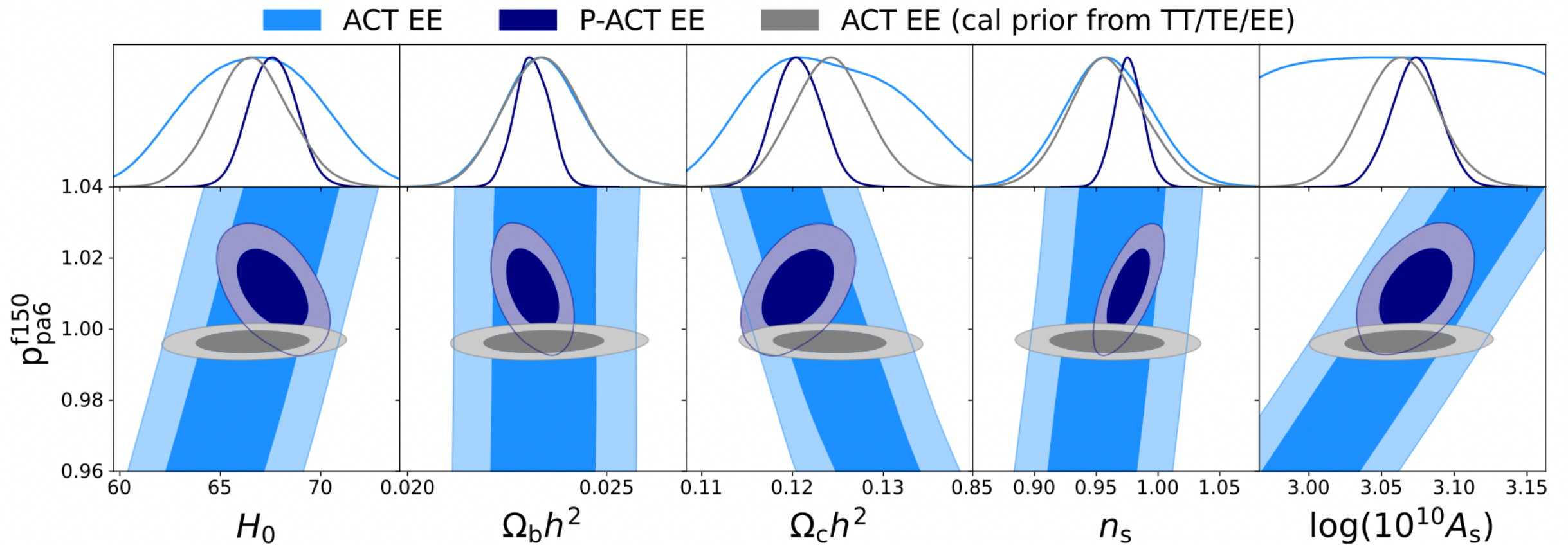


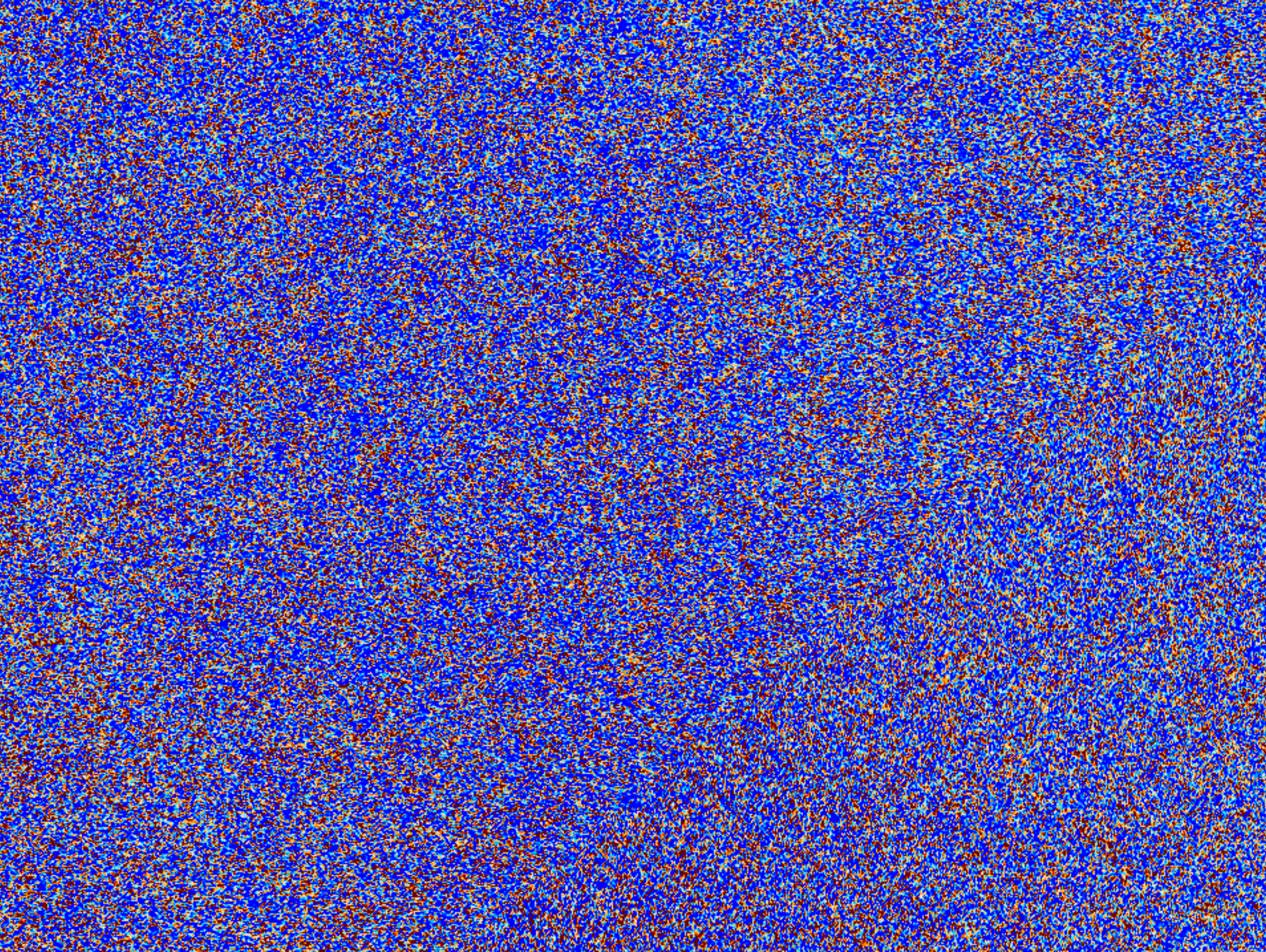
Figure 38. Marginalised posterior distributions of sampled parameters from EE, including the polarization efficiency for PA6 f150. We show constraints from ACT only (including the Sroll2 data to measure optical depth, light blue), P-ACT (dark blue) and ACT when using calibration and polarization efficiency priors from a full TT/TE/EE run (gray).

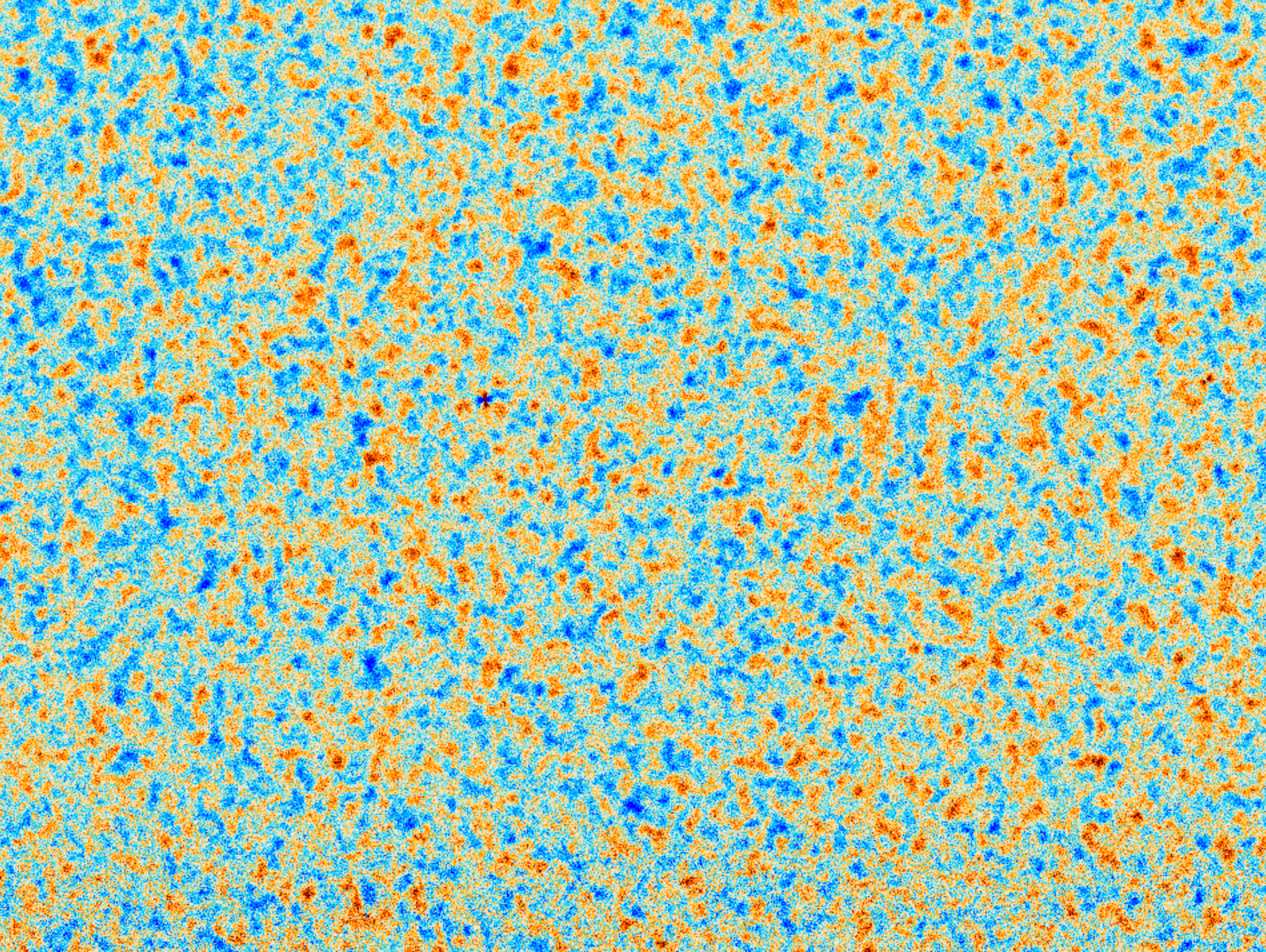
Telescopes

Telescope [\[edit \]](#)

The ACT is an off-axis [Gregorian telescope](#). This off-axis configuration is beneficial to minimize artifacts in the point spread function. The telescope reflectors consist of a six-metre (236 in) primary mirror and a two-metre (79 in) secondary mirror. Both mirrors are composed of segments, consisting of 71 (primary) and 11 (secondary) aluminum panels. These panels follow the shape of an ellipsoid of revolution and are carefully aligned to form a joint surface.







How does model change H₀

Early dark energy: new field that accelerates the expansion prior to recombination, reduces sound horizon.

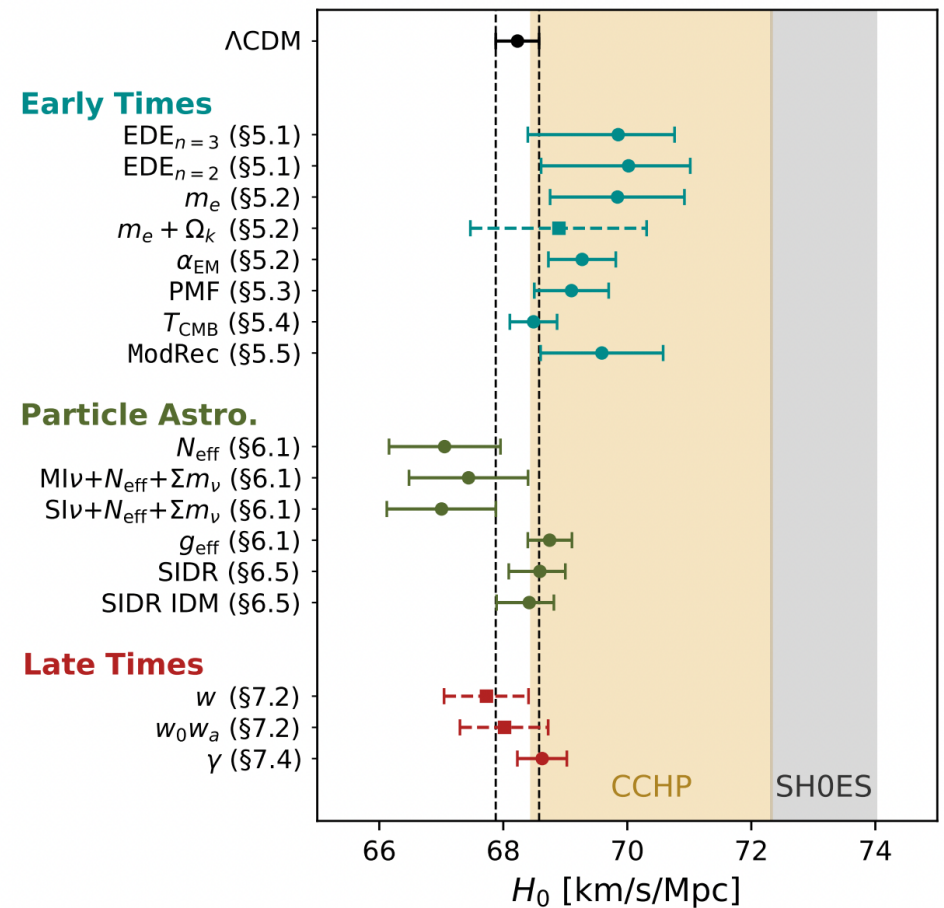
$$V(\phi) = m^2 f^2 (1 - \cos(\phi/f))^n, \quad (10)$$

where m is the mass of the field, f is the axion decay constant, and n is a power-law index. While $n = 1$ is excluded on phenomenological grounds — as the EDE would act as an additional contribution to dark matter at late times — values of $n \geq 2$ constitute viable models. Here, we consider as baseline the $n = 3$ model, as in previous literature (e.g., Hill et al. 2020; Ivanov et al.

Fondamental constant

The dynamics of recombination depends critically on the values of fundamental constants during the decoupling epoch, including the fine-structure constant and the electron mass, we assume that the value of these parameters undergoes an instantaneous, step-function transition well after recombination is completed, but well before the reionization epoch (specifically, we choose $z = 50$ for the redshift of this transition).

these effects). The dominant physical effects are due to changes in the Thomson scattering cross-section, with $\sigma_T \propto \alpha_{EM}^2 m_e^{-2}$, and changes in the energy levels of atomic hydrogen, with $E \propto \alpha_{EM}^2 m_e$. Many additional, subtle effects arise due to the non-equilibrium nature of cosmological recombination — see, e.g., Hart & Chluba (2018); Chluba & Ali-Haïmoud (2016); Planck Collaboration (2015) for a thorough discussion. In general, variations of α_{EM} or m_e change the timing of recombination, with higher values of these constants associated with earlier recombination. Thus, such variations change the physical scales imprinted in the CMB power spectrum, including the damping scale. The new ACT DR6 spectra allow tests of these effects in a qualitatively new regime, deep into the damping tail in TT and across a wide range of scales in TE and EE.

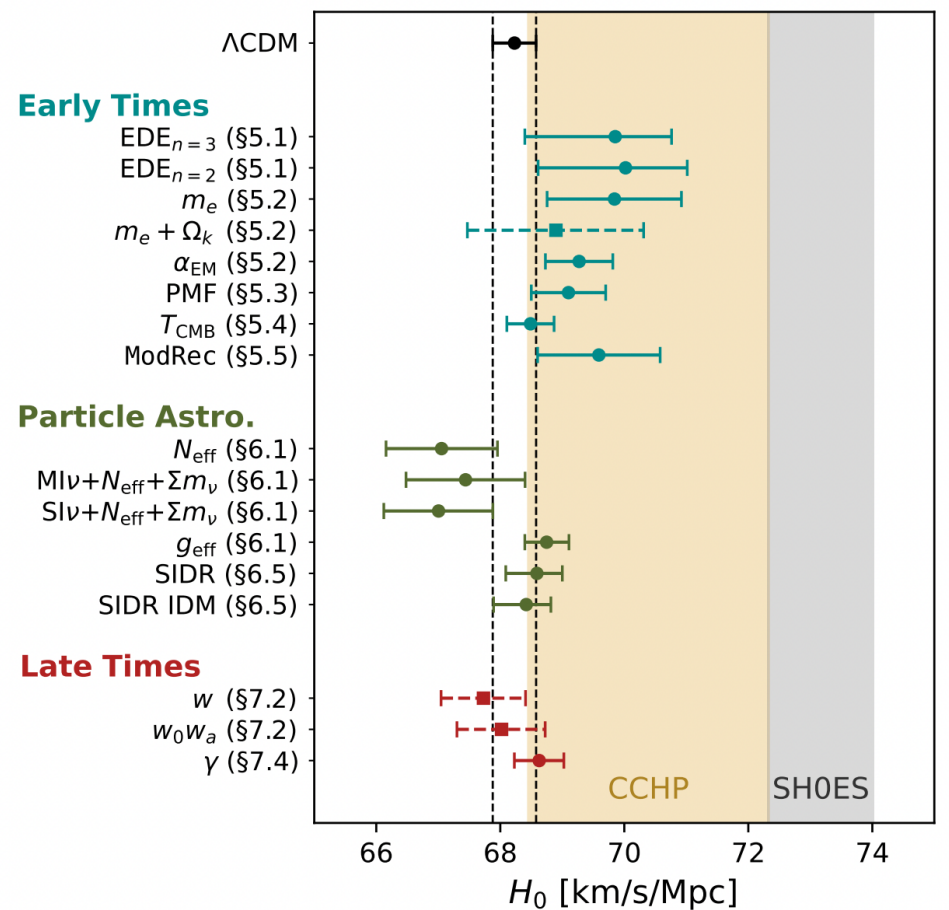


How does model change H₀

5.3. Primordial magnetic fields

The existence of primordial magnetic fields (PMFs) is a compelling possibility. Such PMFs could cause inhomogeneities in the baryon distribution around recombination. Thus, the PMF model is an example of a slightly more generic scenario known as “baryon clumping” (Jedamzik & Abel 2013; Jedamzik & Saveliev 2019). Primordial magnetic fields with a blue-tilted power spectrum can naturally have kpc-scale correlation lengths. Once the photon gas dynamically decouples from the baryon fluid on small scales, the magnetic force causes efficient growth of baryon density perturbations to potentially $\mathcal{O}(1)$ contrasts. These kpc-scale perturbations are not directly resolvable in CMB observations, but they cause accelerated recombination due to

the quadratic source term in the equation describing the recombination rate (Peebles 1968). The corresponding decrease in the sound horizon could then partially reconcile CMB-based determinations of the Hubble constant with local universe measurements (Jedamzik & Pogosian 2020). As magnetic fields are part of the standard model and their generation during early-universe phase transitions is conceivable, PMFs (or baryon clumping models in general) are a well-motivated scenario to potentially increase the CMB-inferred Hubble constant.¹⁷



How does model change H_0

CMB temperature

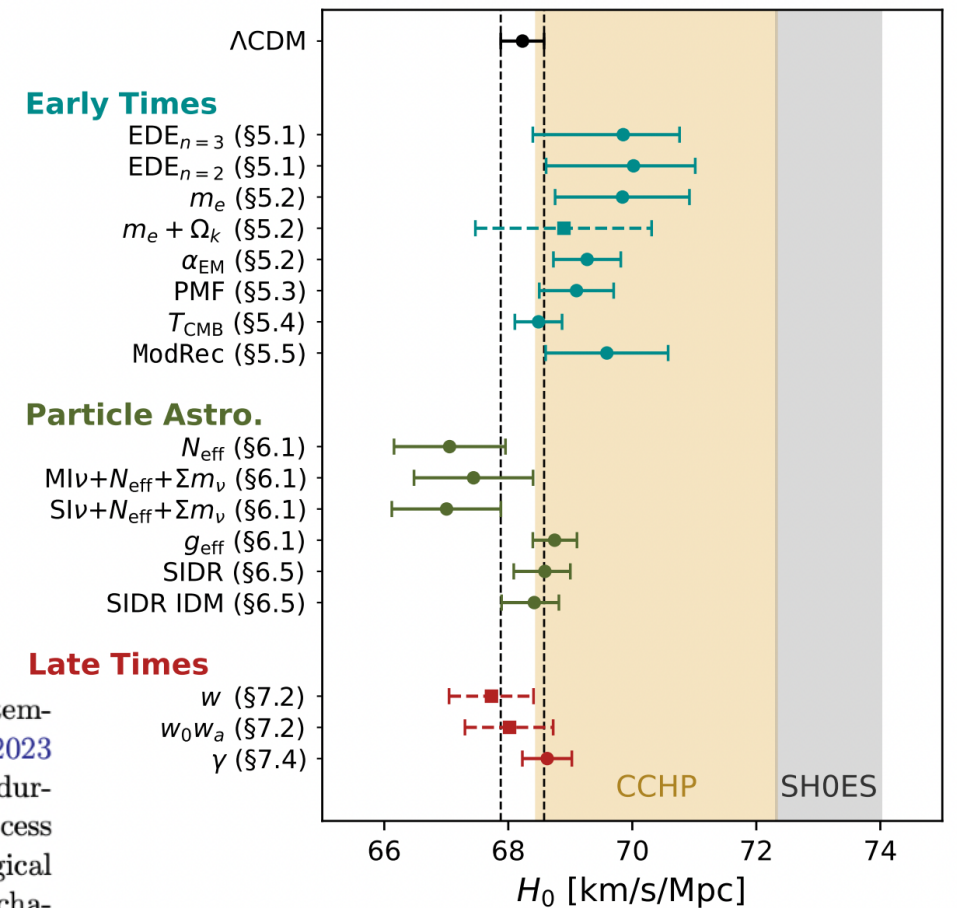
Several studies (e.g., Ivanov et al. 2020a; Wen et al. 2021; Hill & Bolliet 2023) have explored the possibility of increasing the CMB-anisotropy-inferred value of the Hubble constant by changing the CMB monopole temperature, T_{CMB} . In particular, Ivanov et al. (2020a) highlighted a strong negative degeneracy in the H_0 - T_{CMB} plane when the monopole temperature is left free in analyses of *Planck* data. Setting a SH0ES prior on H_0 would then yield a temperature measurement 3σ lower than the combined measurement of $T_{\text{CMB}} = 2.72548 \pm 0.00057$ K (Fixsen 2009) from *COBE/FIRAS* and other data.¹⁸

Obtaining a higher value of H_0 via a decrease in the monopole CMB temperature is difficult. Models with some level of post-recombination reheating can have an

impact by allowing a lower value of the monopole temperature in the early universe (e.g., Hill & Bolliet 2023 propose to convert a fraction of DM into photons during the dark ages). However, although such a process is straightforward to implement in a phenomenological way, it is hard to find a well-grounded physical mechanism to motivate it such that the blackbody spectrum is preserved (see, e.g., Chluba 2014).

Nevertheless, these studies have led to the realization that current CMB anisotropy data in combination with BAO data provide, on their own, a powerful probe of the amount of radiation in the universe.¹⁹ A single-parameter extension to the Λ CDM model, where T_{CMB} is left free, is well constrained. Ivanov et al. (2020a) combine *Planck* 2018 CMB anisotropy and lensing data with BOSS DR12 BAO data (eBOSS Collaboration 2018) and find $T_{\text{CMB}} = 2.706^{+0.019}_{-0.020}$ K (68% CL). Updating this *Planck* result including BAO from DESI, we find a slightly tighter constraint, $T_{\text{CMB}} = 2.696 \pm 0.017$ K. With the addition of the new ACT DR6 spectra, we find a similar constraint

$$T_{\text{CMB}} = 2.698 \pm 0.016 \text{ K (68%, P-ACT-LB).} \quad (28)$$



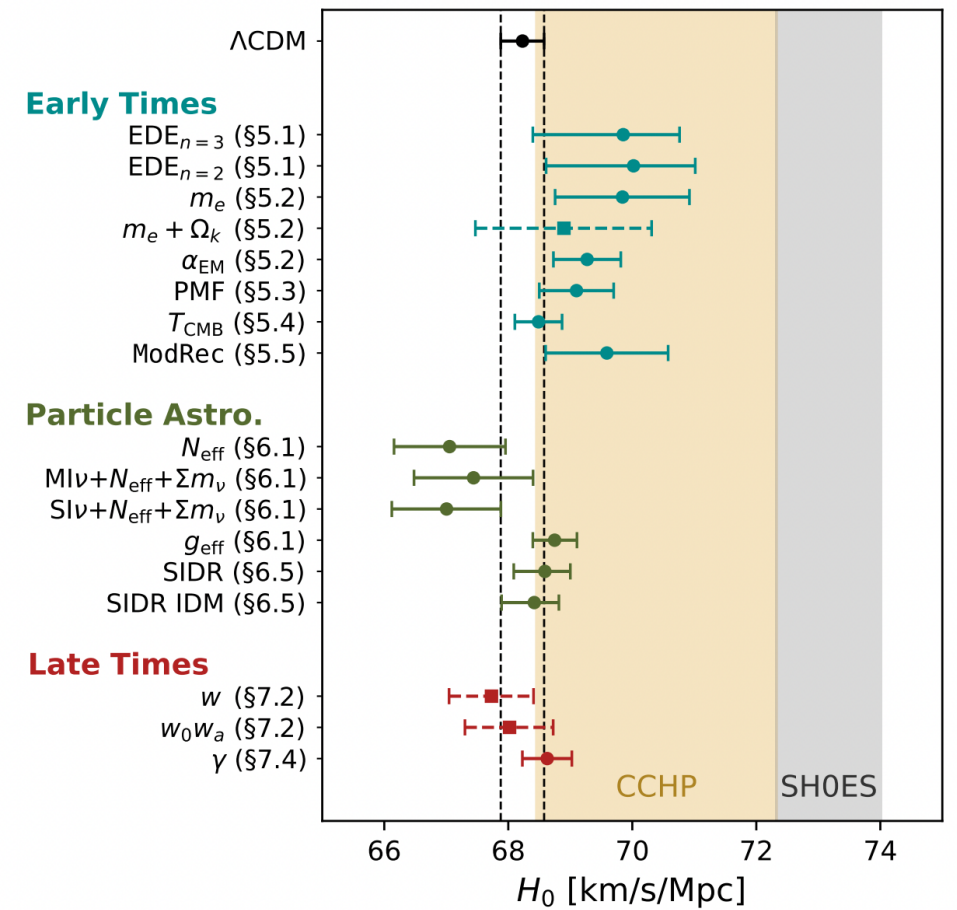
How does model change H₀

Neutrino number

The CMB is able to constrain N_{eff} because its value affects the expansion rate of the universe, especially during the radiation-dominated phase, thereby altering the expansion history just before recombination and the predicted abundances of primordial light elements (Bashinsky & Seljak 2004; Hou et al. 2013; Abazajian et al. 2015; Pan et al. 2016; Baumann et al. 2016a). At the perturbative level, N_{eff} alters the damping tail (high- ℓ region) of the TT/TE/EE spectra, both because the change to the expansion history alters the timescale for diffusion damping and because the free-streaming nature of the radiation damps the growth of perturbations, with the latter also inducing a characteristic phase shift in the acoustic peaks (Bashinsky & Seljak 2004). Combining the *Planck* legacy CMB with *Planck* CMB lensing and BOSS BAO, the neutrino number is measured to be $N_{\text{eff}} = 2.99 \pm 0.17$ at 68% CL (Planck Collaboration 2020c), or $N_{\text{eff}} = 3.06 \pm 0.17$ at 68% CL when we evaluate this estimate using Planck-LB.

With the new ACT DR6 spectra we find $N_{\text{eff}} = 2.60^{+0.21}_{-0.29}$ at 68% CL, combining into

$$N_{\text{eff}} = 2.73 \pm 0.14 \quad (68\%, \text{P-ACT}), \\ = 2.86 \pm 0.13 \quad (68\%, \text{P-ACT-LB}), \quad (30)$$



How does model change H₀

Neutrino self-interactions: heavy mediator

We consider first the case where the mass m_ϕ of the mediator is much larger than the neutrino temperature at all times directly probed by CMB anisotropies (Cyr-Racine & Sigurdson 2014). In this case, the neutrino interaction is effectively a four-fermion vertex controlled by a dimensional coupling constant $G_{\text{eff}} = g^2/m_\phi^2$, i.e., the effective low-energy Lagrangian is $\mathcal{L}_{\text{eff}} = G_{\text{eff}} \bar{\nu} \nu \bar{\nu} \nu$. This is analogous to the low-energy behavior of standard weak interactions, just with G_{eff} taking the place of the Fermi constant $G_F \simeq 1.17 \times 10^{-5} \text{ GeV}^{-2}$. This low-energy limit does not depend on the nature of the mediator, so the analysis here naturally encompasses both the scalar and vector cases. The Boltzmann hierarchy for neutrino perturbations including the collision term \mathcal{L}_{eff} generated by the interaction has been derived by Kreisch et al. (2020).

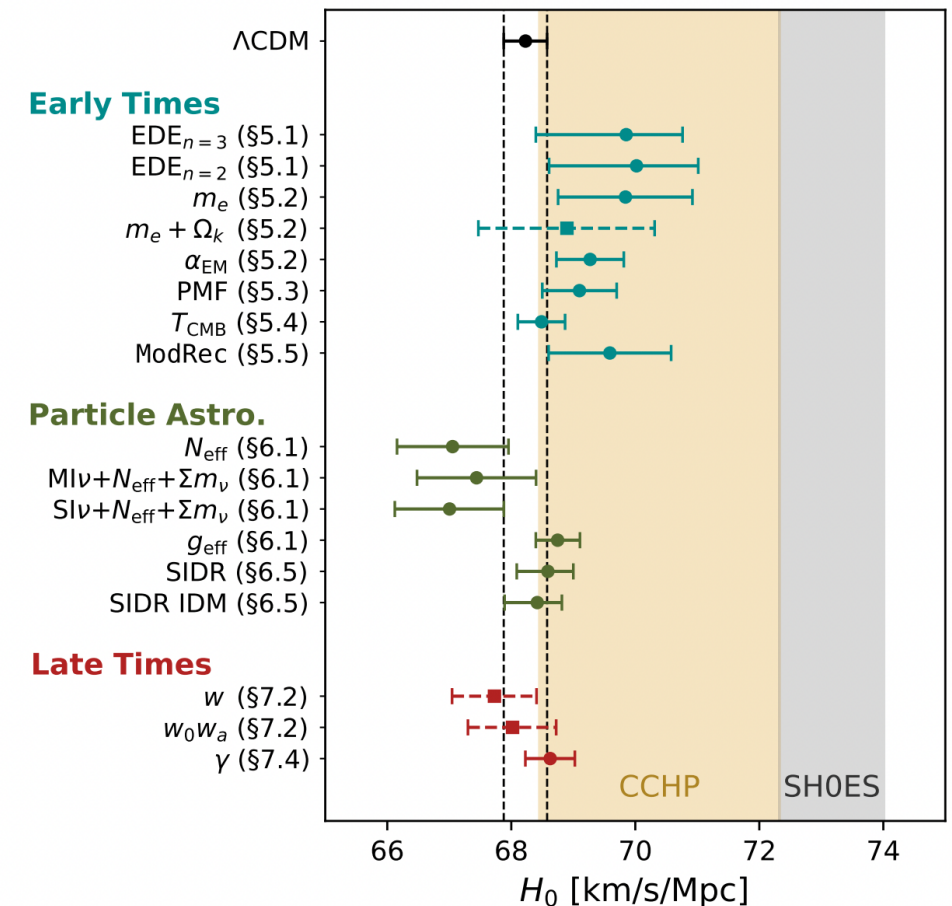
In this scenario, neutrino free-streaming does not start at the time of weak decoupling, but is instead delayed until $T_{\text{fs}} = T_{\nu, \text{dec}}(G_F/G_{\text{eff}})^{2/3}$, where $T_{\nu, \text{dec}} \simeq 1 \text{ MeV}$ is the neutrino decoupling temperature. Neutrino self-interactions through a heavy mediator leave an imprint at angular scales $\theta \lesssim \theta_{\text{fs}}$ (assuming $\theta_{\text{fs}} < \theta_{\text{eq}}$), where θ_{fs} is the scale entering the horizon at $T = T_{\text{fs}}$.

Previous analyses have shown that CMB and BAO data are compatible with, and in some cases prefer, neutrino self-interactions with $G_{\text{eff}} \gg G_F$ (Cyr-Racine & Sigurdson 2014; Archidiacono & Hannestad 2014; Lancaster et al. 2017; Oldengott et al. 2017; Park et al. 2019; Kreisch et al. 2020; Barenboim et al. 2019; Brinckmann et al. 2021; Das & Ghosh 2021; Mazumdar et al. 2022; Roy Choudhury et al. 2021; Poudou et al. 2025). In fact, the posterior for G_{eff} has been found to be bimodal, with probability being concentrated in two distinct regions: a moderately interacting ($\text{MI}\nu$) mode, compatible with no self-interactions, and a strongly interacting ($\text{SI}\nu$) mode. The analysis of ACT DR4 data showed a slight preference for neutrino self-interactions at the $2 - 3\sigma$ level, finding $G_{\text{eff}} \lesssim 10^{-3} \text{ MeV}^{-2}$ for $\text{MI}\nu$, and $G_{\text{eff}} \simeq 10^{-1.5} \text{ MeV}^{-2}$ for $\text{SI}\nu$ (Kreisch et al. 2024).

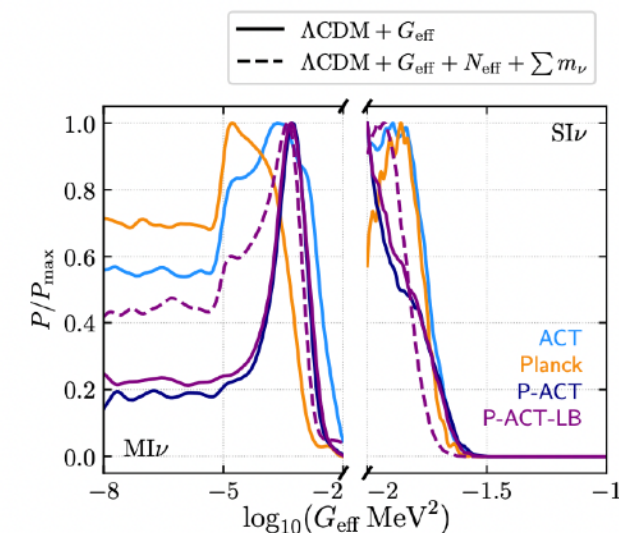
	ACT	P-ACT	P-ACT-LB
$\Delta\chi^2_{\text{MI}\nu}$	-0.2	2.9	3.1
$\Delta\chi^2_{\text{SI}\nu}$	-3.2	-10.6	-7.3
$\sigma_{\text{MI}\nu}$	-	1.7	1.8
$\sigma_{\text{SI}\nu}$	-	-	-

Table 3. $\Delta\chi^2 \equiv \chi^2_{\Lambda\text{CDM}} - \chi^2_{\Lambda\text{CDM} + G_{\text{eff}}}$ from the MAP points of the $\text{MI}\nu$ and $\text{SI}\nu$ regions for different data combinations. When self-interacting neutrino models yield an improvement of the fit over ΛCDM we also report the preference for the model in units of σ . We find no statistically significant preference for neutrino self-interactions.

We start by considering a one-parameter extension of ΛCDM , including G_{eff} as an extra parameter and keeping fixed $\sum m_\nu = 0.06 \text{ eV}$ and $N_{\text{eff}} = 3.044$. To check if the bimodal behavior persists



33



How does model change H₀

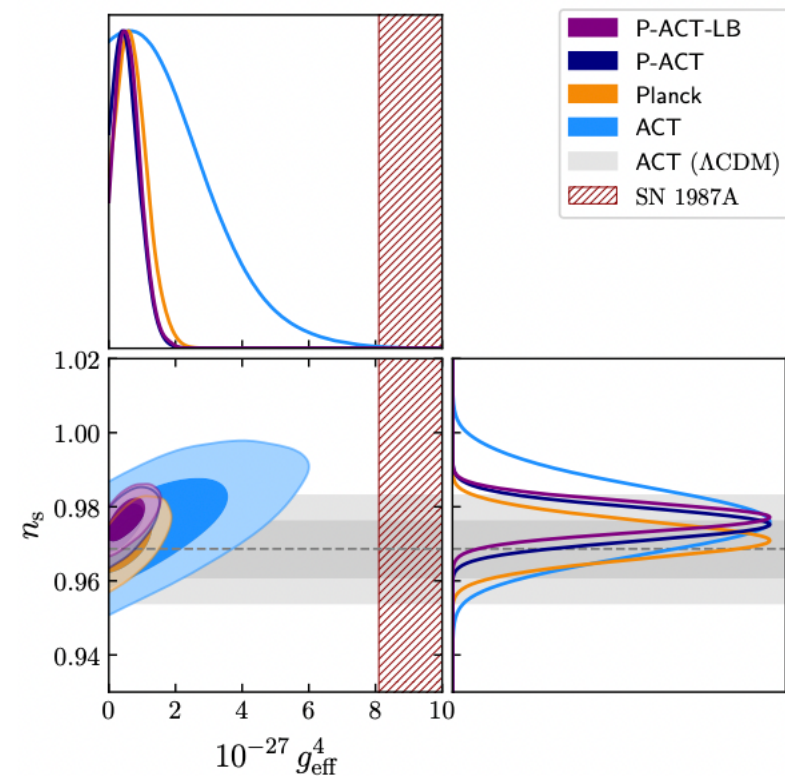
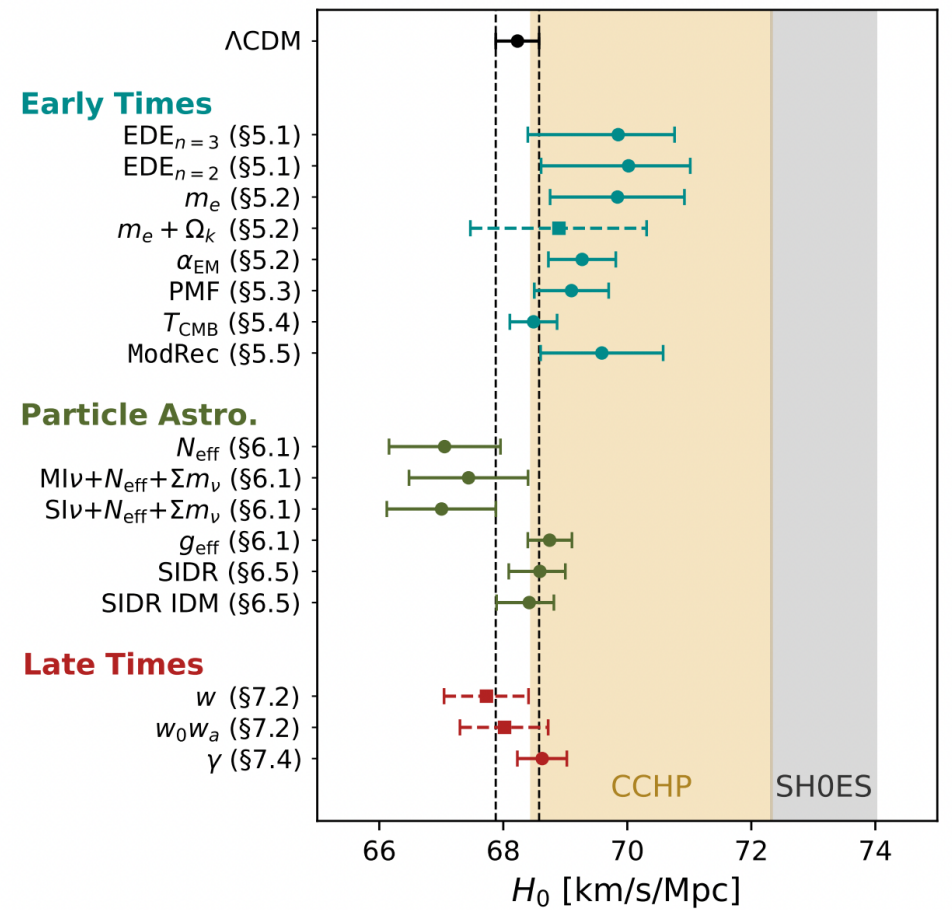
Neutrino self-interactions: light mediator

In this scenario the mediator mass is much smaller than the average neutrino momentum at all times of interest and the scattering rate $\Gamma \propto g^4 T$, so that the ratio between the scattering and Hubble rates increases with time. Neutrinos will then start free streaming at weak decoupling as usual, and become collisional again at later times (Archidiacono & Hannestad 2014; Forastieri et al. 2015, 2019). The effects of collisions are confined to scales between θ_{coll} , the scale entering the horizon when neutrinos stop free streaming at late times, and θ_{eq} . These correspond to intermediate angular scales in the CMB power spectra (larger scales compared to those affected by a heavy mediator) and so we expect less contribution to this limit from ACT DR6.

From *Planck* CMB data, we find $g_{\text{eff}}^4 < 1.5 \times 10^{-27}$ at 95% CL. The new ACT DR6 spectra alone give a limit about three times weaker, with $g_{\text{eff}}^4 < 5.2 \times 10^{-27}$ at 95% CL. Combining the two datasets gives a $\sim 20\%$ improvement on *Planck* alone, with

$$g_{\text{eff}}^4 < 1.2 \times 10^{-27} \quad (\text{95\%, P-ACT}), \\ < 1.3 \times 10^{-27} \quad (\text{95\%, P-ACT-LB}), \quad (38)$$

or $|g_{\text{eff}}| < 1.1 \times 10^{-7}$.



How does model change H₀

Interacting DR-DM

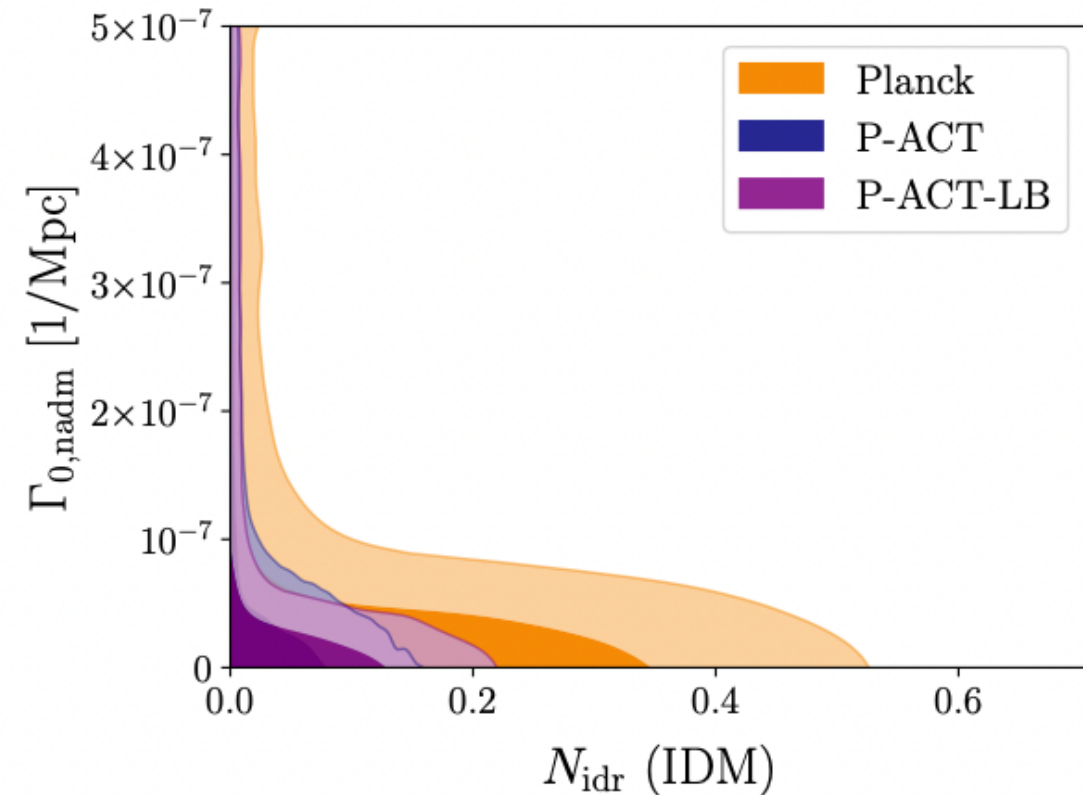
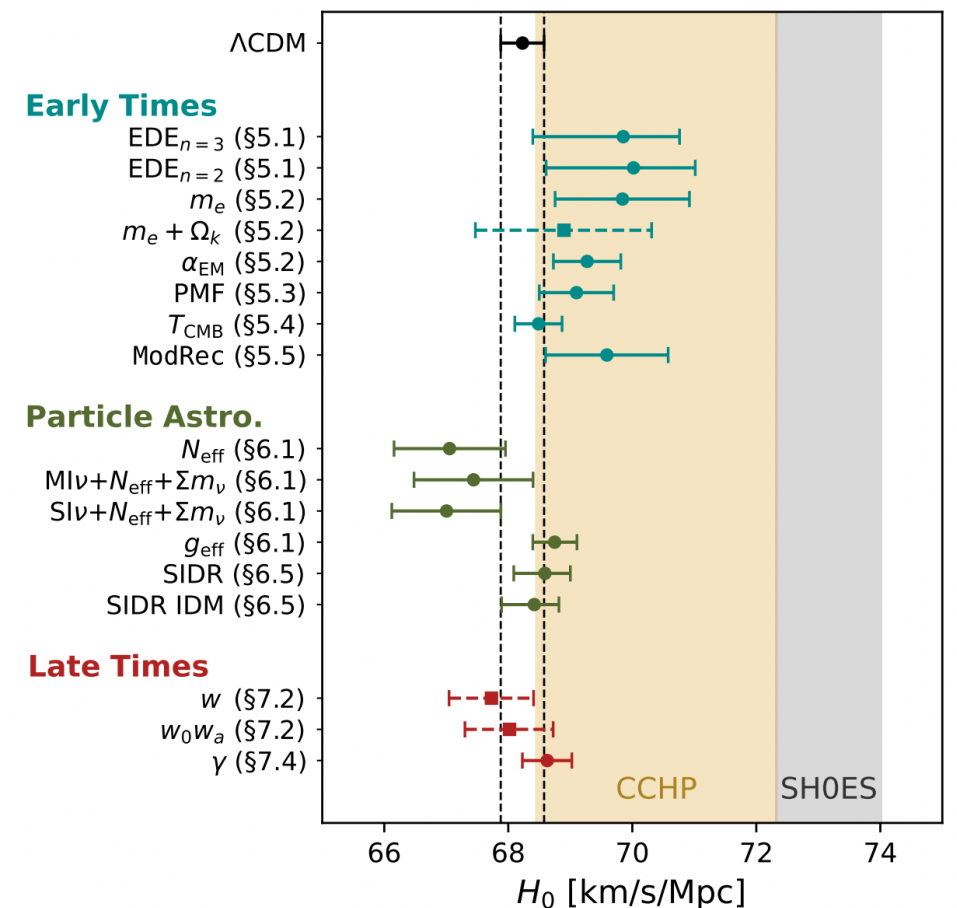


Figure 35. Constraints on the IDR-IDM model. Here the interaction strength $\Gamma_{0,\text{nadm}}$ is given in $1/\text{Mpc}$. The inclusion of ACT DR6 spectra (navy) significantly improves the constraints from *Planck* alone (orange). Inclusion of CMB lensing and DESI BAO data (purple) slightly weakens the N_{idr} upper limit due to small shifts in the best-fit model parameters, but further tightens the constraint on $\Gamma_{0,\text{nadm}}$. The notation N_{idr} (IDM) indicates that the IDR in the model constrained here is interacting with the DM, unlike that in Fig. 34.



How does model change H₀

Self-interacting dark radiation

A wide range of dark radiation (DR) models have been constructed, beyond the simple free-streaming case parameterized by N_{eff} (e.g., Jeong & Takahashi 2013; Buen-Abad et al. 2015; Cyr-Racine et al. 2016; Lesgourges et al. 2016; Aloni et al. 2022; Joseph et al. 2023; Buen-Abad et al. 2023; Rubira et al. 2023; Schöneberg et al. 2023; Zhou & Weiner 2024). These models generically involve self-interactions amongst the DR, interactions between the DR and (a subset of) the DM, or combinations thereof, potentially with non-trivial time-dependence (e.g., due to the temperature of the DR-DM sector falling below the mass of a massive mediator particle). As a first step toward investigating these scenarios, we consider a simple model of (strongly) self-interacting DR (SIDR), for example due to a new gauge interaction in the dark sector. At the background level, this model is identical to N_{eff} , with a free parameter $N_{\text{idr}} \geq 0$ describing the number of additional relativistic species (and hence the additional DR energy density). However, the SIDR and free-streaming DR models differ at the perturbative level: the SIDR forms a perfect relativistic fluid with $w = 1/3 = c_s^2$, with interactions sufficiently strong that no anisotropic stress (or higher-order Boltzmann moments) can be supported. Thus, the perturbative dynamics are characterized fully by the continuity and Euler equations. Unlike free-streaming DR, SIDR can cluster on small scales, thus reducing the impact of Silk damping on the high- ℓ power spectra (at fixed DR energy density). In addition, SIDR generates a smaller phase shift in the power spectra. Thus, CMB fits to the SIDR model can accommodate larger amounts of DR than the free-streaming DR model, which can thus allow higher values of H_0 (e.g., Aloni et al. 2022; Schöneberg et al. 2022; Allali et al. 2024).

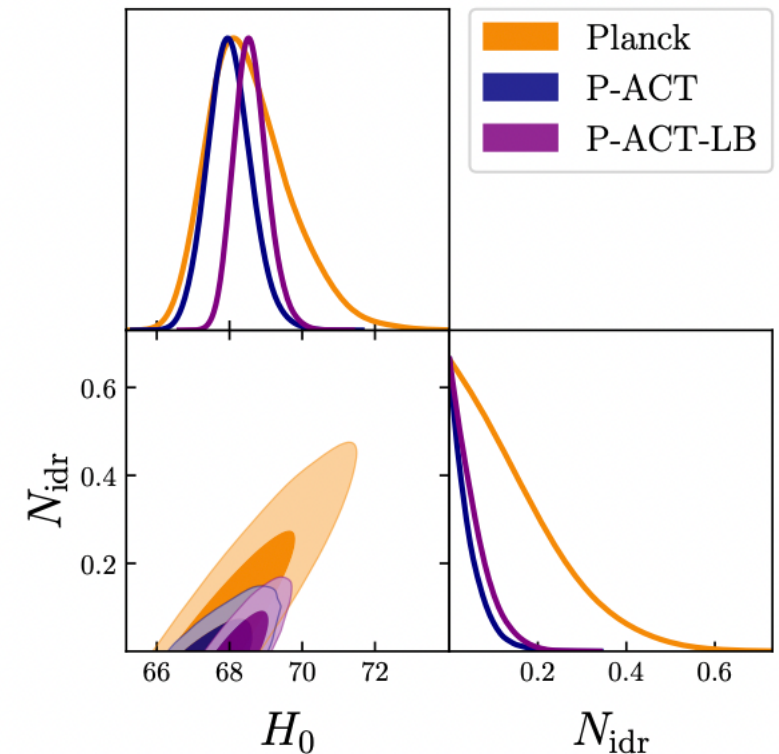


Figure 34. Constraints on the number of strongly self-interacting dark relativistic species, N_{idr} . The addition of ACT DR6 spectra improves the constraint from *Planck* by more than a factor of three (navy versus orange) and notably disfavors values of H_0 above 70 km/s/Mpc that are allowed by *Planck* alone. Inclusion of CMB lensing and DESI BAO data (purple) slightly weakens the SIDR upper limit due to small shifts in the best-fit model parameters, but nevertheless further tightens the H_0 posterior. These are the tightest bounds on SIDR obtained to date.

